Electricity consumption and battery lifespan estimation for transit electric buses: drivetrain simulations and electrochemical modelling

by

Anaïssia Franca
B.Eng, University of Victoria, 2015

A Thesis Submitted in Partial Fulfillment of the
Requirements for the Degree of

MASTER OF APPLIED SCIENCE

in the Department of Mechanical Engineering

Electricity consumption and battery lifespan estimation for transit electric buses: drivetrain simulations and electrochemical modelling

by

Anaïssia Franca
B.Eng, University of Victoria, 2015

Supervisory Committee

Dr. Curran Crawford, Supervisor
(Department of Mechanical Engineering)

Dr. Ned Djilali, Supervisor
(Department of Mechanical engineering)

ABSTRACT

This thesis presents a battery electric bus energy consumption model (ECONS-M) coupled with an electrochemical battery capacity fade model (CFM). The underlying goals of the project were to develop analytical tools to support the integration of battery electric buses. ECONS-M projects the operating costs of electric bus and the potential emission reductions compared to diesel vehicles for a chosen transit route. CFM aims to predict the battery pack lifetime expected under the specific driving conditions of the route. A case study was run for a transit route in Victoria, BC chosen as a candidate to deploy a 2013 BYD electric bus. The novelty of this work mainly lays in its application to battery electric buses, as well as in the coupling of the ECONS-M and the electrochemical model to predict how long the batteries can last if the electric bus is deployed on a specific transit route everyday. An in-depot charging strategy is the only strategy examined in this thesis due to the charging rate limitations of the electrochemical model. The ECONS-M is currently being utilized in industry for the preparations of Phase I and II of the Pan-Canadian Electric Bus Demonstration & Integration Trial led by the Canadian Urban Transit Research and Innovation Consortium (CUTRIC). This project aims to deploy up to 20 battery electric buses for phase I and 60 electric buses for phase II across Canada to support the standardization of overhead fast chargers and in-depot chargers, which in a first in the world. At this time, the developed CFM can not support any final claims due to the lack of electrochemical data in the literature for the high capacity lithium-ion cells used in electric buses. This opens the door to more research in the ageing testing of batteries for heavy-duty applications.

Contents

List of Tables

List of Figures

List of Abbreviations and Symbols

Abbreviations

ABD	Advanced Design Bus
ART	Arterial cycle
BC	British Columbia
BMS	Battery management system
CBD	Central Business District cycle
CC-CV	Constant-current constant-voltage charge
CFM	Capacity fade model
CUTRIC	Canadian Urban Transit Research and Innovation Consortium
DEM	Digital Elevation Model
DOD	Depth-of-discharge
ECON-M	Electricity consumption model
GR	Gear ratio
OCP/OCV	Open circuit potential/voltage
SEI	Solid electrolyte interphase
SOC	State of charge
SPM	Single Particle Model
SSDL	Sustainable Systems Design Lab
TEM	Transmission electron microscopy

Symbols

A	Frontal Area (m^2)
a(t)	Vehicle acceleration (m/s^2)
a_{neg}	Specific interfacial area of the negative electrode (m^2/m^3)
a_s	Specific interfacial area of porous electrode (m^2/m^3)
C_D	Drag coefficient
cap	Total battery capacity (Wh)
C_e	Electrolyte phase lithium concentration (mol/m^3)

C_s	Solid phase lithium concentration (mol/m^3)
C_r	Rolling resistance coefficient
D_s	Diffusion coefficient in the solid state (m^2/s)
D_e	Diffusion coefficient in the electrolyte (m^2/s)
D_e^{eff}	Effective diffusion coefficient (m^2/s)
$E_{charge,grid}$	Energy drawn from the grid to charge the bus (Wh)
E_{TOTAL}	Total energy consumed for a driving cycle (Wh)
$I(t)$	Current (A)
I_{app}	Applied current (A)
i_0	Excahnge current density (A/m^2)
i_e	Ionic current in the electrolyte (A/m^2)
j_{Li}	Current density accross the electrode/electrolyte interface (A/m^2)
j_{side}	Side reaction current density (A/m^2)
F	Faradays constant $(96,487 C/mol)$
F_a	Aerodynamic force (N)
F_{brake}	Braking force (N)
F_g	Grade force (N)
F_{prop}	Force to propel the vehicle (N)
F_r	Rolling resistance force (N)
F_{tot}	Total resistive forces (N)
g	Acceleration due to gravity constant, 9.81 m/s^2
M	Vehicle mass (kg)
M_{eq}	Rotating components equivalent mass (kg)
P_{auxi}	Auxiliary power (W)
P_{charge}	Charging power (W)
P_{inst}	Instantaneous power (W)
Q_0	Volume averaged loss capacity (C/m^3)
R	Gas constant (8.314 J / mol. K)
R_W	Wheel radius (m)
S	Regenerative power split
T	Temperature (K)
t_0^+	Transference number
t_{charge}	Charging time (s)
T_M	Motor torque (Nm)
$T_{M,reg}$	Motor torque in regenerative braking mode (Nm)

T_W	Wheel torque (Nm)
V(t)	Vehicle speed (m/s^2)
U_{neg}	Open circuit potential of the negative electrode (V)

Greek letters

α	Road grade (^{o})
ϵ_e	Volume fractions of the electrolyte
ϵ_{fl}	Volume fractions of the conductive fillers
ϵ_s	Volume fractions of the solid
η	Overpotential (V)
η_{BMS}	Battery management system efficiency
η_{charge}	Charger efficiency
η_{conv}	Converter efficiency
η_M	Motor efficiency
$\eta_{M,reg}$	Motor efficiency in regenerative braking mode
η_{neg}	Overpotential of the negative electrode (V)
η_T	Transmission efficiency
κ^{eff}	Diffusional conductivity (S/m)
ω_M	Rotational speed at the motor (rad/s)
ω_W	Rotational speed at the wheel (rad/s)
ϕ_e	Potential in the electrolyte phase (V)
ϕ_s	Potential in the solid phase (V)
ρ	Air density (kg/m^3)
σ_s^{eff}	Effective conductivity in the solid phase (S/m)

ACKNOWLEDGEMENTS

I am deeply thankful to both of my supervisors, Prof. Curran Crawford and Prof. Ned Djilali at the University of Victoria. By allowing me to pick my research topic, giving me the guidance I needed and helping me through every step of the way I grew self-confidence and a true passion for developing systems modeling and taking on new challenges. Thank you both for your patience, your availability, your continuous support and encouragements.

I'd also like to express my sincere gratitude to Dr. Josipa Petrunic, executive director and CEO of the Canadian Urban Transit Research and Innovation Consortium (CUTRIC), for giving me the opportunity to develop and use the energy consumption model in the phase I of the Pan-Canadian Electric Bus Demonstration & Integration Trial. Thank you for your trust, your push, your energy and your very valuable feedback and advice.

I would like to thank Dr. Julian Fernandez, post-doctoral fellow, for all the relevant advices and feedback he has provided to support my research and professional growth and all his help with editing/reviewing this thesis. Another special thanks is for my colleague and friend Pouya Amid who post-processed the road elevation data for this research, and for my friend Patricia Thomson for her help proof-reading my thesis.

I am grateful to have had Mr. Calvin Tripp as my co-op coordinator and as a mentor who has followed my progresses and never ceased to encourage me and support my professional career throughout my undergrad and graduate studies.

I'd also like to extend my thanks to the research team part of the Transportation Futures for BC project and the SSDL. Working with all of you has been a great pleasure and made time fly. I am also thankful to all the members of IESVic with whom I share many great memories.

Thank you PICS, CUTRIC and MITACS for financially supporting my research.

I am so thankful to my family and best friends from France who have been my biggest fans during this journey. I want to start by giving a special shout out to my mother, who has been my strongest moral support anytime of the day (or night, for the matter...) and to my dad who helped me grow tremendously these last two years. Thank you both so much for being such amazing parents, you are the reason I am striving today.

Thank you Jérémie, Jonathan, Sébastien, my three little birds. I miss the three of

you so much and I am so proud to be your big sister. The thought that I can count on you three and that you've got my back has helped me tremendously over the years, despite the physical distance between us it's like you are next to me. I can't wait until we meet again.

Thank you so much Pierre, Mamie, Claude and Willy. There has been some taught times over the last two years and you have always been there for me to provide your loving support and advice whenever I needed it. Thanks for deeply caring about my success, and continuously encouraging me.

Thank you Mémé and Pépé, for closely watching my life updates and making sure to pray and put a candle for me at church anytime you realized I needed it.

Thank you Fred for checking up on me, for your great advice and always encouraging me to develop self-confidence.

Lastly, thanks to my oldest and best girlfriends Perrine and Manon for your unconditional long-distance support, for your love and for making me laugh real hard no matter what situations I was into.

I am also really grateful to have met wonderful friends in Victoria who have made my time here unforgettable. I am especially grateful to Christina, James and Ajauni who not only made me feel like home in Victoria right away as they are my oldest friends here but who also have supported my growth since I first arrived in Victoria in 2012. You made my time here fly! Another big thanks goes to my girlfriends from Quebec Charlotte and Kim whom I have met less than a year ago but who have had a big joyful impact on my personal life. I can't wait until you all come to visit me in Montreal. Last but definitely not least, I want to thank my boyfriend David for his constant encouragements and help over the course of this experience.

DEDICATION

To the girls and woman who don't have access to education #BecauseIamAGirl

Chapter 1

Introduction

1.1 Motivation and Battery Electric Buses State of the Art

Particle matter (PM) and nitrogen oxides (NOx) in urban air are linked to alarming increases in adults lung cancers, asthma and premature deaths [1]. It is estimated that vehicles contribute to 40-70% of urban NOx emissions, 85% of which is from diesel engines [2]. In 2009, 94% of the Canadian bus fleet operated diesel buses [3], producing a large amount of particle matter and nitrogen oxides (NOx) [4]. Deploying battery electric buses (BEBs) instead of diesel, bio-diesel or hybrid buses is a solution to tackle this public health issue, as this technology does not produce exhaust gases and therefore can improve cities local air quality.

Expanding the use of BEBs can effectively reduce greenhouse gas emissions. This step towards the decarbonization of transportation goes along Canada's engagement to the Paris Agreement signed by 175 parties around the world to limit global warming to 2^oC above pre-industrial levels [5].

Other advantages of BEBs compared to diesel and hybrid buses include less noisy

operation thanks to the electric motor and the simple transmission system which makes its application suitable for densely populated areas.

Additionally, BEBs can effectively recover power during braking, which can be problematic for trolley electric buses [6]. For regenerative braking to function in trolley buses, there has to be another bus requiring to use this surplus generated energy in the power lines at the same time, which is challenging to operate due to many variables during operations.

Furthermore, BEBs are up to six times more efficient compared to buses using compressed natural gas (CNG) according to Proterra, one of the largest american bus manufacturer [7]. Currently, the scientific community challenges the benefits of low tailpipe emissions of natural gas automotive technologies because the extraction and storage of natural gas comes with high risks of methane leakage that can can worsen the impact on climate change [8] and water pollution [9].

Battery electric buses for transit applications have been compared to fuel cell (FCB) and fuel cell hybrid buses (FCHB) in [10]. It was found that BEBs have a smaller energy fuel consumption on average compared to FCBs and FCHBs. Moreover, FCB are facing many technical challenges that prevent their large-scale adoptions, such as the lack of global technical regulations for hydrogen vehicles [11] and hydrogen production and distribution being capital and energy intensive [12].

Several factors, such as passenger safety, comfort, accessibility and reliability can be social barriers to the wide use of public transit [13]. In [14], the authors discussed a phenomenon called the "car effect", stating that people tend to show biases towards the use of personal vehicles, even when using a car is not in the person's best economic interest. This irrational bias is partially explained by the fact that in western societies, car is a symbol of freedom.

Despite these barriers, transit systems including buses, trolleys and light rail,

subways etc... present many advantages over the use of passenger cars. According to the American Public Transportation Association, travel delays would increase by 27 percent without public transportation [15]. Public transportation can protect the environment, improve cities air quality, provide support in emergency situations and reduce dependence in foreign oil. Financial savings is without a doubt one of the main benefit of public transportation. The American Public Transportation Association has developed a tool that assesses the potential savings of using public transportation for commuting instead of personal vehicles depending on the characteristics listed in Table 1.1 which shows the results of a common 2008 scenario. It should be noted that these estimations were calculated using data collected during the financial crisis of 2008 with a gas price of $4/gallon which is twice the average of June 2018 prices. Today's savings would be less than the $1,843 shown in the table but still substantial.

Table 1.1: Estimated savings from using public transportation using national averages for June 2008 [16]

Car's gas mileage: 20 MPG
Price of gas per gallon: $4
Number of miles in round trip commute: 24.22 miles
Size of car: SUV
Daily parking cost: $5
Daily round trip commute cost using public transportation: $3.5
Yearly cost of commuting with a car: $2,683
Yearly cost of commuting with public transportation: $840
Total savings: $1,843

Buses compared to other transit modes such as subways are less expensive and offer the most flexibility in terms of mobility. It is common in cities to have bus rapid transits, for which only major stops are serviced. Municipalities with a low population density such as Victoria BC (495 people/km^2) rely heavily on buses as the only public transport. On the contrary cities such as Vancouver (5,249 people/km^2) use a combination of very well connected trains, boats and buses to facilitate transit,

though busing remains the only way to get around the entire city as trains require considerable civil infrastructures that can be challenging to build and operate in highly populated areas.

A diesel bus is replaced every 12 years as part of a fleet, compared to approximately 6 years for cars [17]. Fleets ownership models vary greatly with the location and policies in place in the municipality. A public transport bus fleet can be owned by a municipal or by transit authority or it can have mixed funding (public and private). For example, BC Transit operating over most of the province of British-Columbia (BC) has two main sources of funding: the government (provincial and municipal) and passenger fares. The Utah Transit Authority, operating in Salt Lake City, is funded from the same main sources and with private investors. Buses are operated by drivers working for the transit authority.

Regarding the improvements of the user experience, transit agencies have made continuous IT efforts to develop user-friendly applications able to facilitate commutes and help users plan for their trips. Applications showing the real-time location of buses on a map are becoming more popular in large and smaller cities (Victoria and Vancouver in BC).

BEB manufacturers offer a wide variety of bus sizes and battery capacities to serve diverse transportation specifications. Different bus models, such as typical 12m long transit bus, coach bus or school bus are being deployed. For short routes, smaller battery packs are recommended. Bus manufacturers also use different types of battery chemistries and charging strategies. Table 1.2 shows different electric bus specifications from various manufacturers in North America for a transit application. The characteristics that are not publicly disclosed are marked with the symbol "(?)". As shown in this table, a wide range of technology is currently available on the market, including different battery systems and battery chemistries. It is important to note

that the capacity shown for each bus technology is the total installed battery capacity. Depending on the battery chemistry, manufacturers recommend different ranges of operating state-of-charge for their batteries, e.g. from 10-90% or 5-95%, to limit battery degradation. This implies that 10 to 20% of the installed battery capacity should not be used. Another important element to note is that manufacturers do not disclose their battery warranties and lifespan, or if they do the testing conditions are unknown (e.g: BYD refers to 4,000 cycles which is not indicative of the actual lifespan). The warranty on battery ranges from 6 years to 4,000 cycles (above 10 years if considering one charge/discharge per day).

Various pilot projects aiming to develop and expand BEB fleets while testing different charging strategies are flourishing in North America [22], Asia [23] and Europe [24] [25]. Table 1.3 shows some demonstration projects that have been implemented or are currently ongoing around the world.

To date, around 173,000 electric buses have been deployed around the world, 98% of which are in circulation in China [30].

To conclude this section, the key challenges to the adoption of BEBs are:

- the confidence in the technology since it is recent as shown in Table 1.3
- the lifetime of the batteries that are shorter than a typical diesel bus (replaced every 12 years) as shown in Table 1.2
- the performance that can be affected by the route on which the bus is deployed

The energy consumption and lifespan analyses developed in this thesis involve several factors and considerations that are reviewed next, including: impacts on the environment and the electricity grid; the impact of drivetrain and route on energy consumption; and the modeling of battery degradation processes. Progress in each of these topics is reviewed in the next sections.

Table 1.2: 12m-long electric bus characteristics for different manufacturers in North America

Criteria	**BYD K9 [18]**	**Proterra E2 [19]**	**Proterra FC+ [19]**	**New Flyer Xcelsior Electric [20]**	**Green PowerBus EV350 [21]**
Battery chemistry	Iron-Phosphate (LFP)	(?)	Lithium Titanate (LTO)	Nickel Manganese Cobalt (NMC)	Iron-Phosphate (LFP)
Charging capacity (kW)	80	120	350	300	320
Battery capacity (kWh)	324	660	105	300	320
Battery capacity (Ah)	200	(?)	(?)	(?)	(?)
Estimated maximum range (km)	259	563	100	193	300
Battery lifespan	4,000 cycles	6 year warranty	6 year warranty	(?)	(?)
Curb weight (kg)	14,000	14,996	12,473	14,864	(?)

Table 1.3: BEB deployment project around the world

Location	**Starting/ending date**	**Bus deployed**	**Manufacturers**	**Charging type**
Geneva, Switzerland [26]	Spring 2018 (?)	12	ABB and HESS	Overhead high-power charging, 600kW
Edmonton, Canada [27]	January 2016 - February 2016	2	BYD and New Flyer	Trickle-charging (60 kW, slow) En-route charging (300kW, fast)
San Joaquin County, USA [28]	May 2013 - Ongoing	12	Proterra	In depot (slow) and fast charging
London, UK [29]	September 2016 - Ongoing	73	BYD, ADL	In depot (slow)
China [30]	2016 - Ongoing	170,000	Yutong,BYD,Nanjing	Slow and fast charging

1.2 Environmental and Grid Impact of Charging Battery Electric Buses

The essential components in a BEB drivetrain are the battery packs. BEB lithium-ion battery can restore the energy accumulated during charging or during the use of regenerative braking to propel the vehicle. Several methods for charging BEBs are commercially available. The most common techniques used are slow charging (in-depot or at terminal stations) and fast charging (at bus stops and terminal stations) [31]. A third less commonly used method consists of swapping the discharged batteries with charged ones. Charging can be achieved through a direct physical connection between the charger and the bus (plug-in or conductive) or wireless [32]. The wireless charging infrastructure or inductive charger offers some advantages over plug-in methods. One of the main advantages of wireless charging is its very high power efficiency for the power transfer between the bus and the charging pad [33]. In [34], the life cycle greenhouse gas (GHG) emissions is assessed, for both conductive and inductive technologies and it was found that the wireless charging system consumes less energy

and emits slightly less GHG compared to a plug-in charging system over the systems lifetimes. Nevertheless, this study failed to take into account the emissions related to the electricity generation mix, which could increase the GHG emissions of the fast charging infrastructures.

Electric cars chargers are categorized according to their charging power levels [35]:

- level 1 is typically an at home charger with an expected output power up to 2 kW
- level 2 is a "primary" charger with an expected output power in the 8-19 kW range
- level 3, or "DC fast charging", can have an output power between 50 kW and 100 kW

Level 2 chargers can be used to charge electric buses with small battery packs, such as school buses. The power level 3 is usually considered as slow/in-depot charging for electric buses. This is currently being used by BYD and Proterra as shown in Table 1.2. For electric buses, fast charging occurs above 120 kW.

In Canada during the winter of 2016, two electric buses were deployed in Edmonton using two different charging techniques, namely trickle-charging and on-route fast charging. Marcon Engineering was the consulting company hired to determine the feasibility of introducing BEBs in service. Their study on the feasibility of the project for both charging strategies found that BEBs can lead to potential environmental and economic net benefits [27]. Most of the research carried out around BEBs focuses on the optimization of charging locations and infrastructure cost [36] [24], vehicle scheduling for fast charging [37][38] and battery sizing [39].

BEBs is a relatively new technology: the first BEB was deployed in Shanghai in 2009. Therefore, transit agencies take high business and technical risks when deciding

to purchase an electric bus. To shield the transit agencies from these risks, a business model designed to facilitate the adoption of BEBs is described in [40]. An enabling company was created to purchase 8 electric buses and their chargers. This company acted as a customer with the bus and charger manufacturers, the bus operator, the city council, the electricity operator, the power distributor and the electricity supplier. The company first purchased the buses and chargers and then leased them to the operating company. This has been shown to be a successful business case, though it raised a couple of concerns for regulatory and innovation policies. The majority of demonstration projects do not communicate the business model used to operate and own the bus and charging infrastructures in the literature.

In [41], the authors evaluate the electricity consumption of an electric bus using real-life data collected from the deployment of a BEB fleet with an ultra fast charging technology. The impact of fast charging on battery cost reduction is investigated. However, the impact of fast charging on the electric grid wasn't considered in that paper. According to Karakitsios et al. [42], fast chargers can potentially create network problems at the distribution level by disrupting the voltage profile and line loading which can create network losses. As shown in Table 1.3, fast chargers can supply up to 600 kW of power at their peak when buses charge, which can represent a significantly large load for the distribution network. There is currently a gap in the literature to identify the impact of fast charging for large BEBs fleet on the power grid, though this topic is being widely investigated for electric cars [43] [44] [45].

In current electricity market structures, customers are classified according to the installed capacity (kW) required and the energy (kWh) required for the operation. Electricity for large general customers is billed according to the following scheme:

- a basic cost, in $/day, covering administration fees
- a demand or delivery cost, in $/kW, covering the cost of installations

- an regulatory or energy cost, in $/kWh, covering the cost of electricity alone

Depending on the Canadian jurisdiction, electricity market prices can either vary hourly or stay constant. In Ontario, the Independent Electricity System Operator (IESO) manages the power system in real-time with pricing changing hourly. Conversely, in British Columbia, BC Hydro is the main electricity provider with fixed pricing no matter how the demand fluctuates. Demand costs are generally the highest cost in the bill, and depending on jurisdiction rates it could potentially make the adoption of BEBs more expensive than the deployment of diesel buses [46] [47].

To mitigate the potential negative impact of fast charging, adding an energy storage system (ESS) to buffer the instantaneous power draw from the grid is a promising solution that has been investigated for electric cars in the literature. In [48], ESSs are characterized into different categories, namely mechanical, electrochemical or electrical. ESS are devices that can store energy on various forms and restitute it as electricity.

Battery energy storage (BES) systems is one of the most popular types of ESS. It has the ability to reduce both the charging costs of BEBs and avoid large infrastructure modifications in the original grid system (including feeders and distribution transformers). In case of a grid failure, the ESS can offset the electricity supply challenge so that the buses can keep running as scheduled for a small period of time. In [49], a sizing optimization algorithm is proposed to install a BES for an electric bus fast charging station. In this paper the optimally sized BES is predicted to shave peak load reducing operating costs and decrease the investment cost by reducing the required capacity of the transformer and feeder. These results are obtained in the case of a time-of-use electricity pricing, thus more work is required to assess the feasibility of BES for different grid and electricity pricing systems such as the one used in British Colombia based on how much energy and power is consumed. Other

storage methods, such as flywheels, capacitors or ultra-capacitors are considered to be attractive technologies because of their durability and power density [50], though they are not yet widely available.

As battery electric buses are being deployed, a key step is to develop standards for both on-route and in-depot charging to be used by bus manufacturers around the world. Adopting standards at an early stage of development reduces infrastructure costs later on, as more BEBs are purchased. As shown in Table 1.3, different projects use different charging power and strategies. The on-going project "Pan-Ontario Electric Bus Demonstration and Integration Trial" in Canada facilitated by the Canadian Urban Transit Research and Innovation Consortium (CUTRIC) aims to gather several large bus and charger manufacturers to test and develop standards to be used throughout Canada to unify the industry and facilitate the large scale adoption of BEBs [51].

1.3 Literature Review of Modeling for E-bus Feasibility Studies

Feasibility analysis on battery electric bus fleets deployment in city networks has been investigated in several studies [52, 37, 53, 38, 27]. The energy consumption of the bus is used to predict the project operational costs and is influenced by the road topography, the battery weight, the weather and the load variation [53]. This section will discuss the state-of-art for modeling the energy consumption of electric buses.

1.3.1 Drivertrain modeling

The total energy consumed by an electric bus is the aggregate of three loads:

- the energy consumed by the traction system to propel the vehicle

- the energy required to heat the bus or to operate the air conditioning
- the energy consumed by the rest of the electrical system, such as lights or control systems [54]

In [53], the authors developed a discrete time-step energy consumption model using the sum of the kinetic, potential and rotational components involved in the vehicle propulsion. Losses due to air friction, curve and rolling resistance and external loads such as air conditioning are accounted for and balanced out in the vehicle energy equation to get the overall energy consumption. The energy used from the vehicle's battery or gained through regenerative braking can be found by scaling the energy consumption by a propulsion or a regeneration efficiency, respectively. One of the important assumption this model uses is a constant propulsion or regenerative efficiency throughout the driving cycle. This should be brought into question as these efficiencies varies depending on the torque and rotational speed, as shown in commercial electric motor efficiency maps.

A different backward approach is used in [52] to determine the energy consumption. Using a specific driving cycle for urban buses, the vehicle longitudinal dynamics are found as a function of velocity. The defined equations are time dependant. Aerodynamic, rolling and climbing resistance forces as well as accessory load forces are summed to get total force acting on the vehicle. The torque is calculated from the longitudinal dynamic equation. The electric motor map is then used to interpolate the rotational speed and get the instantaneous energy use or regeneration at a given motor efficiency. While this approach has shown reliable results for the test driving cycle it has used, it has failed to take into account that the motor rotational speed is directly linked to the wheel speed which can lead to inconsistencies.

More recently, in [41], the authors have attempted to calculate the energy consumption of a transit bus subjected to test driving cycles or real-life cycles. The power

drawn or supplied to the battery is calculated using a constant motor efficiency which as previously stated can lead to inaccuracies in the final results. Additionally, the power regained from regenerative braking is obtained by dividing the power at the wheel by the motor efficiency, when it fact it should be multiplied. The power drawn from the battery should be greater than the actual power at the wheel, on the other hand the power supplied to the battery should be smaller than the power at the wheel to account for losses. To the knowledge of the author, the previous research done on this field always uses assumptions that can negatively affect the results.

1.3.2 Input loads and component specifications

To achieve an accurate energy consumption simulation, it is crucial to properly generate a vehicle model containing the main aerodynamic properties and components' efficiencies. Researchers use published data from electric bus manufacturer, such as the Proterra FCBE 35 bus in [52] or the BYDs ebus-12 2015 series in [38].

Accurately modeling the auxiliary or accessory load is also important in the determination of energy use. Auxiliary power is defined as the power consumed by the heating, cooling and electric systems. This load can significantly contribute to increasing the energy consumption and it is sensitive to external temperature variations. The energy models described in [52] and [53] consider the power or force generated by the load as constant, without accounting for its variations depending on weather conditions. In [39], the auxiliary power is modelled by two constant values, 9 kW for an articulated bus on regular days and 21 kW on hot and cold days. These values are based on data collected during the H2-Bus-NRW project deploying electric hybrid 18m fuel cell buses in Germany.

The feasibility study in [37] focuses on examining the worst-case scenario for auxiliary load during a hot summer day where cooling is continuously used. The dynamic

behavior of the BEB auxiliaries with respect to the temperature have never been modelled for time-based energy consumption modeling of an electric bus. Implementing such feature can improve SOC calculations by making it more accurate.

In addition to the auxiliary load variation, the overall mass of the bus while in service is frequently changing due to the flow of passengers getting on and off which also impacts the energy consumption. Rogge et al. [37] calculated that for an 18m fully packed bus, the passenger mass represents 37.5% of the maximum gross vehicle weight. This study considers the worst-case scenario only. The authors in [55] accounted for a constant average load of 20 passengers, while other authors in [53] used data recorded with a passenger counting system to get an approximation of the bus mass at any point in time. Considering the weight of the bus in the worst case scenario is a good strategy to ensure the sizing of the battery can sustain this scenario. However, it is insufficient to optimize the charging strategy. Therefore, it would be interesting to implement a stochastic feature to model the buses' weight throughout the operating days.

The next important factor to consider in energy modeling is the driving cycle of the bus. A driving cycle is a representation of the speed of the vehicle over time. It greatly depends on the traffic, the road topography and the bus stops during the operation. In order to define a driving cycle, the bus route properties including the traveled distances and coordinates, the topography and the dwell time at each bus stop should be know. In [39], the authors first used an internet mapping service (Google Maps) and converted the route direction in global positioning systems (GPS) data. Another tool was then used to obtain the elevation data collected from the NASAs Shuttle Radar Topography Mission (SRTM) and the National Elevation Dataset (NED). The topography of a given route impacts not only the driving cycle but also the climbing resistance and the amount of energy gained by regenerative braking. In particular

cases, such as the ones depicted in [52] and [56], the route is considered flat and the energy model for the bus doesn't include route topography.

1.3.3 Field trials

Heavy-duty testing driving cycles are available for simulation and widely used by bus manufacturers. Testing driving cycles are constrained driving patterns developed to set standards for vehicles before they enter the market, in order to estimate their CO2 emission and overall energy consumption. In the case of electric vehicles, the vehicle range can be measured when tested under the conditions defined by the testing cycle. These testing cycles are useful to compare the energy consumed by an electric bus in real-life and the energy simulated. In Europe, the Dutch Urban Bus driving cycle and Braunschweig-cycle are widely used, while the Central Business District (CBD) or Manhattan Bus Cycle (MBC) are used in the USA [19]. The authors in [52] compared the simulated energy consumption of their system using the CBD driving cycle with the published energy consumption measured by Proterra when their bus performed the CBD cycle. A similar approach was used by Burmeister et al.in [38] to validate their model, using the Standardized on-road test cycles (SORT) developed by the international Association of Public Transport.

When a case study is implemented, such as in the Milton Keynes Demonstration Project described in [25], data such as the velocity and road altitude can be recorded, for certain days of the project, by the fleet operator. However in some cases data are not available and the actual driving cycles have to be modelled. Simulating an accurate driving cycle without measuring data for electric bus can be complex because it depends on many parameters. In [57], the authors developed an algorithm to generate arbitrary driving cycles based on the characteristics of the original cycle for buses. The arbitrary driving cycle has a similar speed distribution and power spectra

compared to the original pattern, and can be defined with a different duration. This modeling approach requires an accurate driving cycle to start with, which might be unavailable when modeling electric bus deployment before a real life implementation. The Institute of Transportation Systems at the German Aerospace Center has developed an open-source traffic simulation tool that only requires information relative to the route and chosen vehicle in order to simulate an accurate driving cycle [58]. This simulation package, called SUMO (Simulation of Urban Mobility) is a microscopic model in which each vehicle is individually simulated. Information relative to the road, such as its topography and GPS data, are inputs, as well as the main vehicle characteristics. The output of the simulation is the velocity of the targeted vehicles at any time. In [59], a 2D simplistic version of SUMO that does not take into account the height variations of the road was used to generate a realistic driving cycle for one plug-in hybrid vehicle designed at the university of Salento. A 3D add-on feature of SUMO was developed by Maia et al. [60] to incorporate topographic data as an input, which resulted in a more accurate driving cycle. Modeling the driving cycle is also possible by combining testing cycles to fit a specific road conditions as demonstrated in [52] where a combination of the MBC and City Suburban Cycle (CSC), representing suburban driving pattern, was used to simulate the a traffic pattern inside and on the periphery of the Ohio State University Campus.

In 2014, the Milton Keynes demonstration project in the UK successfully converted a diesel fleet operating route to electric buses [25]. The fleet is composed of eight buses in total. The chosen route is 24km long and operates 17 hours a day at a 15 minutes frequency. Inductive opportunity charging as well as in-depot charging were implemented to recharge the system, which increased the range of each vehicle.

To assess the performances of the project, the average energy consumption of each bus was estimated and compared with the actual energy consumption recorded dur-

ing the first five months of the project. The authors found from the recorded data that the energy consumption was affected by extreme weather conditions causing a variation in the auxiliary load. The driver's performance affects the energy consumption significantly. The average energy consumption for 46 drivers was recorded. The minimum and maximum average consumption per mile were 1 kWh/mile and 2 kWh/mile, respectively. Another factor that affected the energy consumption was the topography of the road which was responsible for 1-2% of energy use. Finally, the efficiency of the charging system was calculated by comparing the power drawn from the grid and the power at the battery pack terminals, which averaged 78%. Overall the Milton Keynes project analysis has shown that the actual performances of the buses are close to the ones initially predicted, and the project was deemed successful.

1.4 Modeling the Degradation Phenomenon in Lithium-Ion Battery Background Information

The lithium based family of batteries is the most popular technology for transportation applications due to its high energy and power densities, low weight and fast charging abilities. Other chemistries, namely lead acid or nickel metal hydride battery (NiMH), have been previously used for automotive applications. A qualitative comparison is shown in Table 1.4, while a graphical comparison is shown in Figure 1.1.

Within the lithium-ion based family, several postive electrode materials are currently commercialized [63, 64]:

- LCO Lithium Cobalt Oxide ($LiCoO_2$)
- LMO Lithium Manganese Oxide ($LiMn_2O_4$)

Table 1.4: Comparison of lead acid, NiMH and Li-Ion batteries [61]

Characteristics	Lead acid	NiMH	Li-Ion
Weight	Poor	Fair	Good
Volume	Poor	Good	Good
Capacity / Energy	Poor	Fair	Good
Discharge power	Good	Fair	Good
Cost	Good	Poor	Poor
Calendar life	Poor	Good	Fair

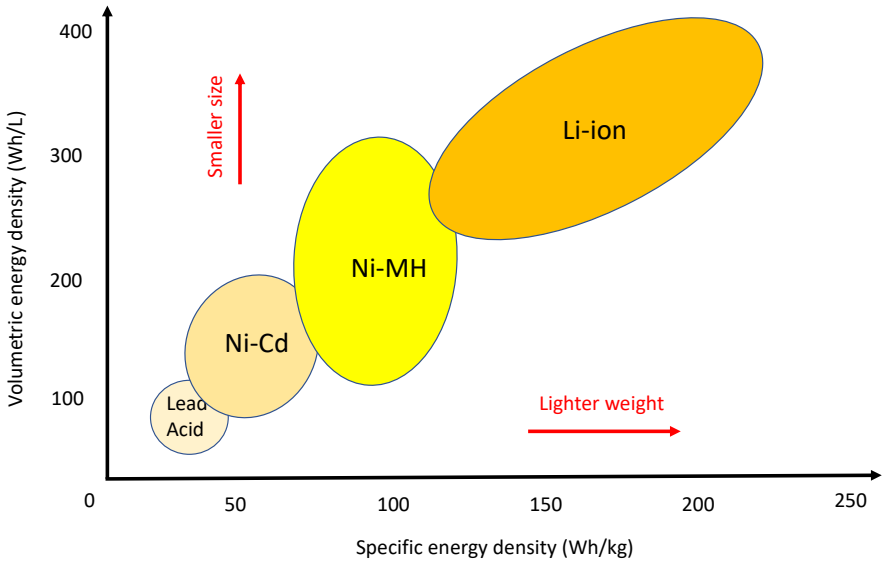

Figure 1.1: Energy density comparison of size and weight of the main types of battery chemistries in automotive applications, adapted from [62]

- NCA Lithium Nickel Cobalt Aluminium Oxide ($LiNiCoA_lO_2$)
- NMC (NCM) Lithium Nickel Cobalt Manganese Oxide ($LiNiCoMnO_2$)
- LFP Lithium Iron Phosphate ($LiFePO_4$)

Table 1.5 summarizes the different applications, advantages, output voltages and specific energies of each lithium-ion chemistries currently commercialised.

NMC and LFP chemistries are most commonly used in the EV industry, LFP being more safe and stable and NMC being more powerful. Current research focuses

Table 1.5: Comparison of batteries with different negative electrode materials within the lithium-ion family [65, 64]

Characteristics	**LCO**	**LMO**	**NCA**	**NMC**	**LFP**
Nominal Voltage (V)	3.6	3.7	3.6	3.6	3.2
Specific energy (Wh/kg)	150-200	100-150	200-260	150-220	90-120
Application	Small electronics	Power tools, electric powertrain	Medical devices, automotive power	EVs	EVs, ESS
Advantage	High specific energy, good cycle life	High power, inexpensive	Good energy and lifecycle	High power, capacity and lifecycle	Very high life time, very safe
Disadvantages	Limited power	Limited life cycle	High charge can cause thermal runaway	Patent issues	Low energy

on trying to increase the specific capacity and lifetime of lithium-ion batteries by testing new positive electrode materials that allow high coulombic efficiency and good power capability [64]. One key research aspect is decreasing the risk of short-circuits by improving the separator technology, thus improving the safety of the battery [66].

Some of the main limitations of Li-Ion batteries are that their capacities and power outputs decay with time [67]. Much research has been undertaken to push the boundaries of the current lithium-ion cell limitations, especially by investigating new positive electrode materials [68]. Currently, sulfur is an attractive material because of its high theoretical capacity [68] and its cheap price [69]. However, Lithium Sulfur battery suffer from high electrical resistance, capacity fading and self-discharge, therefore more research is required to improve their overall performance [69]. Additionally, recent years have seen a rise in interest for lithium-air batteries, which also have a remarkably high theoretical capacity compared to what is being sold in the market currently. However, the biggest challenge preventing its adoption for electric vehicle applications is its limitations on the charge and discharge currents [70].

Though the future may hold breakthroughs and discoveries on new battery materials, current lithium-ion chemistries will be prevalent in the near term. This section will provide a literature review on the research done to capture the performance and the effect of degradation on lithium-ion cells.

1.4.1 Lithium-ion battery fundamentals

A battery is a device that converts electric energy into chemical energy during the charge, and the opposite occurs during discharge. The basic components of the battery are cells. Cells are connected in series and/or in parallel and assembled in a mechanical enclosure to form a module. The battery pack itself is assembled by connecting multiple modules in series or parallel to achieve the desired power capac-

ity. When assembling lithium ion cells, safety is one of the most important concerns since the battery can be subjected to extreme operating conditions such as over-charge/over-discharge, heating or crush which can cause the electrolyte to leak, which itself can lead to smoke, fire or even explosion [71].

Most cells in the automotive industry are either prismatic (left in Figure 1.2 and Figure 1.3)) or cylindrical (right in Figure 1.2 and Figure 1.3).

Figure 1.2: A prismatic and two cylindrical cells [72]

Each cell has two electrodes (a negative and a positive), separators, two terminals (a negative and a positive), an electrolyte that can be a liquid, a gel or a solid material and an enclosure [74]. In lithium-ion batteries, the negative electrodes are composed of graphite, carbon, titanate or silicone [75] while there is a wide array of active material at the positive electrodes.

Two main processes govern the cell dynamics during operation. In the discharge mode, ions contained in the cell migrate from the negative electrode through the electrolyte towards the positive electrode, causing a difference in potential (or voltage).

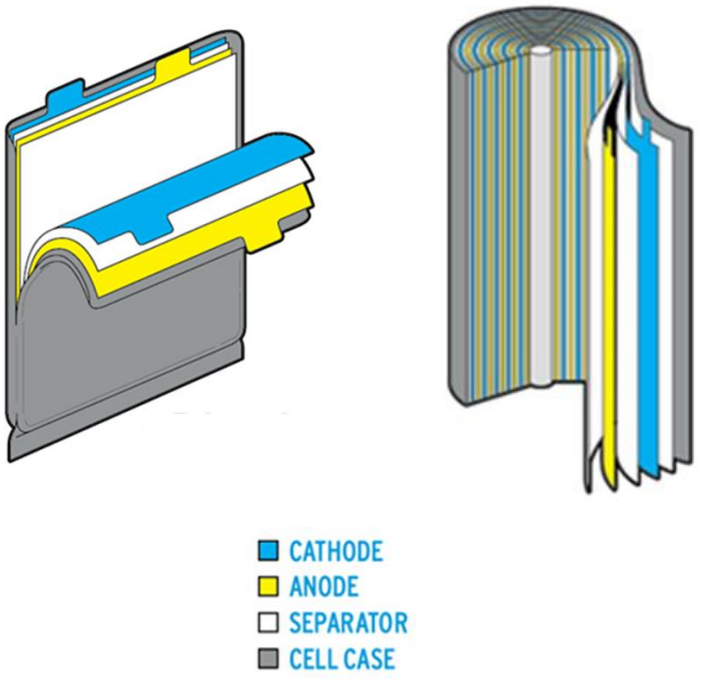

Figure 1.3: A cutaway vierw of a prismatic and a cylindrical cell [73]

This difference generates an electron flow which creates electricity that is collected by the current collector at the terminals to power a load. The general discharge chemical reaction for a lithium-ion battery is shown below.

$$Li_xC \rightarrow C + xLi^+ + xe^- \tag{1.1}$$

In the charge mode, the reverse reaction occurs where electricity is used to push the ions towards the least attractive electrode (negative electrode).

Figure 1.4 shows a schematic of the charging process in a battery. The performance and characteristics of a battery are described as follow [76]:

- the battery capacity, expressed in amp-hour, represents the quantity of electrons

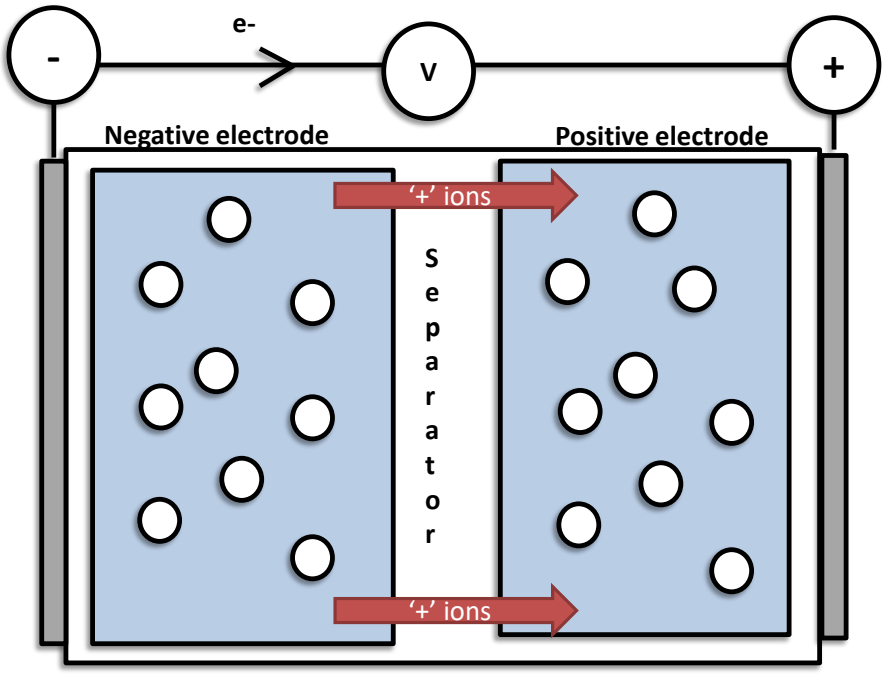

Figure 1.4: Discharge process in a battery

that move between cell terminals

- the cell nominal voltage, expressed in Volts, characterizes the ions inclination to migrate from their elevated energy state to their discharge state in the second electrolyte
- the energy density, in Wh/L, is the nominal battery energy per unit volume
- the state-of-charge (SOC), expressed as a percentage of the total remaining battery capacity. It is defined as $SOC(t) = cap(t)/cap_{max}$ where $cap(t)$ is the current battery capacity at a given time t in kWh or amp-hour and cap_max is the initial capacity of the battery in kWh or amp-hour

When designing the battery module, the basic layout can either use fewer large

cells or many small cells [71]. Some of the main advantages of the "many small cells" design configuration includes improved safety and a higher quality production while the advantages of the "fewer large cells" configuration are lower assembly costs, better reliability since the number of component is reduced, and better volume efficiency. Both configurations have different disadvantages, the final design choice is should be a trade-off.

1.4.2 Available modelling methods for characterizing battery degradation in electric vehicle

Modeling the lithium-ion cell performance can be done through different approaches listed below.

1. Physics-based / electrochemical models intend to simulate the physical and chemical phenomena occurring in the cell during its utilization or storage. These models can be very complex because they capture the transport phenomena and electrochemical kinetics at a small scale [77]. Because of their high computation time, they are not suitable for system level design exercises [78].

2. Equivalent circuit based models, which are tools that capture the major electrical and thermal properties of the battery while avoiding detailed calculations of internal electrochemical processes. These models use battery parameters that can be identified from measurements [79].

3. Performance based model use empirical equations to model battery ageing. Ageing tests are conducted on battery cells under several conditions, from which the correlations between stress factors and capacity fade and impedance raise can be identified. The impact of the ageing factors can be obtained, as well as a descriptive expression of the battery performance level over its lifetime [75].

4. Analytical model with empirical data fitting is a fourth type of modelling method available. The battery lifetime is predicted by means of extrapolation from test results and field data. Four methods are commonly used in this type of model:

    - the coulomb counting method: estimates the battery state-of-health (SOH) by a simple integration of current over time [80]
    - the fuzzy logic approach: computing method based on "degrees of truth" rather than the usual "true or false" (1 or 0) Boolean logic, based on the assumption that the ageing is a steady stochastic process and focuses on mining the relationship between external excitation and object response rather than the degradation mechanism [81]
    - the state observation method: estimates the SOC, SOH and state-of-life (SOL) using a Particle Filter (PF) framework [82]
    - the Artificial Neural Networks (ANN) or Neural Networks (NN) [83] method: learning from input and output data by altering internal relationships between them to predict the capacity, resistance, or SOH

For the purpose of our research, each modelling method was carefully reviewed and compared to choose an optimum approach that would fit project constraints. These constraints were mostly related to the available testing material on site and available battery chemistries to be tested. The SSDL and ESTP laboratories have fast computers, but there is no experimental setup available at the time to test cell ageing. The electrochemical modeling approach was chosen because it provides a more fundamental approach that requires very little experimental data compared to any other method, and is the most accurate model that exists in the literature.

1.4.3 Electrochemical degradation models

Two types of electrochemical models are described in the literature: the pseudo-2D model (P2D) and the single-particle model (SPM).

Pseudo-2D model

The P2D model is generic and can be applied to most battery chemistries. One of the oldest pseudo 2D-model was developed in 1993 by Doyle [84]. This model was able to predict the galvanostatic charge and discharge of a lithium negative electrode/solid polymer separator cell. Many improvements have been made to this generic model since. In [85], a first principles capacity fade model was developed based on a continuous occurrence of a very slow solvent diffusion near the surface of the negative electrode. In this model, the molar flux equation at the negative electrode is split into two components: one for the intercalation reaction and another for the side reaction that forms a film on the carbon particles leading to the capacity fade, called the solid electrolyte interface (SEI). The derived coupled nonlinear partial differential equations (PDEs) were solved simultaneously. Other authors such as Pinson and Bazant [86] and Safari and Delacourt [87] have developed models that can predict battery degradation under cycling conditions. A consensus is yet to be reached on which approach is the most accurate for specific operating conditions [88].

The pseudo 2D physics-based model is the most widely used by battery researchers because it can solve for the electrolyte concentration, electrolyte potential, solid-state potential, and solid state concentration within the porous electrodes, along with the electrolyte concentration and electrolyte potential within the separator [89].

Figure 1.5 shows the schematic of a pseudo-2D model in which the active material particles are represented spherically, and the solid lithium concentration varies as a function of time, the x-direction and the radial coordinate. The main advantage of

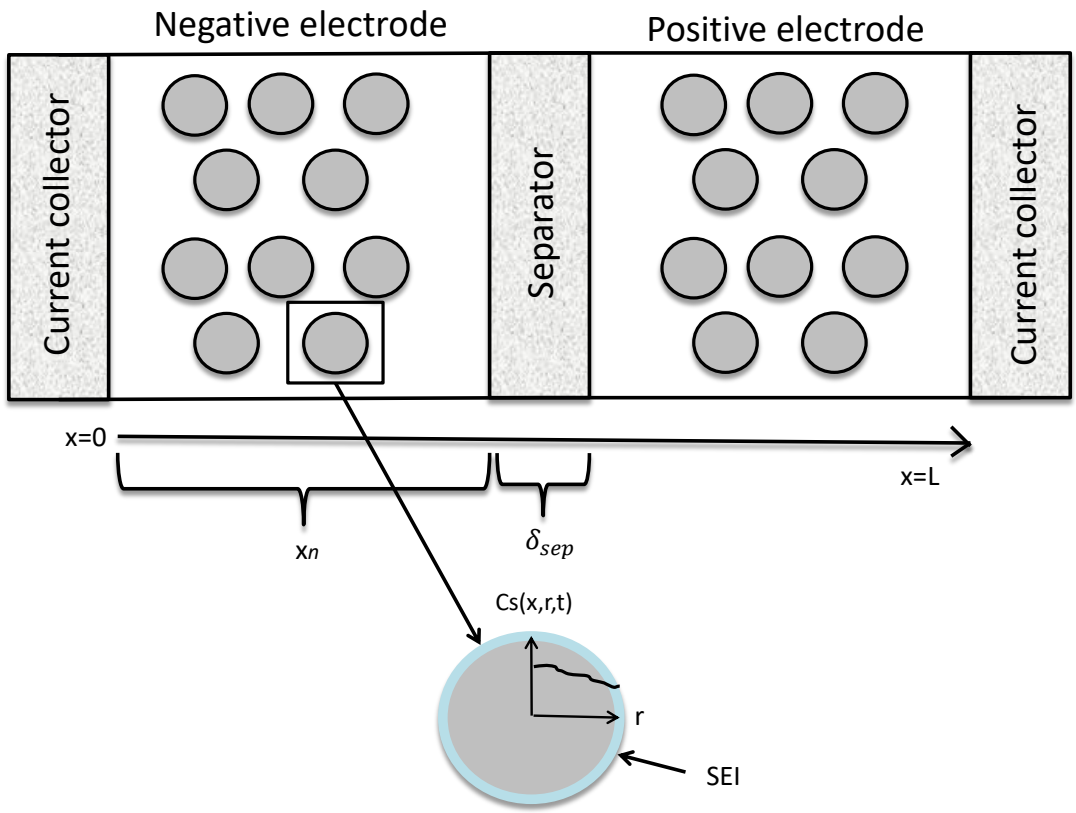

Figure 1.5: Schematic of a pseudo-2D electrochemical model

this method is its high predictive capability because it can capture the main physio-chemical phenomena occuring in a battery in a detailed and accurate way. However, its computational cost is higher than the single particle model (SPM) discussed next.

Single particle model

The single particle model (SPM) is an approach that incorporates the effects of transport phenomena in a simplified manner. Each electrode is represented by a single spherical particle whose area is equivalent to that of the active area of the solid phase in the porous electrode [90] as shown in Figure 1.6.

The particularity of this method compared to the pseudo-2D model is that the diffusion and potential effects in the solution phase are neglected. Zhang et al. in

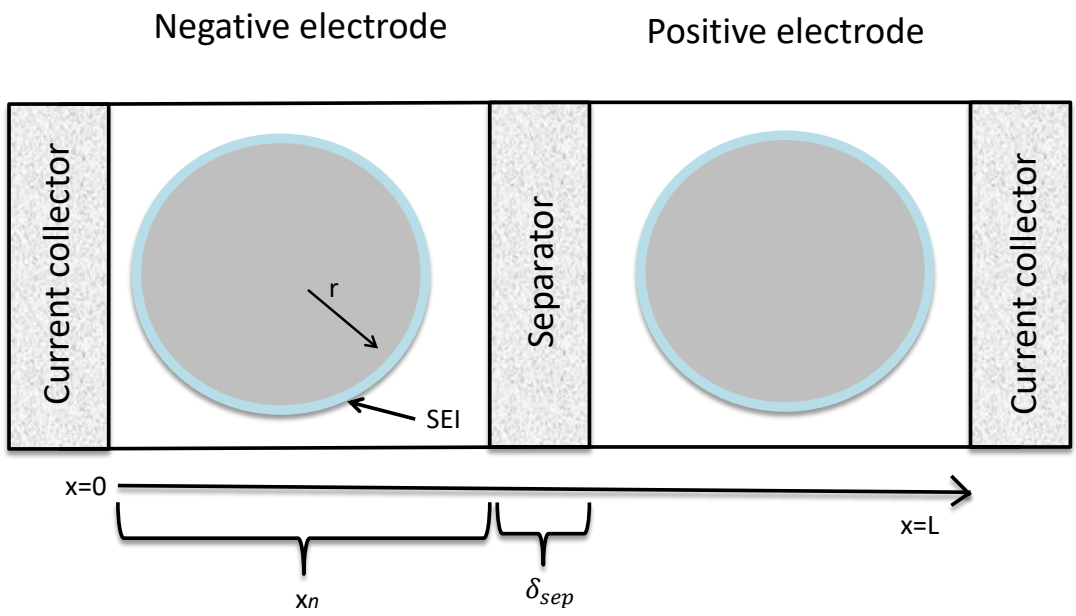

Figure 1.6: Schematic of a single particle model

[91] used a SPM approach to model the lithium intercalation phenomena in a battery. In this model, the concentration of lithium in the solution phase is assumed to be constant which is a valid assumption for low charge/discharge rates [92]. One of the main advantage of this approach is that it can be extended to include other physical phenomena in the cell. For example, Guo et al. [93] applied an energy balance equation to find the thermal behaviour of the cell. The developed model neglected the spatial temperature distribution in the the cell so that the temperature was a function of time only. It should be noted, though, that in an automotive battery configuration the cells are subjected to different temperature boundary conditions and it is not accurate to assume that the temperature is constant throughout the cell. Because of these simplifications, this model allows fast computations but is only

valid for a certain range of operating conditions and set-up (low charge/discharge rates and thin electrodes). In [94], Safari et al. developed an isothermal model for the electrochemical behaviour of a commercial graphite/LiFePO (LFP) at 25^{o}C and 45^{o}C using a non-intrusive analysis based on the electrochemical measurements carried out on commercial cells. In recent years much attention has been paid to lithium iron phosphate (LFP) batteries because of their high thermal stability and energy density. LFP has a poor intrinsic electronic conductivity [39]. A way to overcome this resistivity is to mix the resistive active material with a conductive additive such as carbon.

In [95], Ning et al. have developed a generalized charge-discharge model based on the loss of the active lithium-ions due to electrochemical solvent reduction reaction at negative electrode/electrolyte interface. This model can be applied to charge rates of less than 1C operating between 0^{o}C up to 30^{o}C. This is because simultaneous transport equations in both solid phase and electrolyte phase are solved. The results from this model show good correlations with experimental results, since the relative error in the discharge capacity was found to be less than 2% after 1968 cycles.

The aforementioned SPM model [95] is used in the research work carried out and presented in the following sections. The choice justification on the model to be used are described in section 2.2.2.

1.5 Scope and Contributions

The scope of this thesis is to develop a set of tools that support the deployment of battery electric buses by attempting to answer the following three key questions:

- What are the operational costs and GHG emissions associated with the deployment of BEBs for a given set of selected transit routes?

- What are the available methods that can be used to predict battery degradation associated with a specific battery usage?
- When does the battery need to be replaced on a BEB if it is deployed on a selected transit route?

The research contributions outlined in this thesis are listed below:

1. Developed a drivetrain energy consumption model that assesses the charging cost and GHG emission reduction potential of an electric bus throughout a year for any specified jurisdiction, as overall cost and benefits and varies greatly depending on the jurisdiction
2. Conducted a sensitivity analysis of the energy consumption model for BEB input parameters
3. Coupled an existing SPM model with a degradation model to estimate battery lifetime
4. Applied the battery CFM to battery electric buses driving cycle

1.6 Thesis Overview

This thesis is structured as follow:

- chapter 2 describes the energy consumption model (ECONS-M) and capacity fade model (CFM), how they are coupled together and the model limitations
- chapter 3 presents the case studies and applications of the models
- chapter 4 describes the conclusion and future work including several areas to focus on to improve the CFM

Chapter 2

Model development

This chapter describes the theory and implementation of the electricity consumption model (ECONS-M), followed by the battery capacity fade model (CFM). The final section describes how the two models are coupled.

2.1 Electricity consumption model (ECONS-M) development for an electric bus

This section describes the theory and implementation of the simulation tool developed to assess the energy consumption of a battery electric bus for a given route. This model is referred to as "ECONS-M" (energy consumption model) throughout the thesis report. Using a backward approach, previously defined in section 1.3.1, the model calculates the vehicle longitudinal dynamics as a function of the driving cycle velocity and grade profile. The main output of this tool is an energy consumption profile. There are multiple applications possible for the model, which are shown in Figure 2.1. The main focus of this thesis is to describe the coupling between the energy consumption model and the capacity fade model (CFM) to estimate the

battery degradation associated with a given driving cycle.

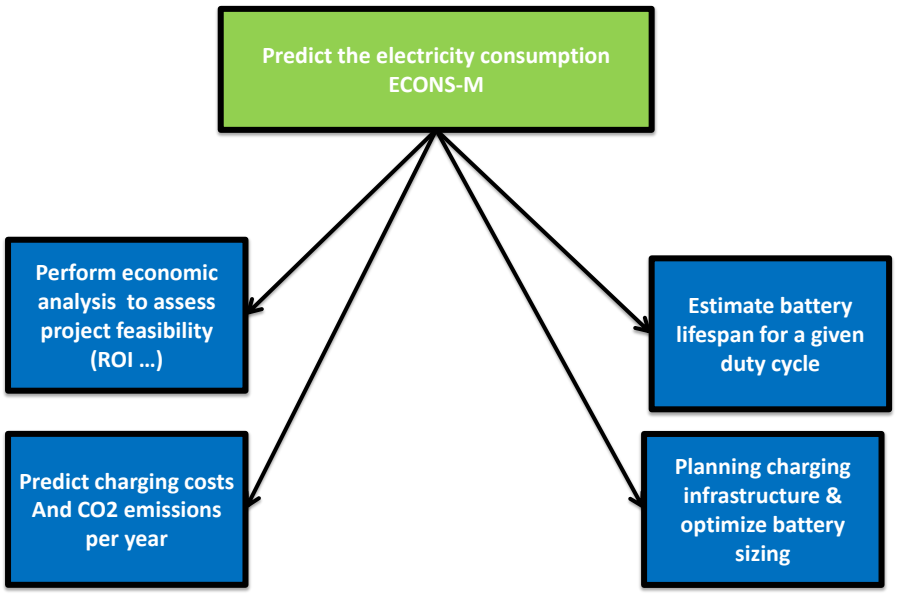

Figure 2.1: ECONS-M: multiple relevant applications

2.1.1 Theoretical Model

For the case of a vehicle in motion, the tractive force can be obtained using a simple 2D application of Newton's second law to describe translational and rotational systems. The most significant forces acting on the vehicle are part of the translational system. Newton's second law is given in equation 2.1; in this case the 2D version is applicable to vehicles going up/down a grade.

$$M \times \vec{a} = \sum \vec{F} \tag{2.1}$$

In this model, the effect of angular moments created by rotating drivetrain components is captured by adding an equivalent mass M_{eq} to the vehicle mass in equation

2.1. This equivalent mass is estimated to be 10% of the vehicle weight [52] for buses.

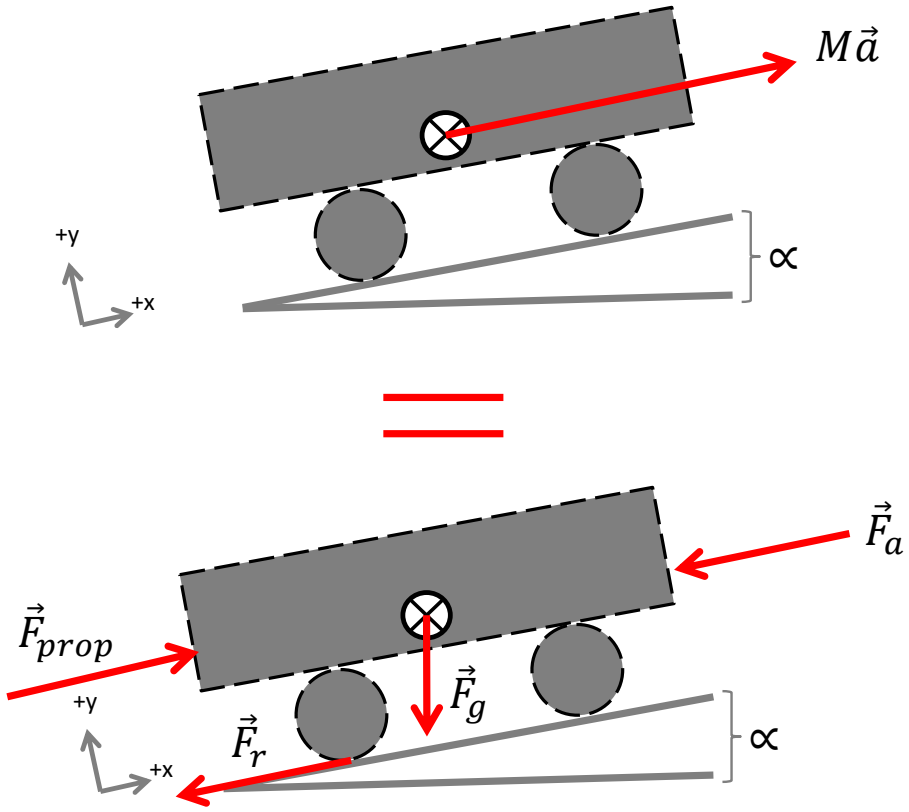

Figure 2.2: Free body diagram of a bus in motion

Figure 2.2 shows a free body diagram of a vehicle in motion. The top and bottom rigid bodies represented are equivalent, according to Newton's second law. The main forces acting on the body are the grade force F_g, the rolling resistance force F_r and the aerodynamic force F_a. F_{prop} represents the force supplied by the motor to propel the vehicle forward by overcoming the external resistive forces. F_{prop} is the unknown in this analysis. Equation 2.1 can be rewritten as:

$$(M + M_{equ}) \times a(t) = F_{prop}(t) - F_{tot}(t) \tag{2.2}$$

F_{tot} is the sum of the external forces acting on the vehicle. The grade force,

aerodynamic force and rolling resistance forces are defined in equations 2.3, 2.4 and 2.5 respectively.

$$F_g(t) = (M + M_{eq}) \times g \times cos(\alpha) \tag{2.3}$$

$$F_a(t) = \frac{1}{2} \times \rho \times A \times C_D \times V(t)^2 \tag{2.4}$$

$$F_r(t) = Cr(V(t)) \times (M + M_{eq}) \times g \times sin(\alpha) \tag{2.5}$$

In these equations, α is the road slope, expressed in degrees. In equation 2.3 and g is the standard gravity constant. In equation 2.4, the air density is represented by ρ, the frontal area of the vehicle is A, the drag coefficient is C_D and the speed is V. Finally, in equation 2.5, C_r is the rolling resistance coefficient, which depends on the vehicle speed and tires conditions. For this study, the rolling coefficient expression used is shown in equation 2.6 [96].

$$C_r(V(t)) = 0.006 + 4.5 \times 10^{-7} \times V(t)^2 \tag{2.6}$$

Once $F_{prop}(t)$ is determined from equation 2.2, the torque at the wheel $T_W(t)$ is found using this relation:

$$T_W(t) = F_{prop}(t) \times R_w \tag{2.7}$$

where R_W is the radius of the wheel. The electric motor torque $T_M(t)$ can be related to the wheel torque using the following relationship:

$$T_M(t) = \frac{T_W(t)}{GR \times \eta_T} \tag{2.8}$$

where GR is the constant gear ratio of the bus and η_T is the constant transmission efficiency.

Additionally, the rotational speed $\omega_M(t)$ of the wheels is found the following relationship:

$$\omega_W(t) = \frac{V(t)}{R_W} \tag{2.9}$$

and related it to the motor rotational speed $\omega_M(t)$ using this equation:

$$\omega_M(t) = \omega_W(t) \times GR \tag{2.10}$$

Once the motor efficiency η_M is obtained from an efficiency map, the instantaneous power consumption of the bus can be calculated using the relation:

$$P_{inst}(t) = P_{cons}(t) = \frac{T_M(t) \times \omega_M(t)}{\eta_M \times \eta_{conv}} + \frac{P_{auxi}}{\eta_{conv}} \tag{2.11}$$

where η_{conv} is the converter efficiency and P_{auxi} is the accessory load. When the bus brakes, the motor becomes a generator. This phenomenon is referred to as regenerative braking and allows the partial recovery of the kinetic energy to recharge the batteries. In case of regeneration, the instantaneous power is:

$$P_{elec,batttery} = T_{M,reg}(t) \times \omega_M(t) \times \eta_{M,reg} \times \eta_{conv} + \frac{P_{auxi}}{\eta_{conv}} \tag{2.12}$$

In equation 2.12, $T_{M,reg}$ is the motor torque calculated when the bus uses regenerative braking. It is calculated using the following equations:

$$(M + M_{equ}) \times a(t) = F_{brake}(t) - F_{tot}(t) \tag{2.13}$$

$$F_{reg} = S \times F_{brake} \tag{2.14}$$

where F_{brake} is the braking force of the bus and S is the power split ratio between the friction brakes and the regenerative brakes. In this model, it is assumed that the

brake split between friction and regeneration is 60-to-40, respectively. This number was obtained after discussions with manufacturers. $T_{M,reg}$ is then found using the same approach as described in equations 2.7 and 2.8.

The energy consumption of the bus is simply the integral of the instantaneous power over time:

$$E_{total} = \int_0^{t_{end}} P_{inst}(t)dt \tag{2.15}$$

The main scope of the ECONS-M tool is to determine the total energy drawn from or supplied to the battery to power the bus over given driving conditions. The approach described in this analysis is a systems approach, for which the main drivetrain components are represented by efficiencies that can be set constant or vary according to various parameters (such as the torque, the speed, etc...). The system used to model the electric bus energy consumption is shown in Figure 2.3.

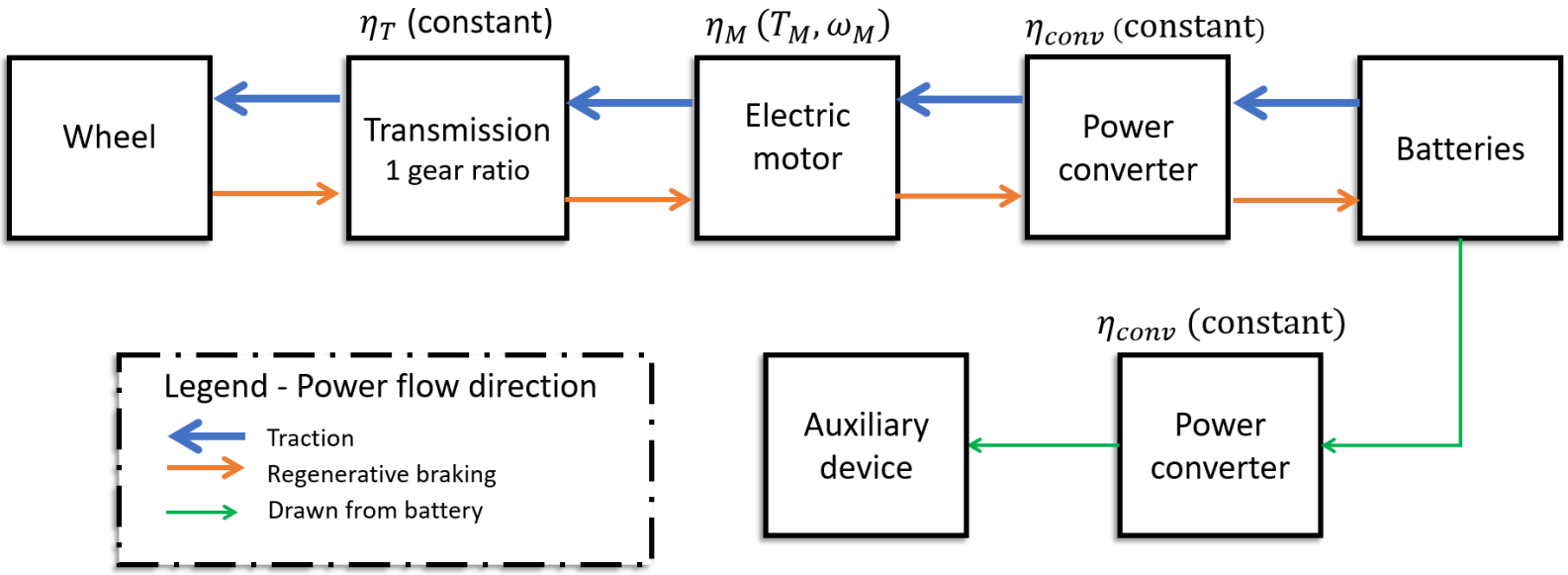

Figure 2.3: ECONS-M's system components

Once the instantaneous energy consumption has been determined, the state-of-charge at each instant t of the battery, assuming an ideal battery, were found using

the following relationship:

$$SOC(t) = SOC(t-1) - \frac{E_{inst}(t)}{cap} \tag{2.16}$$

where $E_{inst}(t)$ is the instantaneous energy used or recovered calculated from the instantaneous power defined in equation 2.11. *cap* is the battery capacity in kWh. In these simulations, the initial SOC is assumed to be 90%. It should be noted that the SOC of the battery pack is expressed as a percentage of the total remaining battery capacity. That is, 100% state-of-charge means that the battery charge level is full, while 0% SOC means that the battery charge level is empty. In real-time in a vehicle, the SOC is often calculated by measuring the current and voltage of the battery to assess how many kWh are used. It should be noted that the electrochemical SOC is different from the battery SOC. Indeed, the electrochemical SOC is a ratio of the remaining lithium concentration ($C_s(t)$ in mol/m^3) over the maximum lithium concentration ($C_{s,max}$ in mol/m^3) in both electrode. It is expressed as $SOC_{electrode}(t) = \theta_{n,p}(t) = C_s(t)/C_{s,max}$.

Finally, charging time and the charging energy for each route was calculated using equations 2.17 and 2.18, respectively. P_{charge} is the charging power of the charger, η_{charge} is the charger efficiency and η_{BMS} is the battery management system efficiency:

$$t_{charge} = \frac{(SOC_i - SOC_f) \times cap}{P_{charge} \times \eta_{charge} \times \eta_{BMS}} \tag{2.17}$$

$$E_{charge,grid} = t_{charge} \times P_{charge} \tag{2.18}$$

The final step of the ECONS-M analysis is to obtain the battery C-rate to be coupled with the degradation model. The C-rate of a battery describes the rate at which a battery is charged or discharged relative to its maximum capacity [76]; 1C

denotes full energy discharge in 1 hour.

To find the battery C-rate, the current flowing from or to the battery is related to the cell terminal voltage using equation 2.19 [97]:

$$V_{term}(t) = V_{OCP}(SOC(t)) - R(SOC(t)) \times I(t) \tag{2.19}$$

where $I(t)$ is the battery current in amps, V_{term} is the potential between the cell terminals in V, V_{OCP} is the open-circuit potential in V and R is the internal battery resistance in Ohm. The open-circuit potential is the voltage in the battery and depends on the instantaneous SOC. The relation between the battery voltage and the SOC is experimentally characterized and varies depending on the battery chemistry and initial capacity.

Additionally, the instantaneous power at the battery can be related to the current and terminal voltage with the following equation:

$$P_{elec,batttery}(t) = V_{term}(t) \times I(t) \tag{2.20}$$

Lastly, once the current has been identified, the C-rate of the battery can be found according to the following equation:

$$C_{rate}(t) = \frac{I(t)}{cap} \tag{2.21}$$

Where *cap* is the battery overall capacity, in Ah.

It should be noted that the main physical equations of this model can be used to assess the diesel consumption of diesel buses, however this was out of the scope of this thesis. It should be noted that ADVISOR can be used in this regard as well, but the data available are out-of-date (2005). Additionally, other tools modeling the power consumption of vehicles such as Autonomie or PSAT can be expensive and require

many input data that can be somewhat challenging to get. Additionally, the solving algorithm and equations used to solve each module are proprietary.

2.1.2 Model Validation

It is challenging to reliably validate the ECONS-M as the technology is relatively new and manufacturers tend to keep information confidential regarding their powertrain performances.

One of the rare source of available information regarding the energy consumption of BEBs is published by the Altoona Bus Research and Testing Center. This research center is based in Penn State University and its goal is to ensure better reliability and performances for buses by providing unbiased comparison of bus models through various test procedures. Many diesel, hybrid and battery electric bus manufacturers participate in this test program and it has become a standard in the industry. These tests focus on the following characteristics:

- maintainability
- reliability
- safety
- acceleration and braking performance
- noise and structural integrity
- fuel economy

In this thesis, the characteristics of a BYD K9 are used to populate the model. This type of electric bus is one of the most widely deployed to this date [98].

The aforementionned Altoona tests were performed on a BYD K9 (model 2013) in June 2014 and results were reported in [99]. The vehicle data form in this report provides the reader with the parameters shown in Table 2.1.

Table 2.1: BYD K9 (2013) characteristics

Parameter	**Value**	**Unit**	**Source**
Curb weight	31,890 - 14,465	lbs - kg	[99]
Seated load weight (curb weight plus 150 lb for every designed passenger seating position and for the driver)	37,290 - 16,914	lbs - kg	[99]
Width	101.5 - 2.57	in - m	[99]
Height	133.0 - 3.38	in - m	[99]
Maximum seated passengers	36	-	[99]
Maximum standing passengers	13	-	[99]
Charger power	80	kW	[100]
Maximum motor torque	700	Nm	[100]
Maximum motor power	180	kW	[100]
Motor maximum revolutions per minute	7500	RPM	[100]

The fuel economy test is a fuel consumption test that is performed for a standard driving cycle called advance design bus (ADB) cycle. ADB cycle is a combination of three driving cycles. First, the Central Business District (CBD) cycle is performed, followed by the arterial (ART) driving cycle. This pattern is repeated, followed by a third CBD cycle and a final commuter cycle to reach the starting point again. The ADB cycle is repeated until the bus battery are depleted, e.g when the state-of-charge (SOC) of the batteries is below 5%.

In the case of the BYD K9, the test is repeated 10 times. The overall test corresponds to a distance of 3.22 km, with an average speed of 20.23 km/h and an average acceleration of 0.89 m/s^2. The CBD cycle, shown in Figure 2.4, is the only driving cycle part of the ADB that is publicly available.

The test is performed with a fully seated passenger load, and the HVAC system switched off. However, other auxilliaries related to the control of the bus represent

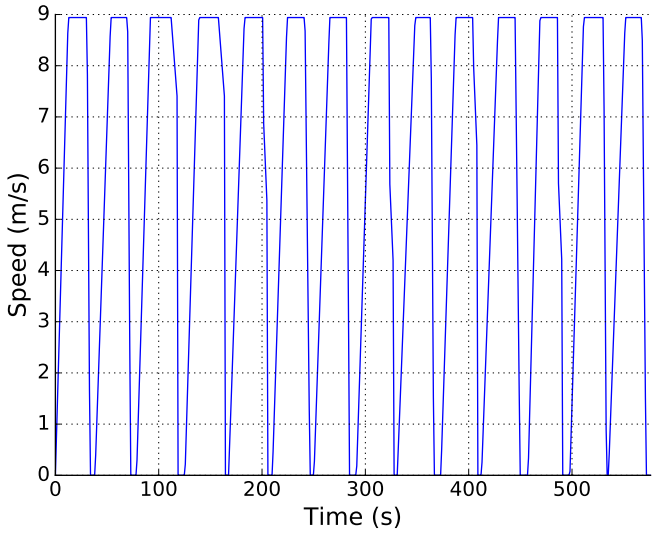

Figure 2.4: Central Business District (CBD) driving cycle (SAE standard J1376)

a load, therefore an additional load of 2.5 kW was assumed as a base load [101]. During the test, a power meter was connected to the bus battery to measure the SOC, current and energy consumption in kWh at any point in time. The SOC and energy consumed after every single drive phase of the cycle are reported. The average energy consumption for the 29 CBD cycles is 1.18 kWh/km. An histogram showing the distribution of the energy consumption for each run performed is shown in Figure 2.5. The vertical red dotted line represents the average of 1.18 kWh/km.

It can be seen that under the same driving conditions, the range of energy consumption varies between 0.72 and 1.56 kWh/km. Table A.1 in Appendix A shows the input parameters used in the ECON-M to reproduce Altoona's test results. Using these input, a result of 1.17 kWh/km was found, which is a 0.8% difference compared to the average energy consumption calculated in Altoona's tests. This comparison allows to assess the accuracy of the model to an error below 5%.

A graphical-user interface (GUI) in Python was developed to easily run the model. A screenshot of this GUI with the parameters used to reproduce Altoona's data for the CBD driving cycle is shown in Figure 2.6.

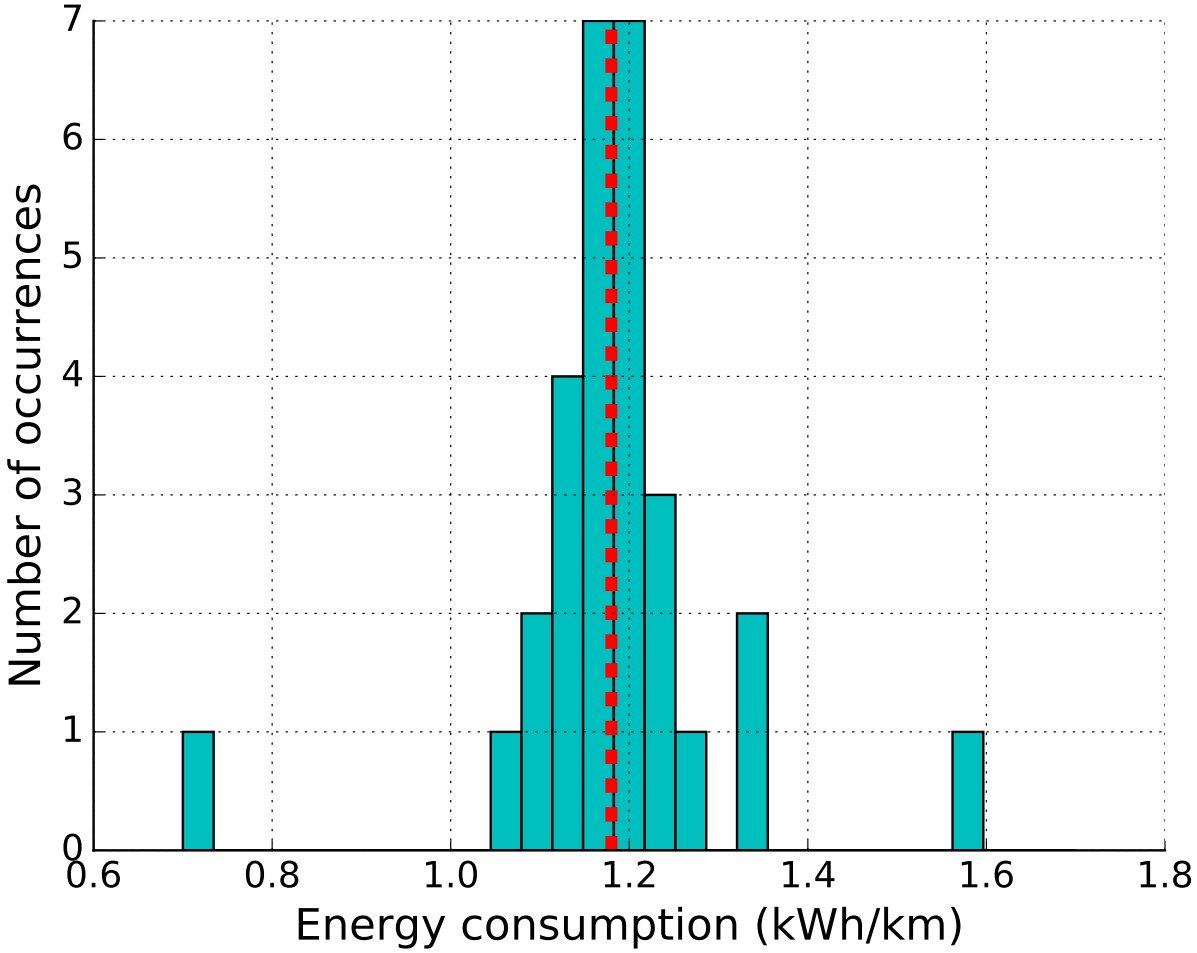

Figure 2.5: Altoona fuel economy test results for a BYD K9 (2013) for each CBD cycle

2.2 Capacity Fade Model Development and Applications

2.2.1 Background on the Degradation Mechanisms in a Lithium-Ion Cell

In a battery, the storage capacity decreases and its internal resistance increases throughout its lifetime reducing the amount of energy available to propel the vehicle [102]. Battery degradation is a complex process because it depends on many

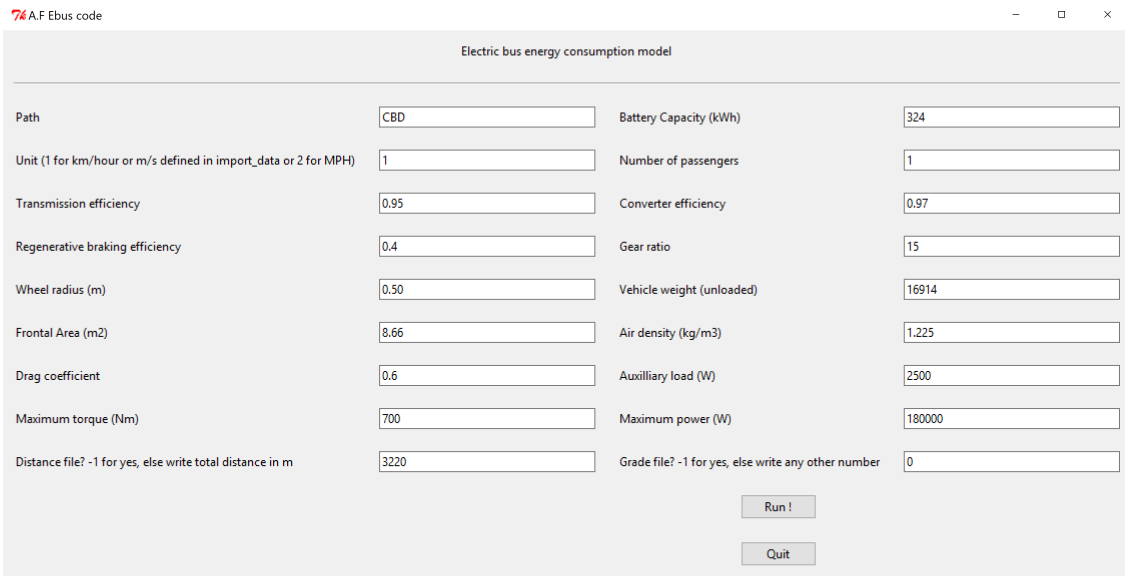

Figure 2.6: GUI developed to run the ECONS-M

factors, including environmental conditions and utilization mode which can be challenging to model. This section describes the main mechanisms that cause battery degradation and the factors that influence it.

Degradation Phenomena in the Negative Electrode

Most negative electrodes in lithium-ion batteries are made of carbon, especially in the form of graphite. Changes occurring at the interface of the negative electrode and the electrolyte are considered to be the major cause of ageing in lithium ion cells [67].

Over time, an accumulation of solid lithium conductive particles agglomerate to form a solid layer at the electrolyte/electrode interface, referred to as the solid electrolyte interphase (SEI). The formation of SEI is triggered by side (or parasidic) reactions occurring in the cell. Depending on the material used in the lithium-ion cell, the SEI can be composed of different coumponds. The commonality between all side reactions forming the SEI for all lithium-ion chemistries is that lithium ions are

consumed to produce a lithium based solid [83]. This solid interphase is naturally created during the first charge of the cell [75]. The SEI forms a permeable layer that allows ions to go through it while blocking electrons or the solvent.

However, the irreversible creation of the SEI decreases the overall number of lithium ions that can cycle through the cell during charging and discharging. The creation of this passivation layer also causes a change in the capacity balance of the cell. The capacity balance is the optimized mass ratio of positive to negative electrode materials to achieve a maximum capacity under steady cycling conditions [103]. It depends on the amount of lithium available for cycling. If this amount is modified, the output energy that the cell can produce will be decreased. Additionally, the presence of the SEI results in an increase in electrode resistance because of the decrease in active surface and cell polarisation [104].

The solvent can interact with the graphite at the negative electrode and corrode it, creating graphite exfoliation which generates gases that can lead to cracks in the SEI structure allowing for its expansion in the cell [75]. This phenomenon mainly occurs during storage and when the cell is subjected to a high voltage.

A high state-of-charge causes a large potential difference between the electrodes, which can accelerate the formation of the SEI. High temperatures can cause the SEI film to break down or to dissolve. This effect frees lithium salts in the solvent causing an increase in the negative electrode effective resistance.

The last identified phenomenon likely to occur at the negative electrode is lithium plating at low temperature. This can lead to a slow lithium ion diffusion into the electrolyte. Under normal operating conditions, lithium ions intercalate into or de-intercalate from the active materials reversibly between the electrodes. Under abnormal operating condition, such as high charge rates or at low charge temperature, lithium ions can be reduced to metallic lithium and deposit as an interphase, forming

a lithium plating [105]. Side reactions from the lithium metal plating accelerate the ageing phenomena.

Ageing mechanism at the positive electrode

The positive electrode degradation is mainly associated with physical degradation of its materials [83], but positive electrode degradation is not the primary cause for degradation in a cell. The chemical reaction occurring at the cathode, or positive electrode, involves the insertion (or extraction) of lithium ions in (or from) metal oxide. This leads to changes in the molar volume of the material which can cause mechanical stresses to the oxide particles and the electrode.

Additionally, the reaction might induce a phase change which will distort the crystal lattice and induce further stresses [106]. This will induce structural changes during cycling, chemical decomposition/dissolution reactions and surface modification [67]. The main consequences of these phenomenon are an impedance increase as well as a capacity fading, causing the positive electrode to age. It should be noted that the degradation of the cathode mostly depends on the SOC and cycling conditions.

Calendar and cycling ageing of batteries

Ageing of a battery can be differentiated in two groups: calendar and cycle ageing.

Calendar ageing is the irreversible loss in capacity due to battery storage whether or not the battery has been charged and discharged. Batteries tend to self-discharge at a rate that depends upon storage conditions [107]. At higher temperatures, side reactions accelerating corrosion and lithium losses can occur and result in capacity fading. Storing the battery at a lower temperature can prevent such effects but creates different challenges due to the loss of material diffusion which can alter the battery chemistry [75].

Cycle ageing refers to the battery deterioration due to its utilization mode when charging or discharging. Both calendar and cycle ageing are accelerated and triggered by common factors listed below. It can be challenging to measure their effects independently in certain cases because these factors have coupled effects on battery degradation.

Factors involved in battery degradation

Many factors influence the rate of battery degradation, especially storage, cycling and the environmental conditions. Operating batteries at high SOC (>95% according to discussions with battery manufacturers) is identified as one of the most important degradation factors. A high SOC enhances the creation of the SEI at the electrode/-electrolyte interface resulting in a capacity decay, power fade and impedance rise [108].

The second important factor is the temperature at which the battery is stored and operates. High temperature in batteries has both a positive and a negative effect on performance. It accelerates the rates of the chemical reactions which leads to a decrease in activation losses and an increase in efficiency. However, it also accelerates side reactions which leads to an increase in the calendar ageing [102]. Low temperatures can increase the degradation rate as it causes lithium plating as previously discussed which itself causes capacity and power fade [67].

Other factors identified in the literature for impacting the battery lifetime performance are the rates of charge and discharge. The higher the discharge rate, the greater the loss in conductivity between adjacent particles in the active material electrode which leads to an increase in internal resistance. If the same amount of charge is drawn from plates that are less conductive, it will lead to uneven current distribu-

tion and an increase in the stress and mechanical fatigue in the cell [109]. In battery electric vehicles, fast charging capability is considered a desirable feature. The storing capacity of the battery strongly depends on the applied charging current [110]. At high current rates during fast charging, the storage capacity of the battery is limited due the increase in internal resistance causing a voltage drop.

The depth-of-discharge (DOD) is an important factor that influences battery degradation. The DOD describes how deeply the battery is discharge. The DOD, in percent, is equivalent one minus the SOC: $\%DOD = 100\% - \%SOC$. The loss of active material particles at the negative electrode due to volume changes during cycling and constant stripping and re-depositing of the solid electrodes is enhanced by high DOD [67].

Lastly, overcharging significantly impacts the battery lifespan. If a cell is overcharged, solvent co-intercalate more which creates gases and subsequent cracks in the battery. This leads to a capacity fade. Overcharging causes irreversible partial decomposition of the anode resulting in an increase of surface resistance and loss of active lithium [102].

Concluding remarks on battery degradation phenomena and factors

Battery degradation is a complex phenomenon, characterized by calendar and cycling ageing. The literature identifies battery average state-of-charge (SOC) and change in SOC, temperature, charge/discharge (C/D), depth of discharge and overcharging as the principle agents in battery degradation [111]. Both calendar and cycling ageing are mostly influenced by the temperature, charging current and average SOC. Cycling ageing also depends on factors that are function of the battery utilization mode [75]. These factors are greatly influenced by the external climate and

the driving cycle. Moreover, factors will react differently if the vehicle is subjected to, for example, excessive acceleration.

Capacity fade and power fade

Capturing the full degradation process of a battery involves predicting both its capacity and power fade. The capacity fade of a battery is mainly affected by the loss of cycleable lithium and/or the loss of active electrode material that can host lithium [112]. The power fade, however, is mainly affected by the film resistance increase of the SEI. In this research, the change in resistance was not considered. Solely the capacity fade was considered to predict the end-of-life (EOL) of the battery.

Power fade is not typically used for the purpose of predicting the EOL of the battery. However, it is a useful information as it communicates how much the vehicle will be limited in its speed and performances after many cycles [83]

2.2.2 The Single Particle Model (SPM)

Definitions of conductivity, transport and diffusion in a porous media

This section provides a short definition on the main transport phenomenon occurring in a battery electrode, which is a porous media. In batteries, the electrodes are usually composites made of active material, conducting materials and binders. The liquid electrolyte penetrates the pores of the solid electrodes at a rate that depends on its porosity. The porosity of the electrodes is a measure of the void spaces in the electrode and is a characteristic that highly influences the performance of the cell. The electrical conductivity of the porous media is also influenced by the porosity and is defined as the degree to which the material can conduct electricity. The ion transport in porous media or migration often consists of an electrolyte phase which has a very high ionic conductivity allowing fast diffusion and a solid phase which has

very little to no diffusivity [113]. Another important physical phenomenon occuring in a cell is the diffusion, which in a porous media is the random movement of molecules moving toward regions of lower concentration in order to reach an equilibrium.

Detailed mathematical model of the cell behaviour

Most of the current rigorous lithium-ion battery models in use are based on the concentration solution and the porous electrode theories proposed by Doyle [84] and Newman and Tiedemann [114].

The concentrated solution theory is used to describe the transport of electrolyte in the liquid phase accounting for ion pairing inside the electrolyte phase [115]. The porous electrode theory is used to model the transport of ions in porous micro-structure [116]. These models describe mathematically the charge, discharge and species transport in the solid and electrolyte phases across a 1+1D structure, neglecting the dynamics in the other two dimensions. The 1+1D structure is a notation describing that 1 dimension is along the depth of the cell, or the "x" direction, and the other is along the radius of the particle, the "r" dimension. This approximation applies to most cell structures along the x-direction where the cell is of the order of 100 μm thick [117]. The main variables involved in the macro-homogeneous 1+1D electrochemical model of a battery are the solid phase lithium concentration $C_s(x, r, t)$ in the positive and negative electrodes, the lithium concentration $C_e(x, t)$ in the electrolyte, the potential $\phi_s(x, t)$ in the positive and negative electrodes, the potential $\phi_e(x, t)$ in the electrolyte, the ionic current $i_e(x, t)$ in the electrolyte, and the molar ionic flux $j_{Li}(x, t)$ between the active material in the electrodes and the electrolyte [118]. These variables are time dependant (t) and spatially dependant (x for spatial coordinate and r for radial coordinate).

The following subsections describes the governing equations simulating the main

physical phenomena in a lithium-ion cell.

Mass transport in the solid phase

A typical porous electrode in a cell is composed by active material, conductive filler, and binder. The active material can be represented by many spherical particles across the electrode. It is widely accepted in the literature that diffusion in the negative and positive electrodes can be modeled using spherical equations of Fick's law shown in equation 2.22 [119], [120]. A schematic of the modelled system is shown in Figure 2.7. Additionally, Figure 2.8 gives a representation a cylindrical cell cross sectional area to be able to locate the modelled system within the cell. Each combination of separators, current collectors and electrodes are put together is series and rolled in an spiral shape to form the common cylindrical battery shape.

The subscripts n and p are indicators that the equation work for the negative and positive electrode. In this equation, D_s is the diffusion coefficient in the solid state (m^2/s).

$$\frac{\partial C_{s,i}(x,r,t)}{\partial t} = \frac{D_{s,i}}{r^2}\frac{\partial}{\partial r}[r^2\frac{\partial C_{s,i}(x,r,t)}{\partial r}], \qquad i = n,p \tag{2.22}$$

The initial conditions are such that the initial solid concentration is known from the type of chemistry used, so that $C_s(x,r,t=0) = C_s^0$. The Newmann (or second-type) boundary conditions used to solve for the concentration of solid lithium are shown in equations 2.23 and 2.24, where r is the sphere radius, j^{Li} is the reaction current given by the Butler Volmer kinetics equation in 2.36 and F is Faradays constant ($96,487 C/mol$) and a_s is the specific interfacial area of porous electrode (m^2/m^3) defined in equation 2.25 where ϵ_s, ϵ_e and ϵ_{fl} are the volume fractions of the solid, electrolyte and current conductive fillers respectively [95].

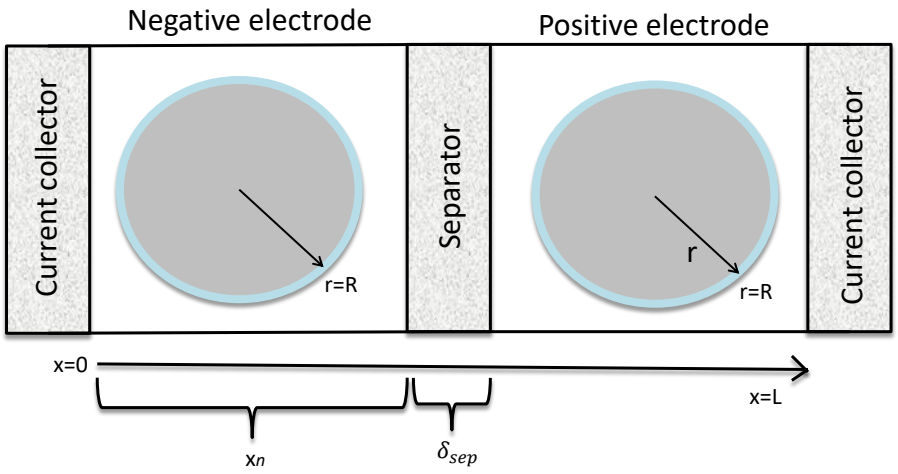

Figure 2.7: Each electrode modeled as a sphere

$$\frac{\partial C_{s,i}}{\partial r}|_{r=0} = 0, \qquad i = n, p \tag{2.23}$$

$$D_s \frac{\partial C_{s,i}}{\partial r}|_{r=R} = \frac{-j^{Li}}{a_s F}, \qquad i = n, p \tag{2.24}$$

$$a_{s,i} = \frac{3\epsilon_{s,i}}{r} = \frac{3 \times (1 - \epsilon_{e,i} - \epsilon_{fl,i})}{r_i}, \qquad i = n, p \tag{2.25}$$

Mass transport in the liquid phase

The mass transport in the electrolyte is described by Fick's law of diffusion in the x direction in equation 2.26. This equation is used to describe the evolution of lithium ion concentration due to flow of ions and electrons [120].

$$\epsilon_e \frac{\partial (C_e(x,t))}{\partial t} = D_e^{eff} \frac{\partial}{\partial x}\left(\frac{\partial C_e(x,t)}{\partial x}\right) + \frac{1 - t_0^+}{F} j^{Li} \tag{2.26}$$

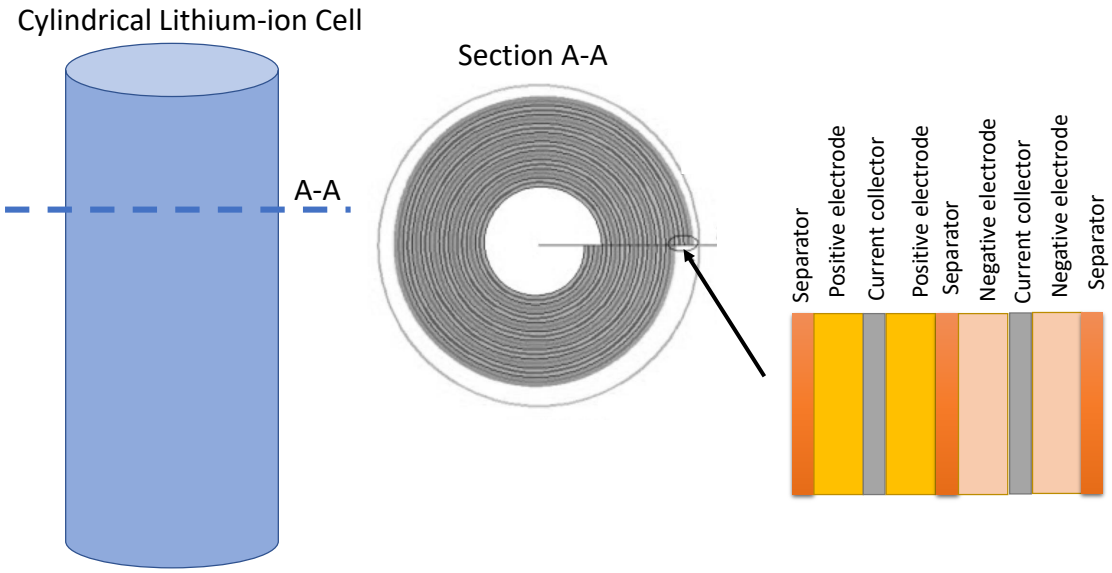

Figure 2.8: Cross sectional representation of a cylindrical lithium-ion cell

In this equation, t_0^+ is the transference number assumed to be constant due to limited available data [95]. The transference number, so called ion transport number, is a measure of the fraction of the total electrical current carried in an electrolyte by an ion. Additionally, the effective diffusion coefficient inside the porous electrode is calculated using the Bruggeman relation in equation 2.27 [84]. This equation captures the tortuous path of lithium ion through the porous electrodes and separator [120].

$$D_e^{eff} = D_e \epsilon_e^{1.5} \tag{2.27}$$

The initial conditions associated with this differential equation describe the fact that there is no flux at the current collectors.

Changes in potential in the solid electrodes

The change in potential in the solid electrodes is described by Ohm's law in equation

2.28 and relates the electrical potential $\phi_s(x,t)$ to the solid phase current i_s [117].

$$\sigma_{s,i}^{eff}\frac{\partial^2\phi_{s,i}(x,t)}{\partial^2 x}+i_s=0, \qquad i=n,p \tag{2.28}$$

The current density carried by the electrons in the solid phase $i_s = a_s j$ is related to the current density carried by the ions in the electrolyte i_e by Kirchoff's law [121]. σ_s^{eff}, the effective conductivity of the solid phase, is found using equation 2.29, also called Bruggeman's relation.

$$\sigma_s^{eff}=\sigma_s\epsilon_s^{1.5} \tag{2.29}$$

The boundary conditions to solve this equation depend on the charge/discharge operational mode: if the applied current is known when the cell is subjected to a constant current charge or discharge I_{app}, equation 2.30 is applied. When the end of charge voltage (EOCV) is known during a constant voltage charge, equation 2.31 is used.

$$-\sigma_{s,p}^{eff}\frac{\partial\phi_s(x,t)}{\partial x}|_{x=0,x=L}=\frac{I_{app}}{S} \tag{2.30}$$

$$\phi_s|_{x=0}-\phi_s|_{x=L}=EOCV \tag{2.31}$$

Additionally, the solid potential is the highest at the electrode/separator interface, which is translated in the equation below:

$$\frac{\partial\phi_s(x,t)}{\partial x}|_{x=x_n}=\frac{\partial\phi_s(x,t)}{\partial x}|_{x=x_n+\delta_{sep}}=0 \tag{2.32}$$

Changes in potential in the electrolyte

In the solution phase, the governing equation for the potential distribution $\phi_e(x,t)$ is derived from the charge conservation law [119]:

$$\kappa^{eff}\frac{\partial\phi_{e,i}(x,t)}{\partial x} - \kappa_D^{eff}\frac{\partial lnC_{e,i}(x,t)}{\partial x} + j^{Li} = 0, \qquad i = n,p \tag{2.33}$$

where κ_D^{eff} is the diffusional conductivity, given by the following relation:

$$\kappa_D^{eff} = \frac{RT}{F}(1-2t_0^+)\kappa^{eff} \tag{2.34}$$

The boundary conditions are:

$$\frac{\partial\phi_e(x,t)}{\partial x}|_{x=0} = \frac{\partial\phi_e(x,t)}{\partial x}|_{x=L} = 0 \tag{2.35}$$

Volumetric rate of the chemical reactions

Butler-Volmer kinetics equation is used to relate the reaction current j^{Li} to the local overpotential η:

$$j^{Li} = a_s i_0\big[exp\big(\frac{\alpha_a F}{RT}\eta\big) - exp\big(\frac{-\alpha_c F}{RT}\eta\big)\big] \tag{2.36}$$

where a_s was evaluated using equation 2.25. The exchange current density i_0 is evaluated according to the following formula [121]:

$$i_0 = \kappa F(C_s^{max} - C_s^{surf})^{\alpha_a}(C_s^{surf})^{\alpha_c}(C_e)^{\alpha_a} \tag{2.37}$$

Simplifications used in the SPM

The main assumption made in the single-particle model (SPM) is that the current distribution is uniform along the tickness of the electrode. Therefore, instead of modeling many small intercalation particles along the electrode, the entire porous electrodes can be modelled as a single intercalation particle [93]. Additionally, the concentration gradient in the electrolyte is neglected. That is, $\partial C_e(x,t)/\partial x = 0$ and $\partial C_e(x,t)/\partial t = 0$. This assumptions lead to significant simplifications in the model that are describe thoroughly in [122].

Numerical discretization and solution procedure

The SPM model used in this research has been implemented in Matlab 2016 by Bizeray et al. [123]. This model [121] is freely available online and implemented in Matlab 2016.

The discretised SPM model described in this section 2.2.2 is a set of ordinary differential equations (ODEs) and differential algebraic equations (DAEs). These equations were first discretized using a method called Chebyshev orthogonal collocation. This spectral method is used to numerically solve the ODEs and DAEs by defining grid points on the extrema of the Chebyshev polynomials of the first kind, which is a sequence of polynomial related to the de Moivre's formula $(\cos(x) + i\sin(x))^n = \cos(nx) + i\sin(nx)$. A thorough discussion on this method is presented in [124].

The discretized equation are then integrated using the solver "ode45" in Matlab to get a numerical solution, or "ode15s" if the former is too slow. The "ode15s" solver is a time adaptive solver which reduces the time steps required during slow transient behavior, therefore reducing computational efforts [125]. According to Matlab's documentation [126], "ode45" is the first solver one should try for most problems to solve equations of the form $y' = f(t,y)$ or problems with a mass matrix $M(t,y)y' = f(t,y)$.

2.2.3 Modelling the SEI growth to predict the capacity fade

The ability to accurately predict the capacity fade of a battery due to its usage can support battery technology improvement and lifetime enhancement. It can also help matching battery life to a particular duty cycle, given a particular battery chemistry. As discussed in the introduction, the most important source of capacity fade in automotive batteries is the expansion of the Solid Electrolyte Interphase (SEI) causing the loss of cyclable lithium in the cell [127].

In this research we use a model developed by Ning et al. [95] to predict the capacity fade of an electric bus lithium-ion battery. In this model, it is assumed that under normal cycling conditions, i.e no overcharge or overdischarge, the capacity fade occurs only during the charge process, e.g when the battery is being charged through plug-in/induction or when regenerative braking occur. That is because the main side reactions causing the SEI growth only occur during charging.

The cell capacity, that is how much energy (in Ah or kWh) a battery can provide before it is fully discharged for a given discharge rate (C-rate), relates to the amount of cyclable lithium in a cell [128]. When this amount decreases, the battery is no longer able to support the same discharge rate for as long as compared to when it was new.

It is assumed that a battery reaches its end-of-life (EOL) when the capacity deteriorates below 70% of its initial value [129]. This would both mean that once the battery reaches its EOL, the bus can only be deployed in short routes and eventually won't be able to complete any route of the transit system, and that the associated output power would drop. If one can predict how the capacity decreases, it can be possible to estimate how long the battery packs can last before being re-purposed [130]. For slow charging electric buses, that can be a game changer as the bus will require longer charging periods during the day which can be a great operational challenge for

transit agencies.

In [95], the loss of cyclable lithium due to the SEI creation during the first cycle is characterized based on the volume-averaged loss capacity Q_1 [131]:

$$Q_1 = \int_0^{t_{charge}} |j_{side}(t)| a_{neg} dt \tag{2.38}$$

where j_{side} is the current density of the side reaction causing the increase in SEI layer thickness and a_{neg} is the specific interfacial area of the negative electrode. t_{charge} is the time during which charging occurs. j_{side} is calculated using the Tafel equation (2.39), where j^0_{side} and α_{neg} are experimentally determined parameters, and η_{neg} is the negative electrode overpotential [95] defined in equation 2.40 .

$$j_{side}(t) = -j^0_{side} exp(\frac{\alpha_{neg} F}{RT} \eta_{neg}(t)) \tag{2.39}$$

$$\eta_{neg} = \phi_s - \phi_e - U_{neg} - j \times R_f \tag{2.40}$$

In equation 2.40, U_{neg} is the open circuit potential of the negative side electrode, j is the local current at the negative electrode and R_f is the resistance of the SEI.

In [95], with every cycling phase, the available lithium decreases according to equation 2.41:

$$C_{N+1} = C_N - \frac{Q_N}{F \epsilon_{neg}} \tag{2.41}$$

where C_{N+1} and C_N are the lithium concentrations at the beginning of the charging cycle "N+1" and "N", respectively. F is Faraday's constant and ϵ_{neg} is the volume fraction of the negative solid electrode and Q_N is the volume-averaged capacity lost due to parasitic reaction in (C/m^3). However, this method is computationally intensive because the SPM model is re-run for every cycle and the capacity lost during the

cycle is re-calculated every cycle. Since this research focuses on finding the capacity fade for a repeated driving cycle pattern, another approach was used to improve computational time based on the results obtained in [95]. Instead of re-calculating the capacity fade for every cycle, the capacity loss is linearized according to equations 2.42 and 2.43:

$$C_{N+1} = C_0 - N \times C_{1,s,neg} \tag{2.42}$$

$$C_{1,s,neg} = \frac{Q_1}{F\epsilon_{neg}} \tag{2.43}$$

where C_{N+1} is the concentration at the beginning of the charging cycle "N+1", C_0 is the initial lithium concentration before the cell has been used, N is the cycle number and Q_1 was defined in equation 2.38.

This assumption was based on the results in Ning's paper for the lithium concentration loss for every cycle, shown in Table 2.2. As shown here, when the cell reaches its end-of-life at cycle number 1968, the maximum difference between the results is 3.56%.

Table 2.2: Linearization of the capacity fade for each cycle based on the results in [95]

Cycle number	**Lithium concentration of the negative electrode (x10^3 mol/m^3) using equation 2.41**	**Lithium concentration of the negative electrode (x10^3 mol/m^3) using equation 2.42**	**Difference (%)**
0	25.39	25.39	0.00
455	24.29	24.29	0.00
822	23.52	23.41	0.50
1124	22.94	22.67	1.14
1545	22.13	21.66	2.13
1732	21.76	21.20	2.56
1968	21.39	20.63	3.56

2.2.4 Coupling the Capacity Fade Model with the SPM Model

As mentionned in the above section 2.2.2, the SPM model used in this research was developed by Bizeray et al. [123]. Solving for the SPM equations is a challenging task, therefore using this tool that was available and validated was preferred rather than re-developing the code in-house. The battery chemistry specification used to test the model against Ning's results are shown in Table 2.3.

The Matlab SPM model uses the output values of the developed CFM that calculates the increase in SEI thickness and the battery capacity for every charging/discharging cycle.

The following steps are implemented to run the two models together:

1. the ECONS-M produces a time-dependant C-rate profile according to the given driving cycle, which is then fed into the capacity fade model (CFM)

2. the CFM implemented in Python passes the input parameters listed in Table 2.3 and the C-rate profile to the SPM model (Matlab)

3. the SPM model simulates the discharge or charge of a lithium-ion cells and produces results, such as the cell voltage, the negative electrode over-potential and the simulation time steps

4. the CFM running in Python reads the results, especially the phase difference between the electrolyte and the solid state of the negative electrode, and the second by second applied current used to calculate the local negative electrode overpotential

5. the CFM running in Python calculates the new thickness of the SEI and the decrease in the available lithium concentration

Table 2.3: Electrochemical model input used to validate the degradation module

Parameter in Bizeray's SPM model [121]	**Value from Ning's degradation model [95]**	**Unit**	**Symbol**
Negative electrode material	MCMB (graphite powder)	-	-
Positive electrode material	$LiCoO_2$ (Lithium cobalt oxide)	-	-
C rate (discharge, constant)	1C	-	-
Nominal battery capacity	1.67	Ah	cap
Current collector resistance R_f	20×10^{-4}	Ω/m^2	-
Thickness of negative electrode	75.50×10^{-6}	m	-
Thickness of positive electrode	74×10^{-6}	m	-
Thickness of separator	25×10^{-6}	m	-
Electrode active surface area	0.087	m^2	-
Positive and negative electrode solid particules' radius	2×10^{-6}	m	r
Initial SOC of negative electrode when fully charged	0.83	-	θ_{neg}
Initial SOC of positive electrode when fully charged	0.48	-	θ_{pos}
Volume fraction of active material (negative electrode)	0.51	-	$\epsilon_{s,neg}$
Volume fraction of active material (positive electrode)	0.48	-	$\epsilon_{s,pos}$
Maximum Solid phase concentration(negative electrode)	30556	mol/m^{-3}	$c_{neg,max}$
Maximum Solid phase concentration(positive electrode)	51555	mol/m^{-3}	$c_{pos,max}$
Diffusion coefficient of Lithium in active material (negative electrode)	3.8×10^{-14}	$m2.s^{-1}$	$D_{neg,s}$
Diffusion coefficient of Lithium in active material (positive electrode)	1.0×10^{-13}	$m2.s^{-1}$	$D_{pos,s}$

6. the CFM calculates the lithium concentration for each cycle according to equation 2.42

7. when the battery has reached its end of life, e.g when the capacity is 70% of its initial value, the process is stopped and the final capacity is checked through a final run in the SPM

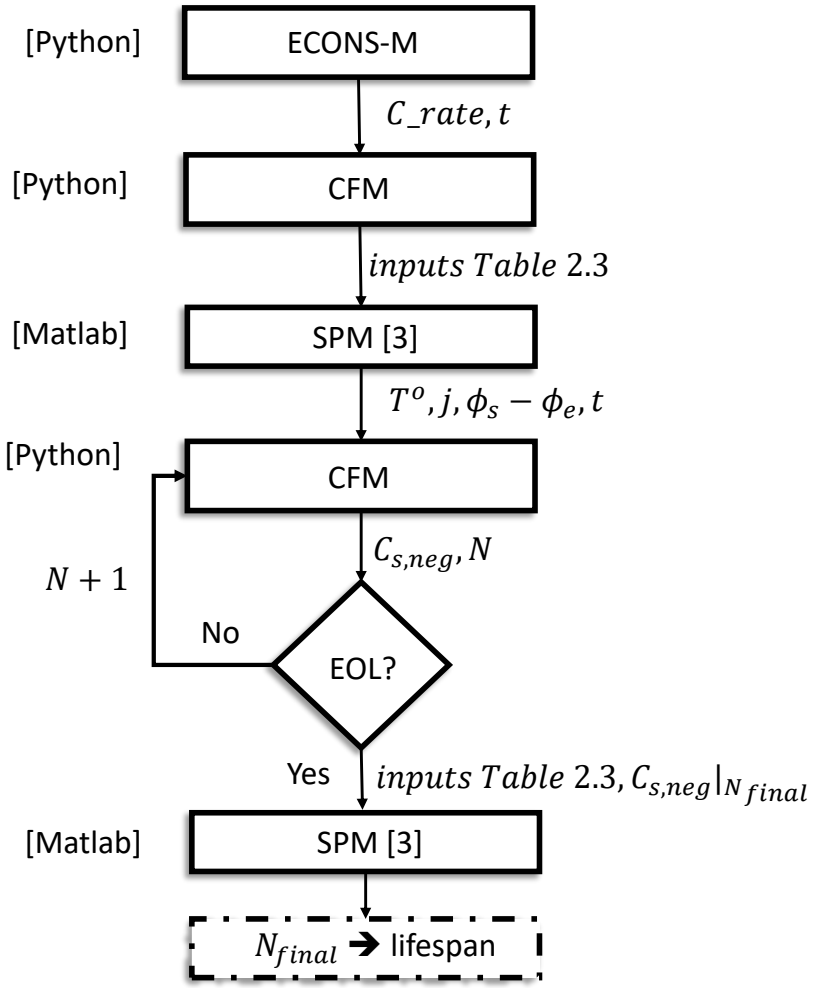

Figure 2.9: Coupling the ECONS-M, the SPM and the CFM

Figure 2.9 shows a flow diagram summarizing the process that has just been described. One limitation of using this coupling tool is that the code in Python has to be implemented in Python 2.7 while the latest version of Python to this date is

3.5. This is because the package *matlab.engine* of Python used to communicate with Matlab is not available for newer versions.

The open circuit potential (OCP) curves of the negative and positive electrodes from Ning's model were digitalized and used in the Matlab SPM code as inputs. The open circuit potential curves of the negative and positive electrodes that were gathered in Ning's research are shown in Figure 2.10 and 2.11, respectively. The x-axis labelled SOC represents the negative and positive electrode SOC θ_{neg} and θ_{pos}, not the overall cell SOC.

The open circuit potential (OCP) plays an important role in the CFM as it allows to find the surface overpotential for the negative electrode in equation 2.40. It is expressed in function of the electrode SOC. It measures the difference in electrical potential between the current collectors of the positive and negative electrode when the system is disconnected from an external load, so when there is no current flowing. The curves obtained for the OCP greatly vary between battery chemistries therefore it requires specialized individual electrode testing.

2.2.5 Model Reproduction and Validation

To ensure that coupling the two models predicts the capacity fade behavior of the cell as accurately as shown in Ning's research [95], two tests were performed:

1. run the electrochemical model charge with the same battery characteristics defined in [95] at 1C for one cycle to ensure the same voltage versus capacity can be reproduced

2. run the electrochemical model charge for many cycle and compare the capacity fade after 455, 822, 1124, 1545, 1732 and 1968 cycle to verify the validity of the produced model against Ning's model

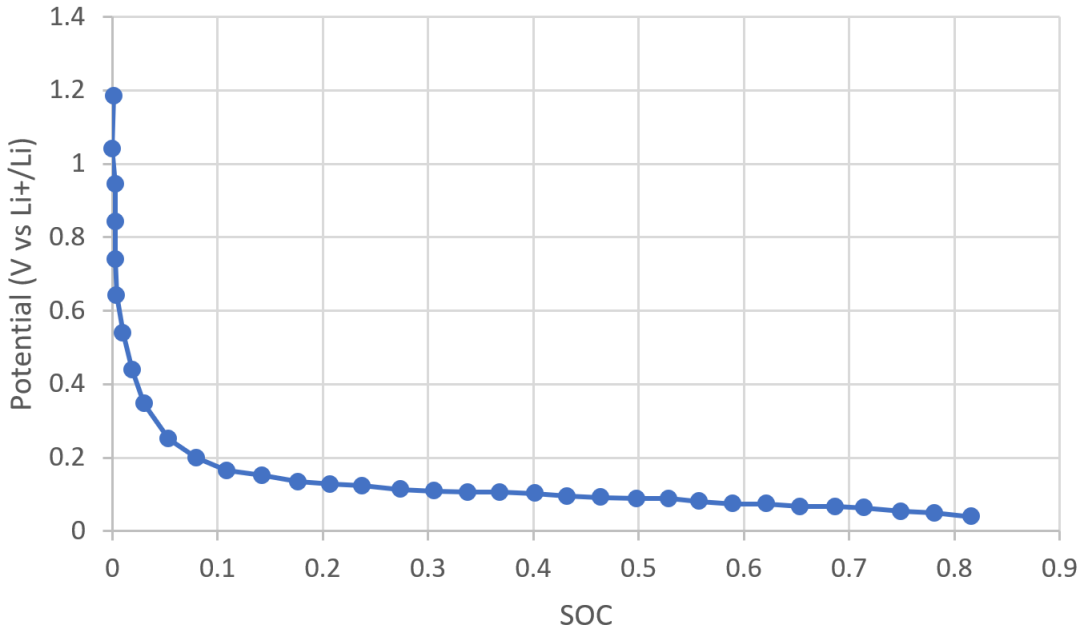

Figure 2.10: Open circuit potential (OCP) of the negative electrode, adapted from [95]

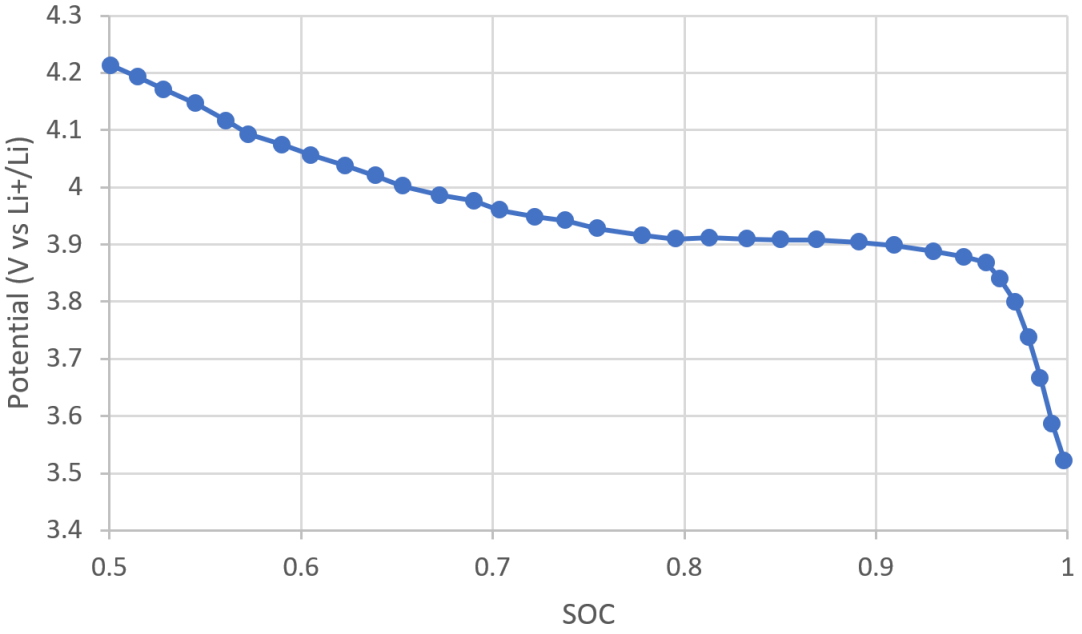

Figure 2.11: Open circuit potential (OCP) of the positive electrode, adapted from [95]

Test the SPM model at a constant C-rate charge

The first test that was required to reproduce Ning's results was to ensure that the cell behavior was well captured by the Matlab SPM model on a simple 1C charge.

The Matlab SPM model run using the parameters listed in Table 2.3 and the comparison between Ning's results and the SPM model are shown in Figure 2.12.

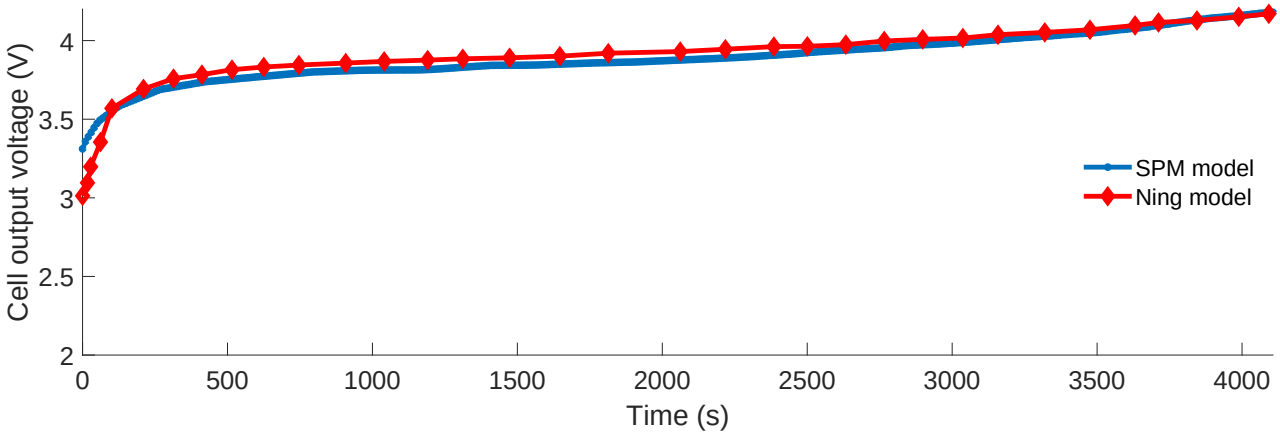

Figure 2.12: SPM model output cell voltage curve compared to Ning's voltage curve [95] for a 1C charge

Ning's voltage curve is shown in the red diamond line while the SPM model voltage curve is the blue continuous curve. The average difference between the two curves was calculated to be 1.15 %, while the maximum difference between the two curves was 9.91% at t=0. This difference can be explained by the fact that the SOC of the negative and positive electrode when the battery is fully discharged wasn't provided in Ning's paper. This means that the OCP of the negative and positive electrodes is different, especially at the beginning of the charging process. Due to a lack of available data in the literature on this specific point, the initial value of the SOC when the battery is discharged was set to 0.8933 for the positive electrode and 0.0068 for the negative electrode. These values were already implemented in Bizeray's Matlab model for the same type of chemistry used in Ning's model. To

back-up this explanation, Table 2.4 shows the maximum and average error difference between the output voltage of Ning's model and of the SPM model for the constant C-rate discharge curve.

Table 2.4: Maximum output voltage difference for the constant C-rate charge curve when modifying the initial positive and negative electrode SOC

Initial positive SOC	**Initial negative SOC**	**Maximum difference (%)**	**Average difference (%)**
0.8933	0.0068	9.91	1.15
0.8933	0.003	5.72	0.88
0.92	0.003	4.97	0.87
0.92	0.0025	4.61	0.87

Test the coupling of the SPM and the CFM for many cycles

The model was then run for a constant 1C rate charge for many different cycles using the parameters shown in Table 2.5. The negative electrode lithium concentration at the beginning of the discharge was compared to the results in [95]. The results are shown in Figure 2.13. At cycle N=455, the difference between the reproduced CFM coupled with the SPM model and Ning's model is 2.4%. The cell was found to reach its end of life after 1968 cycles. At this point, the concentration difference had increased up to 9.05 %, the end-of-life being predicted earlier in Ning' model. It is believed that this error is due to the fact that the charge was solely an imposed constant current, while Ning's model accounts for an additional constant voltage phase. Indeed, this additional constant voltage charge is responsible for a larger capacity fade, therefore the battery end-of-life would occur earlier in Ning's model. This limitation will be discussed next.

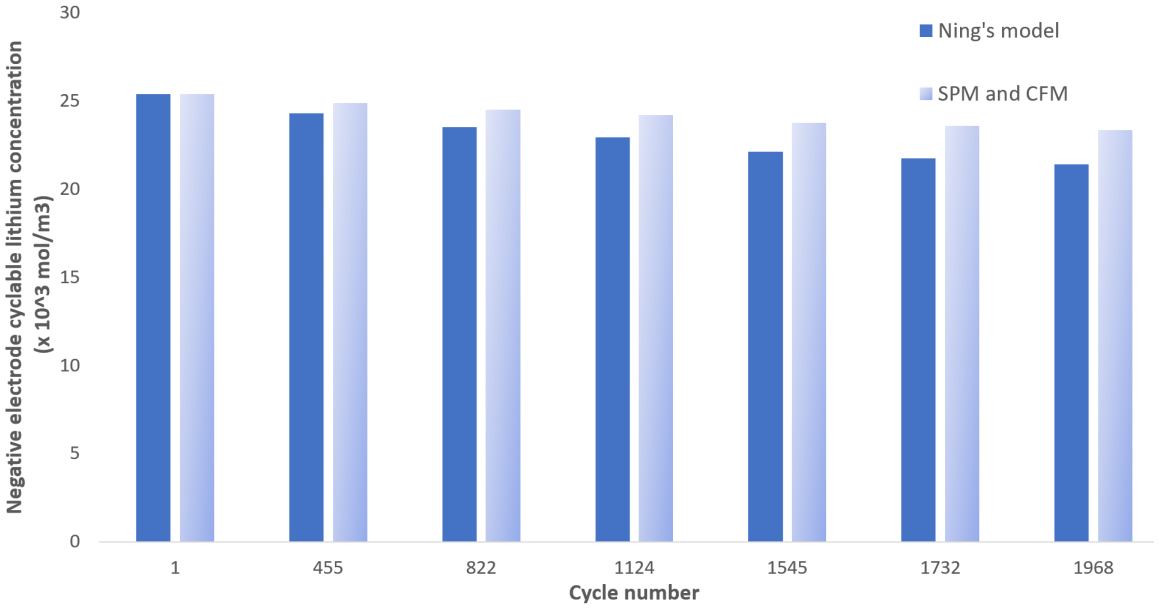

Figure 2.13: Lithium concentration for different cycle (1968 corresponds to the end-of-life of the cell): comparison between Ning's results and the buid-in model results

Table 2.5: Parameter values used to simulate the parasidic reaction [95]

Parameter	**Value**	**Unit**
U_{neg}	0.38	V
j^0_{side}	0.8×10^{-7}	A/m^2
α_{neg}	0.5	-
a_{neg}	735,000	m^{-1}

2.2.6 Model Limitations

The current electrochemical model in use is a single particule model implemented in Matlab [123]. This type of model assumes the negative and positive electrodes can be represented as two solid single circular particles, with the same surface area as the initial electrodes. This simplification involves neglecting the concentration and potential changes in the solution phase between the active material particles in the electrodes [89].

While this model runs faster, one of its main limitation is that it cannot accurately predict the behaviour of the cell at charging and discharging rates greater than 1C

despite what was claimed in [95]. In [90], the authors showed that the percentage error between the simple particle and pseudo 2D models for a discharge rate of 1C is 3.4%. The pseudo 2D model is a more detailed physics based model accounting for variation of lithium concentration across the electrodes and effects of the electrolyte [132]. It can be characterized as an extension of the SPM model. For a 2C discharge rate, it reaches 59.4% therefore the model can no longer predict the cell voltage behavior. This is due to the basic assumption that the concentration in the solution phase is constant during the discharge in an SPM model, which isn't correct at higher discharge/charge rates. For a discharge rate up to 1C, the change in the solution phase concentration is less than 10%, but for a 2C rate it goes up to 40% so this assumption is no longer valid [90]. The SPM model is therefore incapable of predicting the discharge profile in the kinetics-dominated regime.

In [85], the current density of the side reaction is assessed using the equation below:

$$j_{side} = -j^0_{side}\left(\frac{C_s}{C_s*}\right)\left(\frac{C_{Li^+}}{C_{Li^+}*}\right)e^{\frac{\alpha_{neg}F}{RT}\eta_{neg}} \tag{2.44}$$

where j_{side} is the current density of the side reaction, C_s is the concentration of solid lithium, C_s* is the maximum solid lithium concentration, C_{Li^+} is the lithium ion concentration, $C_{Li^+}*$ is the maximum lithium ion concentration, F is Faraday's constant, α_{neg} and j^0_{side} are known experimental parameter, R is the gas constant and T is the cell temperature. It is explicitly stated that there is not much variation in the concentration of lithium ion in the solution phase for low to moderate rates of charge and discharge, which simplifies equation 2.44 further to:

$$j_{side} = -j^0_{side}e^{\frac{\alpha_c F}{RT}\eta_{neg}} \tag{2.45}$$

which is equivalent to equation 2.39 in section 2.2.3 used in [95]. In the introduction

of [95], however, the authors mentioned that their model is applicable not only for mild but also for harsh charge/discharge conditions. From the previous argument that was made, it appears that the simplification cannot in fact hold for large-C rates, as there is a non-negligible lithium concentration difference at the surface of the electrode. Hence, equation 2.44 must be applied throughout the electrodes using the variable concentrations present throughout at high C-rates.

The second model limitation is due to the fact that only a constant-current charge or discharge can be modeled in the Matlab SPM model. In [95], the charging procedure uses a constant current charge (CC) up until a certain voltage is reached. In the experiment conducted in [95] the upper voltage limit is set to 4.0 V. The voltage is held constant until the cutoff current of 50mA is reached. This procedure is called "constant-current constant-voltage" charge (CC-CV). The CV part of the charge avoids the risk of reaching high potentials in the battery that could result in overcharging degradation (i.e. high overpotentials leading to rapid SEI formation) [97]. The Matlab SPM used in this simulation doesn't include a function to switch and use constant current and constant voltage charges. Therefore, the CFM doesn't capture the effect of constant voltage (CV) degradation, not because it is deficient, but because of the limited implementation of the full set of equations.

As shown the previous section, the predicted lithium concentration at the negative electrode at the end of life of the cell was 9.05 % higher than the one measured by Ning et al. In [95], it is said that for a charging rate of 1C, roughly 10% of the capacity was estimated to be supplied by the CV charge mode. Though it is challenging to estimate how much CV charge impacts the battery capacity decay, it impacts 10% of the charging capacity during every charging cycle. This could explain the differences in the results.

The third main limitation lays in the fact that the SEI resistance change was

not included in this model. The growth in SEI results in an increase in internal resistance of the battery cell. This change in internal resistance impacts the cell output power by reducing the battery voltage for a given discharge current rate over time [112]. As explained is section 2.2.1, the end-of-life of a cell is usually predicted using solely the capacity fade (i.e. cyclable Li), as the resistance change is a second-order performance degradation effect. However, the impact of resistance increase is useful to assess the future performance of the batteries and should be considered to have a broader understanding of the battery degradation.

Lastly, another limitation is the lack of thermal model for the battery/cell. The model assumes a constant room temperature throughout the cell during the charge/discharge process. In [133], a lithium-ion cell thermal model is developed to model discharge performance at different operating temperatures. Transport properties, diffusion coefficient, exchange current density and conductivity are variables that all vary with temperature. Additionally, the battery pack modeled in this study is assumed to have an ideal thermal management system, which means that every cells of the pack operate at the same temperature. In reality, cells are more or less hot depending on their location inside the pack. Air cooling is one of the simplest cooling system used by manufacturers to cool a pack and unify its temperature, however the rate of heat transfer from the cells to the air is low due to the limited thermal conductivity of air. If this method is chosen, high mixture rate of the air is required to effectively transfer heat from the system which is difficult to achieve in a space-constraint environment such as an electric vehicle [134]. On the other hand, liquid coolant is a more compact and efficient solution but it can lead to safety hazards if not managed properly due to the use of coolants such as Dexcool.

2.3 Coupling the Electricity Consumption Model with the Capacity Fade Model

The ECON-M and the CFM were coupled in order to assess the battery lifetime when the battery is subjected to real life driving cycles. This method has not yet been investigated in the literature, to the knowledge of the author. Equation 2.19 in section 2.1.1 showed that the current flowing from or towards the battery in case of charging or regenerative braking can be linked to the battery output power and terminal voltage. However, the V_{OCP} and resistance need to be known.

From various conversations with electric bus manufacters, the usual choice for cell capacity is 40Ah. To find the V_{OCP} and internal resistance of the battery, the model in [135] was applied to a 40 Ah LiFePO4 because of a lack of proprietary cell data.

The 0.3C discharge curve was provided by the manufacturer in [136] and digitalized to extract the required information to characterise the V_{OCP} and internal resistance of the cell. The result of the digitalization is shown in Figure 2.14.

From the model in [135], four parameters need to be specified in order to capture the cell voltage behaviour as a function of the current, namely the internal resistance, the voltage drops and the charge at the end of the exponential zone, and the polarization voltage.

First the internal resistance R is characterized using the equation below, where V_{nom} is the nominal voltage of the cell in volts, η is the efficiency of the cell and Q_{nom} is the nominal capacity of the cell in Ah:

$$R = V_{nom}\frac{1-\eta}{0.2Q_{nom}} \tag{2.46}$$

$$R = 3.2\frac{1 - 0.995}{0.2 \times 40} = 0.002\Omega \tag{2.47}$$

Next, to find V_{OCP}, parameters A (equation 2.49), B (equation 2.50), K (equation 2.51) and E_0 (equation 2.52) need to be determined.

$$V_{OCP}(SOC(t)) = E_0 - \frac{K}{SOC(t)} + A \times exp(-B \times Q(1 - SOC(t))) \tag{2.48}$$

A is the voltage drop during the "exponential zone" shown in Figure 2.14. The end of the exponential zone is achieved when the rapid initial voltage drop stabilizes. The end of the nominal zone is achieved when the voltage starts to drops abruptly [137].

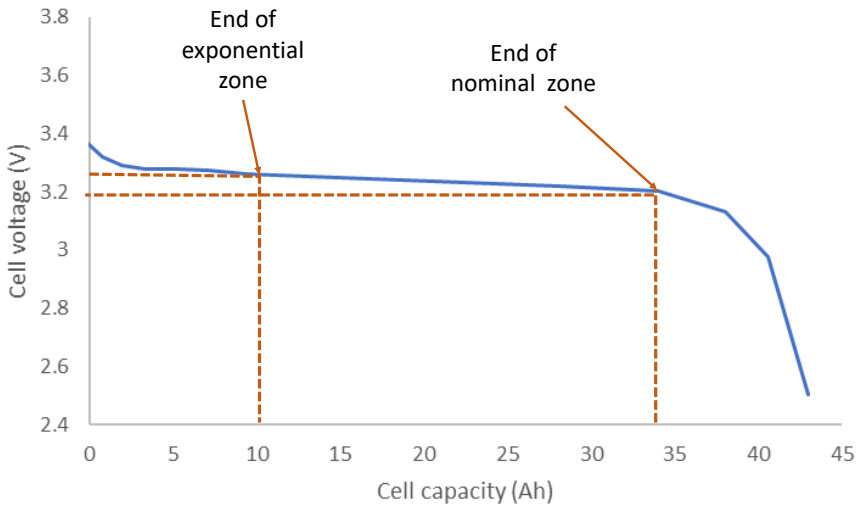

Figure 2.14: 0.3C discharge curve: defining the exponential and nominal zone

$3/B$ represents the charge at the end of the exponential zone, K is the polarization voltage and E_0 is a voltage constant.

$$A = E_{Full} - E_{Exp} = 3.26 - 3.27 = 0.09V \tag{2.49}$$

$$B = \frac{3}{Q_{exp}} = 3/10 = 0.3(Ah)^{-1} \tag{2.50}$$

$$K = \frac{(E_{full} - E_{nom} + A(exp(-BQ_{nom}) - 1))(Q - Q_{nom}))}{Q_{nom}} = 0.014V \tag{2.51}$$

$$E_0 = E_{full} + K + Ri - A = 3.31V \tag{2.52}$$

Finally, to find the terminal voltage, this equation is used:

$$V_{term} = E_0 - \frac{K}{SOC(t)} + A \times exp(-BQ(1 - SOC(t))) - Ri(t) \tag{2.53}$$

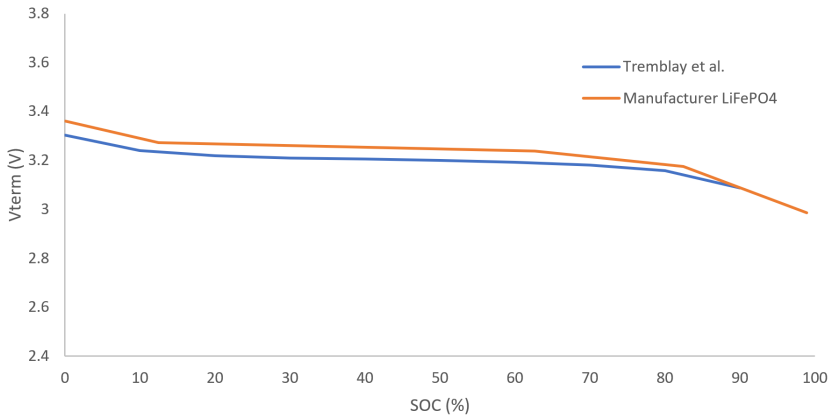

Figure 2.15: 0.3C discharge curve: manufacturer data versus model prediction

Figure 2.15 shows the difference between the manufacturer data versus what the results from using parameters A,B, K and E_0 in equation 2.53 for a constant discharge current of 12 A (0.3 C rate). The maximum difference between the two curves is 2.6%, which validates the model used in [135] for this particular cell. This difference can be explained by the fact that since every discharge curve is different, it can be somewhat

challenging to accurately find the end point of the exponential and nominal zones.

We want to model a 324 kWh and 540V, or 600 Ah battery pack as used in the BYD K9 electric bus [138] because it is the type of BEB with the most publicly available data in the litterature that uses low C-rate charging. A possible configuration for this battery is to have 600 Ah / 40 Ah = 15 branches of cells connected in parallel. The total voltage of each branch would be $324kWh/600A = 540V$. We know that the nominal voltage of a 40 Ah lithium iron phosphate cell is 3.2V [136]. Therefore, each branch needs to have $540V/3.2V = 169$ cells in series. A schematic of the modelled battery pack is shown in Figure 2.16.

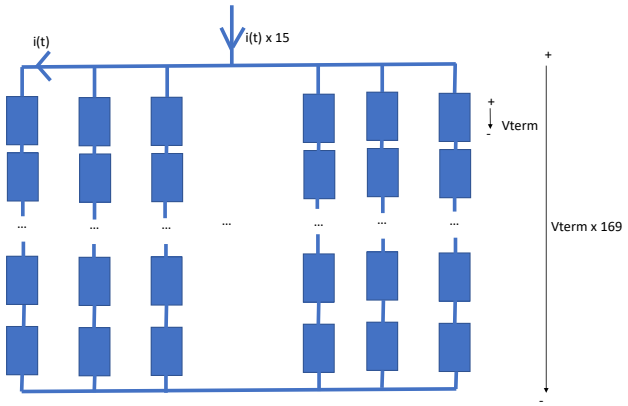

Figure 2.16: 324 kWh and 540 V battery pack representation

Assuming the ideal case in which every cell of the battery packs behaves the same way and an ideal battery management system, the overall battery current is equal to the current flowing through each branch multiplied by 15 branches. Using the same approach, the terminal voltage of the battery voltage multiplied by 169 cells. The charging and discharging current required to power the vehicle is found by solving simultaneously equations 2.53 and 2.54, which related the output power of the battery to the cell voltage and current. The second-by-second current array is then transformed into a C-rate (current divided by the battery capacity of 600 Ah) and fed into the SPM / battery degradation model with a C-rate that changes every

second.

$$P_{elec,batttery}(t) = V_{term,cells}(t) \times N_{cells,series} \times i(t) \times N_{branch,parallel} \tag{2.54}$$

2.4 Chapter Conclusion

In this chapter, two models are described: the electricity consumption model (ECONS-M) and the capacity fade model (CFM). Both models are coupled to convert a real-life BEB driving cycle into a C-rate profile, then fed into the CFM.

The ECONS-M is a first-principle based dynamic analysis that uses the speed of the vehicle as a function of time to obtain the acceleration and forces acting on the bus [131]. This allows to calculate the torque of the electric motor, considering the transmission efficiency and the gear ratio as constants. Regenerative braking is also included in this analysis. The model was tested using standardized Altoona's driving cycle, and the average energy consumption measured and modelled showed a difference of 0.8%.

The CFM is based on an single particle model (SPM). This type of model assumes the negative and positive electrodes can be represented as two solid single circular particles, with the same surface area as the initial electrodes. This simplification involves neglecting the concentration and potential changes in the solution phase between the active material particles in the electrodes. In this research, we solely consider the change in lithium concentration to estimate the decrease in battery capacity. The reproduced capacity model is run against Ning's results [95] and shows that the capacity decrease calculation has up to a 9.05% difference when the battery reaches it's end-of-life, which is explained by the fact that the charging strategy only uses CC charge instead of a CC-CV charge modeled in Ning's research. The model

limitations are also discussed. These limitation include the fact that the model is only valid at low charging rates (less than 1C) and that the increase in internal resistance is not considered in this study.

Finally, the coupling methodology between the two models consists in obtaining a second-by-second C-rate profile for the batteries, which is then scaled down to the cell level. This cell level C-rate is then fed into the SPM and CFM to assess the cell lifetime, assuming every cell of the battery pack degrades at the same rate.

The next chapter focuses on direct applications of the two models. Especially, the ECONS-M is used to project electricity prices and GHG reduction potential for a selected route in Victoria, BC. The CFM is then applied to this selected route to assess the battery lifetime under these conditions.

Chapter 3

Case studies and applications of the ECONS-M and CFM

This chapter describes the applications of the ECONS-M and the CFM. First, the energy consumption of a 2013 BYD K9 bus was assessed for a real-world route in Victoria BC. This chapter describes how the driving cycle data were recorded and the road grade profile obtained and presents a sensitivity analysis for the ECONS-M followed by projections of the financial benefits of the BEB along with potential emission reductions. The second part of the chapter discusses how the CFM can be used to project the lifetime of lithium-ion batteries subject to real-world driving cycles. Lastly, other possible applications of the model, future research and improvements are discussed.

3.1 Energy Consumption of a BEB for Real-World Transit Route

3.1.1 Speed and GPS Coordinates Inputs

Data Gathering

An essential input of the ECONS-M is the driving cycle of the bus, which includes the speed and the road elevation profile versus time. A Tracking Key GPS Logger 2 from LandAirSea, so called "passive GPS tracker", is used in this study. One of the advantages of using a passive GPS tracker is that it stores the recorded data instead of sending them in real-time, therefore there is no monthly-fee associated with its operation. The sampling rate can also be varied. This tracker records the GPS coordinates of the vehice.

The sampling rate for this study was set to be 1Hz. A 12.9 km long Westward and 13.3 km Eastward route was selected. It is representative of a typical Victoria transit system route through universities, downtown and residential areas and as such is frequented by many students and workers. The hours of operation are between 5AM and 1AM the following day (20 hours of operation) on weekdays and 6 or 7AM until 1AM or 11PM on Saturdays and Sundays, respectively. A bus leaves both terminals every 10 to 20 min, therefore there is always at least two buses on this route, one in each direction. Additionally, the buses drive through an important bridge and up and down a steep hill.

To record the data the device has to be placed horizontally with the top face facing up as shown in Figure 3.1. There is a strong magnet at the bottom that makes it easy to position inside the bus. Note that the bus was a double-decker each time the data were recorded. The technical specifications indicate that the GPS Tracking

Key receives signals from the 24 Department of Defense satellites orbiting the Earth, and its GPS location accuracy is +/− 2.5m [139].

Figure 3.1: GPS Tracker Key setup to record the bus speed, elevation and GPS coordinates on a double decker

One issue is that there is no power button on the GPS: it automatically turns off after a few seconds without detecting a motion. This was problematic during the data gathering phase as it would stop recording data for a few minutes at a time after the bus stopped at a traffic light for about 1 min. For this reason, the experiment was repeated 3 times and the dataset with least jumps in the data was used in this analysis.

Table 3.1: Characteristics of the chosen transit route in Victoria, BC

Parameter	**Westward direction**	**Eastward direction**	**Unit**
Average speed	25.7	27.5	km/hr
Total distance	12.9	13.3	km
Average acceleration	1.5	1.3	m/s^2
Final deceleration	-2.7	-2.5	m/s^2
Average grade	-0.04	0.2	deg
Time to complete the route	45.3	40.1	min

The results after riding the bus for the selected route in each direction are shown in Figures 3.2 and 3.3, respectively. Table 3.1 shows the main characteristics of the driving cycle for the chosen route in Victoria.

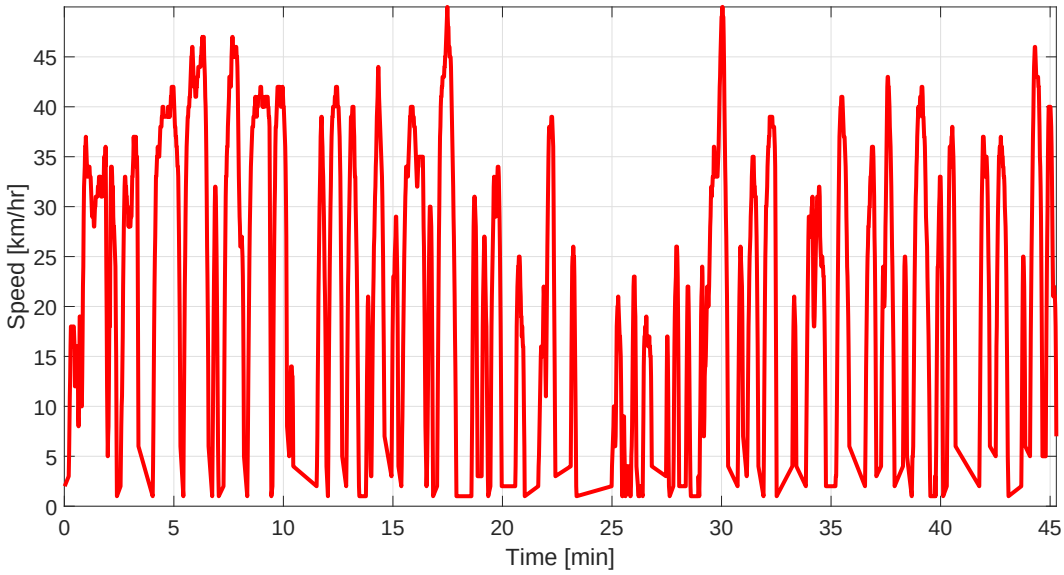

Figure 3.2: Raw driving cycle recorded in the Western direction

Data Post-processing

Using GPS data points, the elevation data can be obtained using a Digital Elevation Model (DEM). There are many DEM databases available, including the Space Shuttle Radar Topography Mission (SRTM) or the JAXAs Global ALOS 3D World which both have a spacial resolution of about 30m. The National Elevation Dataset (NED) is the U.S. Geological Survey that covers the United States, Canada, and Mexico that has a resolution of up to 1/9 arc-second (3m) in certain areas. The NED model is publicly accessible and updated every 2 months from diverse source data. For Victoria area, the resolution is 1/3 arc-second, which is the highest seamless DEM resolution for the U.S to this date [140].

Another tool that can be used to extract elevation profiles is Google Maps API, used in Google Maps and Google Earth. Google's data comes from many different sources, but Google has yet to release detailed information regarding the accuracy of their road elevation profiles [141].

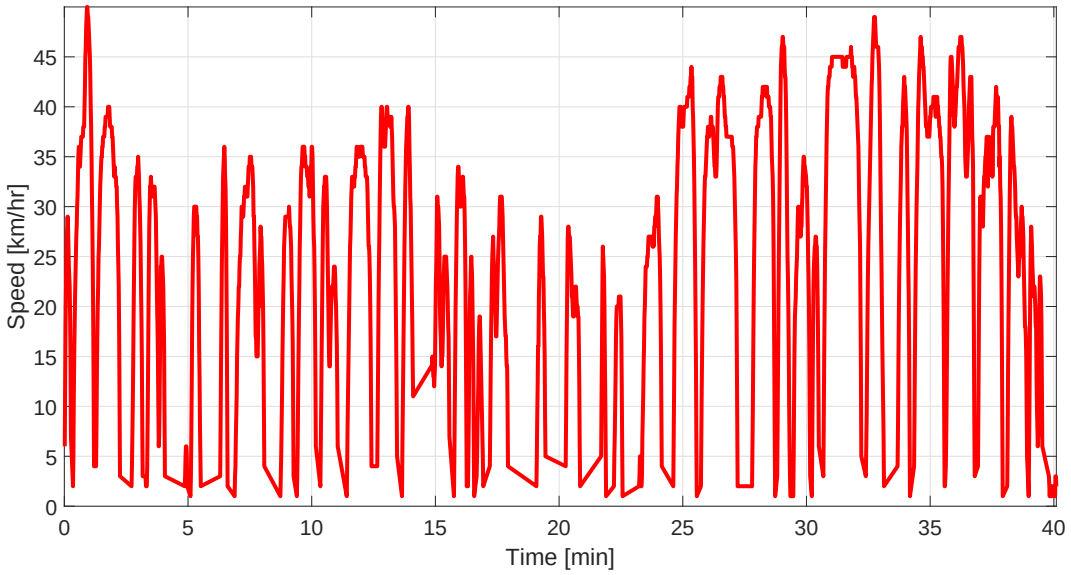

Figure 3.3: Driving cycle recorded in the Eastern direction

Once the GPS data is recorded, it can be loaded into the online platform LandAirSea [142]. The data is stored in ".LAT" format which is specific to this website and cannot be read by other software. This platform displays the displacement of the vehicle on a map generated by Google Maps API at the time recorded. The elevation profile and speed of the vehicle are calculated using information from Google Maps' database. The GPS coordinates, speed and elevation profile can be downloaded as CSV or KLM files from this platform. The KLM format provides geographic annotation and visualization that can be loaded into different tools, such as Google Earth or GPS Visualizer.

The elevation data obtained from Google Maps API shows spikes in altitude as indicated by the red line in Figure 3.4; such spikes are unlikely to occur in real-life. As such, the NED DEM database which has a known accuracy and is freely available was used to extract elevation data from the GPS coordinates. Additionally, due to the inaccuracies of the DEM, it is crucial to apply a filtering method to smooth the elevation profile. Pouya Amid, a PhD student at the University of Victoria part of

the Sustainable Systems Design Lab (SSDL) developed a computation tool in Matlab to smooth the obtained elevation profile using Savittzky-Golay filter. His help was required to complete this task.

Using this smoothing algorithm, a more realistic elevation profile, shown in the blue line in Figure 3.4, was obtained. The realistic elevation profile, besides being smoothed, shows an offset between 2-4m compared to the raw data. This is due to the fact that the DEM and the Google Maps API give different elevations for the same GPS coordinate. For instance, if one looks at the first GPS point recorded (latitude: 48.46616211, longitude:-123.3090495) the elevation height is 63.35m using the NED DEM. For the same point, the resulting altitude is 58.6m when using Google Maps API, which corresponds to a 7.5% difference when compared to the DEM result. This explains the offset observed in Figure 3.4.

It should be noted that DEM databases do not account for man-made constructions such as bridges, therefore the data need to be filtered when the bus crosses a bridge. In this elevation profile, it can be seen that the bus crosses over a bridge in both directions when the altitude drops down to 0m (sea level). To correct for this, the altitude at these points was assumed to be the same as the one given by Google Maps API. A flat road was assumed for this small portion of the trip.

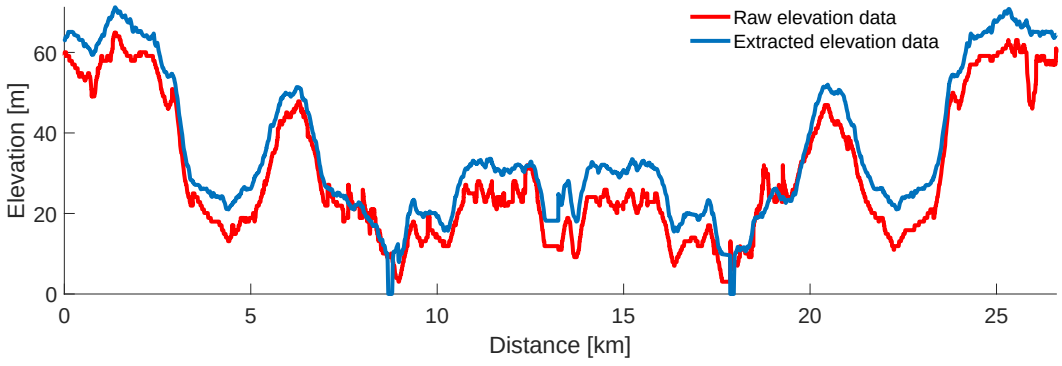

Figure 3.4: Raw elevation data for the whole trip (both directions)

The resulting road grade in degrees in shown in Figure 3.5 for the East direction. Since the difference in altitude between two GPS points and the actual travelled distance is known, the road angle is simply determined by triangulation.

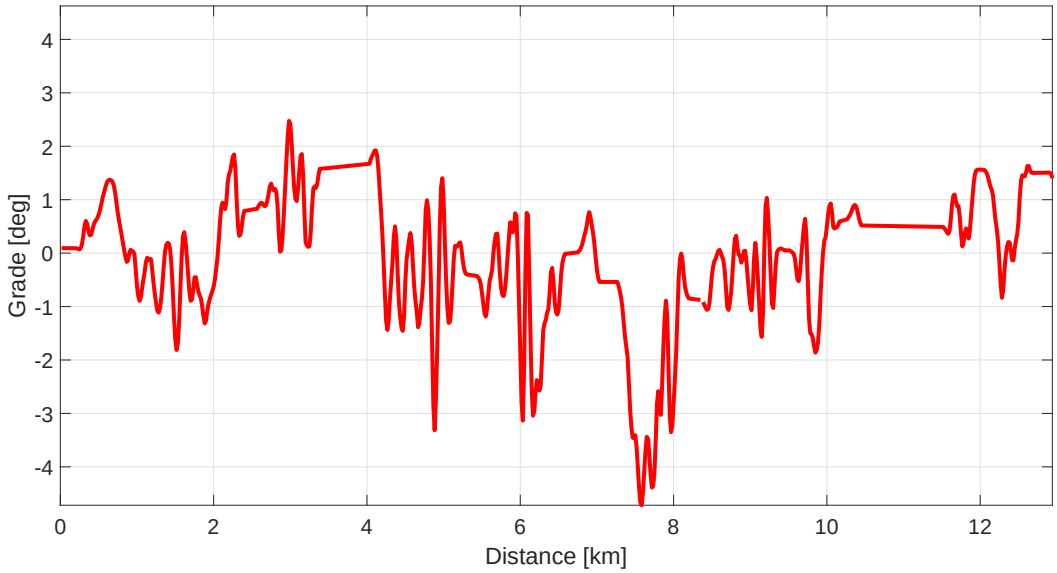

Figure 3.5: Road grade (deg) for the East direction travel

Once the grade profile is obtained, a second post-processing manipulation of the data is necessary, as the recorded speed does not drop to 0 at any point in time. As such, when the speed drops below 5km/hr, it was set as 0. This assumption was made based on the study of the driving cycles and GPS coordinates on the LandAirSea online platform. These corresponded to bus stops or possible intersection or traffic stops. There was no traffic jam during the time the data were recorded. It should be noted that since grade and speed are both being derivatives of elevation and position, signal noise is inherently amplified in base measurements. The effect of this change is shown in Figure 3.6.

During the data gathering phase, the sampling frequency was not maintained at exactly 1Hz over the test. The device would stop recording when the bus stopped for a few seconds, then start collecting data again. A 1D interpolation function was

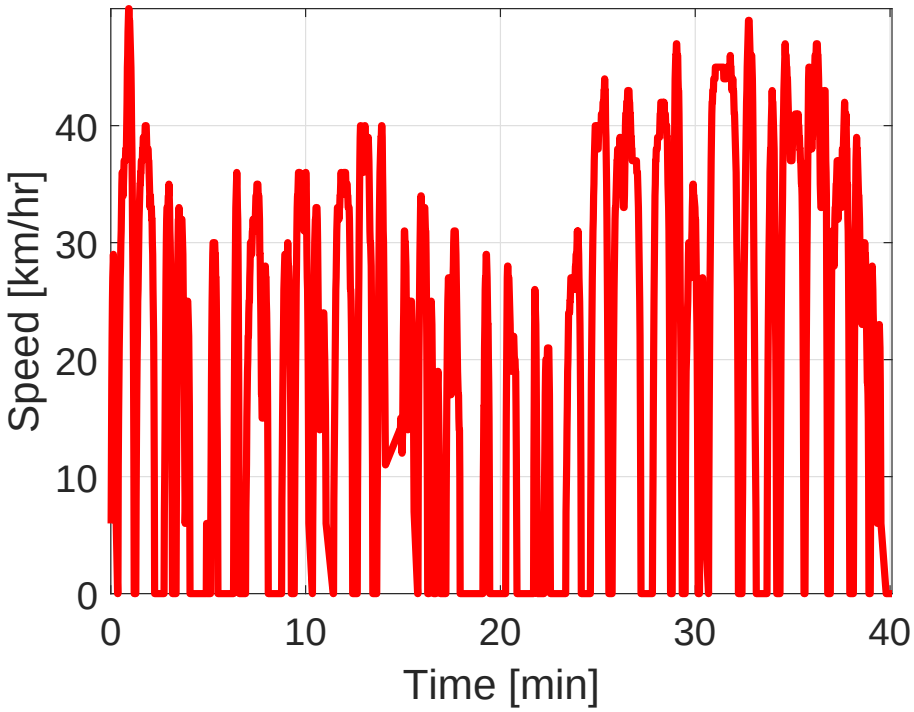

Figure 3.6: Driving cycle recorded in the Eastern direction with post-processed data

therefore used to obtain the speed, time, grade and travelled distance array used in the ECONS-M for every second.

3.1.2 ECONS-M Sensitivity Analysis

To better assess how the ECONS-M results are influenced by input parameters, a sensitivity analysis was performed. During the Milton Keynes demonstration project in 2014, the energy consumption for the buses were recorded. The driver's performance was found to have a significant impact on the energy consumption of the electric buses [25]. Up to 0.62 kWh/km difference in energy consumption was measured between two different drivers corresponding to 100% difference in energy consumption.

Zhou et al. [143] reported that though the drivers were asked to not change their behavior when driving the e-buses in Macao, different drivers would drive at different

speed under similar road conditions (13 km/h versus 17 km/h) which indicates it can be a challenge for drivers to control their driving pattern. Frank et al. in [144] modeled the effect of driving style on energy consumption and developed an "eco-driving application" informing the driver of her/his energy efficiency. This application can be very useful for battery electric bus drivers.

Senstivity analysis for energy demand in electric cars has been investigated in [145] but to the best of the author's knowledge, such an analysis is yet to be done with electric buses input parameters. This research did not focus on capturing the driver impact on the energy consumption due to lack of data. Instead, different parameters, identified in [145], were varied over a range of values assumed or found in the literature to study the impact of each parameter on energy consumption. This method is called a "parametric sweep".

The parameters listed below were all related to the bus physical characteristics and varied for the sensitivity analysis:

1. Drivetrain efficiency
2. Mass of the vehicle
3. Mass of the passengers
4. Coefficient of rolling resistance
5. Frontal area
6. Auxiliary load
7. Drag coefficient

The analysis was performed for a test driving cycle with a constant speed of 25 km/hr on a flat road. Table 3.2 summarizes the range of value for each parameters, the sampling variation and the nominal value.

The ranges for the curb weigh, passenger number and frontal area were obtained by comparing all the available Altoona reports for 12-m long battery electric buses [146, 147, 99, 148]. The individual passenger weight was chosen to be 75 kg.

Table 3.2: Sensitivity analysis performed with electric bus parameters

Parameter	**Min value**	**Max value**	**Variation Step**	**Nominal value**	**Unit**
Motor efficiency	80	95	1	88	%
Curb weight of the vehicle	12,414	14,864	100	14,465	kg
Passenger number	0	71	1	0	-
Coefficient of rolling resistance	0.006 [149]	0.01 [150]	0.0001	0.00800	-
Frontal area	6.2 [101]	8.9 [149]	0.1	8.9	m^2
Auxiliary load	0	10 [151]	0.1	0	kW
Drag coefficient	0.6 [101]	0.8	0.01	0.66	-

The results of the energy consumption sensitivity analysis are shown in Figure 3.7. The energy consumption in kWh/km was normalised compared to a basecase. This basecase used the input shown as nominal values in Table 3.2. In Figure 3.7 the basecase corresponds to the value "1". For each parameter, the boxes represent the energy consumption range compared to the basecase when the model is run with the maximum and minimum values of Table 3.2. For example, when looking at the "Motor eff" case which stands for the motor efficiency, the box indicates a span of 0.16. This means that the output of the model using a maximum motor average efficiency of 95% or a minimum efficiency of 80% showed a span of 16% difference in energy consumption when normalized with the results of the basecase.

This gave a good insight as to which parameters impact the energy consumption the most within a range of feasible values found in the literature. In Figure 3.7, the parameters with the largest impact are listed from left to right. This means it is crucial to correctly model the auxilary power use and the tire rolling coefficient to obtain realistic results. Interestingly, these results coincide well with the sensitivity analysis performed by Asamer et al. [145] for electric cars. However, the impact of the passengers weight when the bus is empty compared to when it is fully loaded was

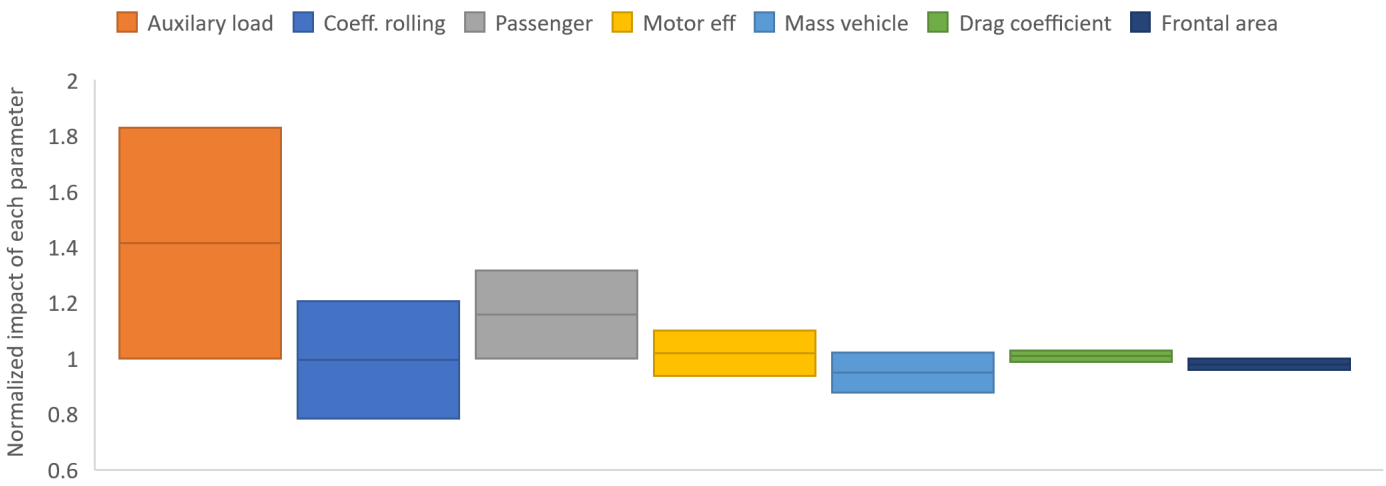

Figure 3.7: Normalized energy consumption: sensitivity analysis results for parameters regarding the bus physical characteristics for a constant speed and flat road

also found to be much more important than for an electric car.

Other important factors include the motor efficiency and the mass of the vehicle which do not greatly vary between manufacturers. Finally, other factors such as the drag coefficient or the frontal area had a limited impact on the energy consumption calculations; i.e when these parameters were varied within a reasonable range, there was not much change in the associated resistive forces.

The impact of the average speed was considered next in the analysis. In Figure 3.8, the energy consumption output is compared to the basecase run at 25km/hr. It shows that the greater the speed, the greater the impact on the energy consumption is. At average speeds lower than 35 km/hr, the impact of average speed is minimal compared to higher speeds.

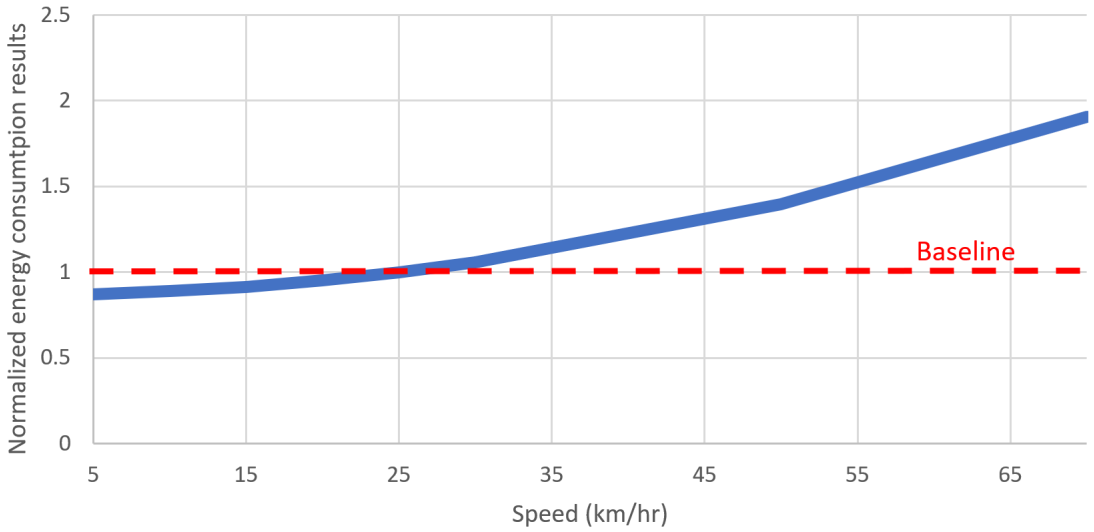

Figure 3.8: Normalized energy consumption sensitivity analysis results for varying speed using the basecase bus input on a flat road

3.1.3 Electricity Cost Compared To The Diesel Cost and Potential CO2e savings

The ECONS-M model is used to estimate the energy consumption of a 2013 BYD K9 on the transit route chosen in Victoria, BC. The model uses the input parameters shown in Appendix A. The driving cycle for the East direction is shown in Figure 3.6 in section 3.1.1.

It it assumed that throughout the run, a constant auxiliary load of 2.5kW is drawn and an average of 15 passengers remain onboard. The recommended SOC usage window for Lithium Iron Phosphate batteries is between 10-90 % therefore it is assumed the bus starts its route at a 90% SOC [136]. The calculated energy and final SOC is shown in Table 3.3.

Table 3.3: Results from the ECON-M for the selected route of Victoria, BC

Parameter	Westward direction	Eastward direction	Unit
Energy consumption	0.9	1.1	kWh/km
Total energy consumed	12.4	14.2	kWh
Final SOC after one way	85.9	85.2	%

If the bus does a round trip, it will consume in total 29.0 kWh. The total battery capacity is 324 kWh. That is, it can perform 10 round trips before the battery state-of-charge is depleted to 10% and the bus has to return to depot to charge. Assuming a 5% SOC buffer to return to the depot for its charge, the bus can only actually complete 9.5 trips. The BYD in-depot charger is 80 kW, with a rated voltage of 400V and a maximum current of 126 A. The charger efficiency is assumed to be 91% [152]. When the bus arrives into the depot it has to charge back to a 90% from a 10% SOC: $90\% \times 324 - 10\% \times 324 = 259.2kWh$.

The time to charge the battery, assuming a constant output power from the charger, is:

$$\frac{259.2kWh}{80kW \times 0.91} \times \frac{60min}{1h} = 3hr33min = 213min.$$

The energy consumed from the grid is:

$$\frac{213min}{60min/hr} \times 80kW = 284.8kWh.$$

It takes 85 min for the bus to complete a round trip run. Assuming the bus stops for 5 min after completing one direction of the route, the total trip is 95 min. As explained in section 3.1.1 the selected route operates for 20 hr per day. As modeled, the BEB can operate for 15 hr before requiring a 3 hr charge.

To estimate the diesel costs of operating a diesel bus on the selected route in Victoria, an average fuel consumption of 55.5L/100km is used as reported by BC Transit in [153]. Diesel costs are assumed to be \$1/L after discussions with different Canadian Transit authorities. In Table 3.5 the yearly fuel consumption for the specific route is obtained assuming the bus performs 9.5 runs per day for 7 days a week, 52.2 weeks per year.

The electricity rate for the charge of the modeled BYD K9 are obtained using BC Hydro's most up-to-date rate structure. BC Hydro is the main provider of electricity in British Colombia and the unique electricity supplier in the Victoria area. The

in-depot charger falls into the Medium General Service category. It should be noted that this rate structure is different compared to a residential consumer charge as it contains an additional $/kW "demand charge". This rate structure applies to customer with an annual peak demand between 35 and 150 kW. The in-depot charger has a 80 kW peak demand, charging the vehicle with a CC-CV cycle (with varying power). BYD buses have integrated on board chargers, therefore grid AC power can be directly delivered to the bus. Other manufacturers using in-depot chargers don't usually include a charger within the bus, therefore extra charging and power supply installations are required in the depot.

Table 3.4 summarizes the different charges of this rate structure. The demand charges are calculated for the maximum demand over a 15-min period average over a month. In the simulation, the BEB stays plugged in until it is fully charged; therefore the peak demand is 80 kW over this period. In addition to these charges, different discounts and additional taxes are applicable.

- 1.5% on entire electricity bill if electricity is metered at primary potential (assumed to be true)
- Rate Rider: 5% on entire electricity bill, covers additional and unpredictable energy costs
- Transformer owner discount (per kW): $-0.25
- GST and PST (taxes): 12% on the final electricity bill

Table 3.4: BC Hydro Medium General Service rates [154]

Charge	**Value**
Basic charge	$0.2429 per day
Demand charge	$4.92 per kW for a 15-min interval per month
Energy charge	$0.0880 per kWh

The results of the cost analysis are summarized in Table 3.5. Under the electricity price structure considered, the largest part of the electricity bill is the energy charge, though the demand charge portion is also substantial. Overall, the total savings are up to $34,215 per year for the energy/fuel charges to operate the electric bus compared to the diesel one.

Table 3.5: Yearly operational benefits of deploying the BEB compared to diesel buses

Parameter	**Value**
Total distance (km)	26.2
Price of diesel ($/L)	1
Fuel consumption (L)	50,476
Diesel price ($)	50,476
Basic charge ($)	88.65
Demand charge ($)	4,723
Energy charge ($)	9,148
Total electricity cost ($)	16,261
Fuel cost ($)	50,476
Savings ($)	**34,215**
Savings percentage	**67%**

The rate structure studied in this section is valid for the entire province of BC. In Ontario, however, electricity price is set by a supply/demand market with prices changing hourly, and the demand and energy charges depend on the electricity supplier of the jurisdiction. Certain jurisdiction's prices may be less favourable than the cheap rates experienced in BC, and perhaps even unfavourable for the adoption of BEB. Future work will consist in studying different rate structures across Canada to assess the feasibility of deploying BEBs based on the current charges implemented. This can drive policies changes and decision making in this area to ensure electricity rates for these projects do not handicap the deployment of BEBs.

It is also important to assess the emissions of the electric bus from the electricity production and compare them to the diesel emission to estimate the potential $CO2_e$ reduction.

CO_{2e}, or $C0_2$ equivalent, is a metric that describes the effect of different greenhouse gases in a common unit [155]. The most commonly known GHG is CO_2, but methane and nitrous oxide have for instance a higher GHG potential than CO_2. As an example, 1kg of methane emitted corresponds to 25kg of CO_2 emitted in terms of global warming impact.

BC Hydro reports that 92% of its energy supply comes from hydro power - that is a "clean source". It also reports an average emission factor of 11 tonnes CO_{2e}/GWh generated [154]. Other real marginal emissions, such as those related to a unit change in electricity demand, are more complicated and out of scope of this thesis. In [156], the BC Ministry of Environment has identified the direct emissions from heavy duty diesel vehicles to be 2.63 $kgCO_{2e}$/L of fuel. Diesel buses are considered to be heavy duty vehicles just like freight and delivery trucks.

Using these emission factors, the yearly CO_{2e} emission savings for the selected route are shown in Table 3.6. The percentage of potential emission reduction is shown in the last row. The projected emission reduction are up to 99% for the deployment of BEBs.

Table 3.6: Yearly CO_{2e} savings from deploying the BEB compared to diesel buses

Parameter	**Value**
Yearly electricity use (MWh)	104.0
Yearly fuel consumption (L)	50,476
Emissions from the grid (tCO_{2e})	1.1
Emissions from diesel use (tCO_{2e})	132.7
Yearly tCO_{2e} saved	**131.6**
Percentage of tCO_{2e} saved	**99%**

3.2 Estimate the Battery Lifetime Using the Capacity Fade Model

The scope of this section is to describe how the ECON-M and the CFM are used to estimate the battery lifetime of a BEB subjected to real-life operating conditions.

The first step is to obtain a C-rate profile for the given driving cycle using the methodology described in sections 2.1.1 and 2.3. By solving equations 2.53 and 2.54 the current and voltage of the cell are obtained. The current and voltage that each cell would be subject to during the recorded driving cycle for the transit route in Victoria are shown in Figure 3.9 and 3.10, respectively. As expected during discharge, the overall trend of the voltage is to decrease as the battery is depleted. In this figure, positive and negative current correspond to the battery powering the drivetrain and to regenerative braking respectively.

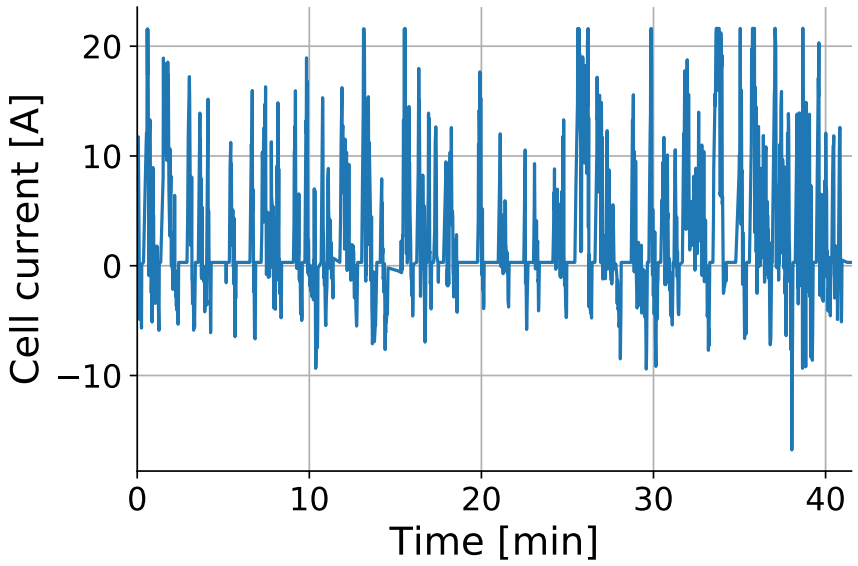

Figure 3.9: Cell current for the East direction driving cycle

The C-rate of the battery to be input to the CFM is shown in Figures 3.11 and 3.12.

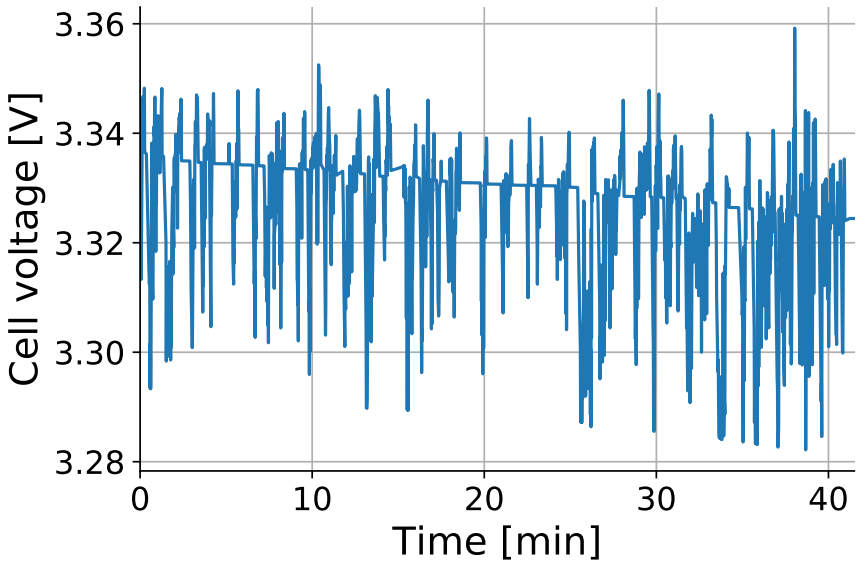

Figure 3.10: Cell voltage for the East direction driving cycle

The bus is charged with an assumed constant current charger at the rated current, 126 A which corresponds to a C-rate of 0.21, i.e less than 1C and within the model validity range as noted in section 2.2.6. The overall C-rate profile to be fed into the degradation model was built-up to include 9 East direction trips, 10 West direction trips, followed by a 213 minutes CC charge. This process is repeated 7 days a week, 365 days a year.

To the knowledge of the author, there is no study available in the literature listing all the parameters required to run the CFM for a LFP cell like the ones used in a BYD K9. Therefore, the parameters listed in Table 2.3 are used in this study. It should be noted that these parameters are not for the actual BYB cell chemistries, and the following study is therefore an illustrative example aiming to showcase the possible CFM outcomes. Chapter 4 details the different experiments required for future work to populate this model with BEB cell-specific data.

The results of the CFM are shown in Table 3.7. Interestingly, the capacity fade in the West direction is slightly higher than in the East direction, even though the

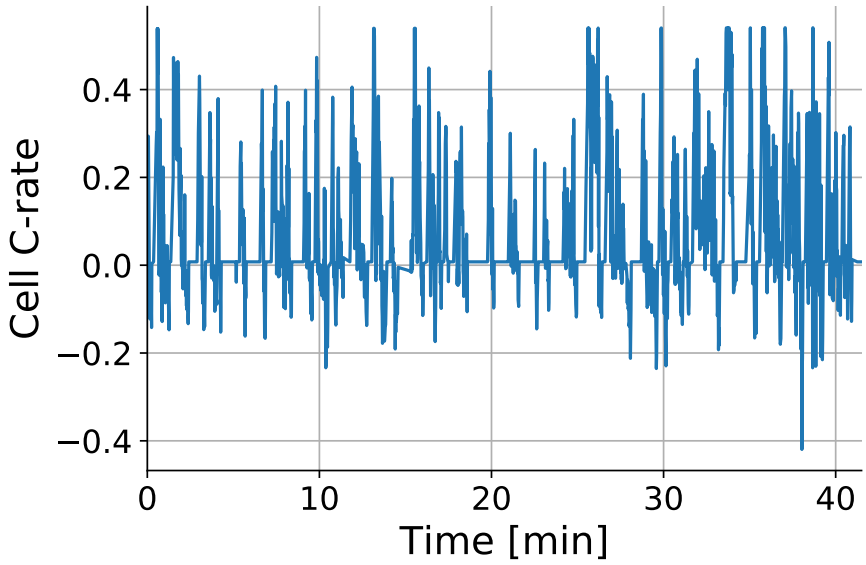

Figure 3.11: Cell C-rate for the East direction driving cycle

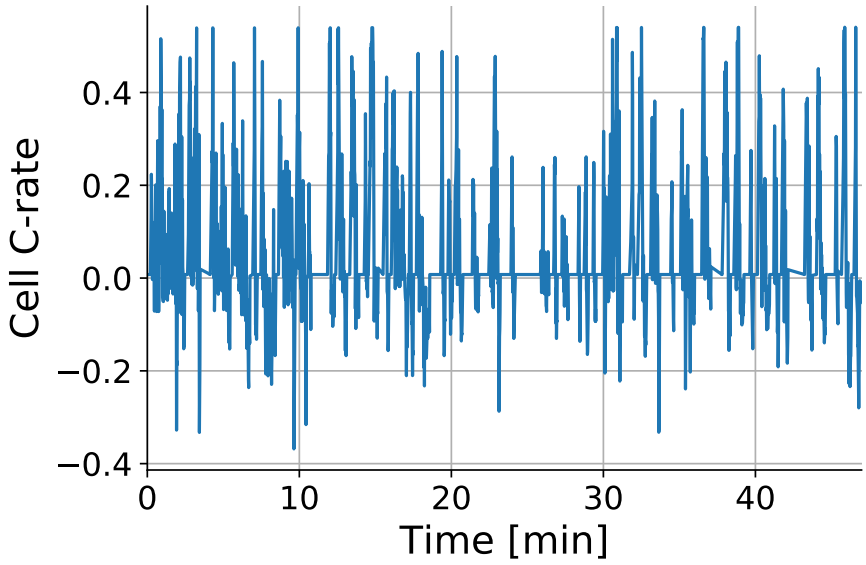

Figure 3.12: Cell C-rate for the West direction driving cycle

energy consumption of the East direction is higher. This is due to the fact that in the West direction, there are more regenerative braking events occurring than in the East direction. Since the model captures the degradation occurring during the charging events only, the more such events, the more capacity fade.

Table 3.7: Daily capacity fade resulting from the driving cycles

Parameter	Value
Capacity fade in the West direction (mol/m^3)	3.8
Capacity fade in the East direction (mol/m^3)	3.4
Capacity fade from charging (mol/m^3)	1.1
Total daily capacity fade (mol/m^3)	8.3

The battery end-of-life is deamed to have been reached when the capacity has decreased by 4,000 mol/m^3 [95]. Using the results provided in Table 3.7 the lithium cobalt oxide batteries would only last for 481 days or 1.31 years when subjected to the assumed BEB driving conditions which is far too short for an electric vehicle application.

As previously discussed, there is virtually no data in the literature for high capacity LFP or NMC batteries which are commonly used in BEBs. Therefore it is not possible to make any quantitative claims with regards to the CFM at this point of the research.

The developed Python Code for the CFM is shown in Appendix B.

3.3 On the Applications of the Models

In this chapter, different possible outcomes based on the modeling results were described. The ability to project the energy consumption of an electric bus for a given driving profile can support the planning and optimization of the charging strategy. Whether the buses use in-depot charging, terminus charging or on-route charging, there are many parameters such as the location or the output power of the chargers that need to be considered in the planning phase of a deployment project.

In this thesis, we explored two different applications of the ECONS-M: prediction of the electricity charging cost for a year and the potential GHG savings compared to a diesel, CNG or hybrid bus in use within the fleet; and support of decision making and assessing if the bus schedule allows sufficient downtime for charging, if fast charging is the chosen strategy. Current bus schedules have been optimized for diesel buses, which usually fuel upon their return to depot. It is likely that for routes with high traffic the bus schedule does not allow enough time to charge the bus on route or at the terminals. Schedules will therefore need to be revised to accommodate electrification.

The application of the CFM goes beyond estimating the lifetime of the simulated battery for a specific route. It can also predict the performance of new chemistries applied to automotive applications. In section 3.2, it was shown that lithium cobalt oxide batteries are not a good fit for BEB application as they would reach an EOL before 2 years.

If input cell parameters become available to feed the CFM and validate it, the model could also support financial planning of a deployment project to determine when the bus operator will need to replace the battery packs of the bus. Different routes will have a different impact on battery degradation. In section 3.2 it was shown that the East and West directions of the same route result in a different degradation profile due to a different pattern of regenerative braking. With proper planning, the operator can decide to change the routing of a bus after a certain number of years to maximize the battery use before it reaches its EOL.

3.4 Chapter Conclusion

The goal of this chapter was to give an overview of possible applications of the model for a particular transit route selected in Victoria, BC. First, the driving cycle (speed

versus time) of the vehicle was recorded using a GPS tracker. The data were gathered every second to obtain an accurate profile of the vehicle speed. The GPS coordinate were then used to obtain the road grade using a DEM database.

This input was then fed into ECONS-M to simulate a 2013 BYD K9 using an in-depot charging strategy. The energy consumption and battery SOC are assessed, as well as the maximum amount of runs possible before the battery is depleted. A sensitivity analysis has shown that the auxiliary load, coefficient of rolling resistance and passenger weight were crucial parameters to accurately estimate energy consumption. The yearly savings of deploying a battery electric bus compared to a diesel bus from a strictly operational standpoint, are $34,215, corresponding to a 67% saving. The yearly CO_{2e} savings are 131.56 T which corresponds to a 99% reduction, making the electric bus deployement extremely attractive in British Columbia to mitigate emissions.

Battery lifetime was estimated using the CFM with lithium cobalt oxide chemistry inputs due to a lack of available data on LFP electrochemical inputs (actual BYD cell). Though this results doesn't allow conductive results at this point, it opens the door to more research questions and the need to generate degradation testing on battery electric bus cells.

Lastly, the possible applications of the model were discussed. It should be noted that the ECONS-M has been used in several studies done for different transit agencies across Canada as part of Phase I of the Pan-Canadian Electric Bus Demonstration & Integration Trial led by the Canadian Urban Transit Research and Innovation Consortium (CUTRIC). This specific application will be discussed further in the Conclusions.

Chapter 4

Conclusion and Recommendations

4.1 Conclusion

This thesis reviewed the development and application of two models to support decision making for the deployment of battery electric buses: the energy consumption model (ECONS-M) and the CFM. In the introduction, a literature review on the different BEB feasibility studies and deployments was provided, along with a review on how to model the degradation phenomena in lithium-ion cells.

Deploying BEBs in transit route is somewhat challenging, as the technology is relatively new and the existing system is not yet optimized to adapt full fleet electrification. The ECONS-M and the CFM were developed to tackle these challenges that need to be addressed during the planning phase of deployment projects and to provide valuable insights to the industry.

The second chapter of this thesis described the background of the two models as well as the theoretical equations behind them. It also explained how the models are coupled to convert a real-life BEB driving cycle into a C-rate profile to estimate the battery lifetime. The models are route specific.

The ECONS-M is a first-principle based dynamic analysis that uses the speed of the vehicle as a function of time to calculate the energy consumption of the bus, in kWh/km. The model was tested using standardized Altoona's driving cycle, and the average energy consumption measured and modelled showed a difference of 0.8% for a 2013 BYD K9, which is a 324kWh battery electric bus using in-depot charging strategy.

The CFM uses a single particle model (SPM) to predict the cell potential versus time. The main assumption of the SPM is that the electrodes can be represented as solid single circular particles. This neglects the concentration and potential variations in the solution phase between the particles in the electrodes. In this research, we solely considered the decrease in lithium concentration to estimate the capacity decay, and did not include the resistance increase. The CFM implemented in this thesis follows Ning's model [95] but models a CC charging strategy rather than the CC-CV used in Ning‘s research.

The model limitations were also discussed in the second chapter. The main limitations of this model are:

- valid for C-rates up to 1C
- the resistance increase isn't accounted for
- it is not possible to implement a CC-CV charge using the SPM model developed by Bizeray et al. in Matlab as it is, though equations to be solved in a CV context are well known

Lastly, the ECONS-M and the CFMs were coupled to generate a second-by-second C-rate profile based on real-life operating conditions. This profile was then scaled down to be applied to the cell level. The cell lifetime is then assessed using the CFM.

The third chapter studied the direct applications of the two models. The ECONS-M was used to show the financial benefits of deploying a BEB versus a diesel bus and the $CO_{2,e}$ reduction potential for a selected route in Victoria, BC. The CFM was also used to provide an insight on the battery lifetime if the bus was to drive under the specified conditions.

A sensitivity analysis was performed for the ECONS-M. The results showed that the auxiliary load, coefficient of rolling resistance and passenger weight have the highest impact on the energy consumption and therefore should be carefully selected to obtain a realistic output.

A GPS tracker was used to record the speed and GPS coordinates of a bus driving through the selected route. Post-processing of the data was required to smooth the elevation and speed profiles to obtain a more realistic pattern.

Using this driving pattern with the characteristics of a 2013 BYD K9, the yearly financial and emission savings of deploying a BEB were obtained from the ECONS-M. This thesis demonstrates the advantages of deploying BEBs in British Columbia, where the electricity is generated 92% from clean power source. Compared to a diesel bus, 67% of financial savings can be achieved on the operational costs and 99% savings can be achieve on the $CO_{2,e}$ emissions.

Lastly the C-rate profile was generated using the ECONS-M and fed into the CFM to estimate the battery lifetime. However, due to a lack of available data in the literature on electrochemical characteristics of battery used in BEBs, the CFM was run using the inputs of a typical lithium cobalt oxide cell. This is the type of battery used to power small electronics, such as cellphones and laptops which means that it does not suit a heavy duty vehicle application. This highlighted the fact that more research is required in this area to accurately predict battery lifetime of electric buses, which is a growing industry.

4.2 Main Contributions

The main contributions of this thesis are detailed below.

1. A drivetrain energy consumption model (ECONS-M) that assesses the energy consumption of a BEB was developed. This model was used to assess the potential GHG and financial savings if a 2013 BYD K9 was to be deployed on a selected transit route in Victoria instead of a typical diesel bus. Large energy cost savings were demonstrated and shown in chapter 3. It should be noted that operation, maintenance and procurement costs are outside the scope of this thesis. This type of GHG and financial benefits analysis for electric buses had not been performed before. This model is currently set-up to use Canadian electricity rate structure and transit schedule, but its scope of application can be broadened internationally.

2. A sensitivity analysis of the ECONS-M identified the main factors impacting energy use of a BEB; these are the auxiliary load, coefficient of rolling resistance and the passenger load. This had not yet been investigated.

3. The ECONS-M helped demonstrate the environmental and financial benefits of deploying BEBs in British Columbia, where the electricity is mainly generated from clean energy sources.

4. An existing SPM model was coupled with an in-house developed CFM to estimate battery lifetime under a BEB driving cycle. This novel approach provides a potentially powerful tool for long term planning. Its features were illustrated for generic $LiCoO_2$ batteries but its application to the type of batteries used in BEB's will have to await open availability of input data.

5. The battery C-rate resulting from the driving cycle was produced by the ECON-

M and input into the SPM / CFM. This allows the SPM/CFM to directly read simulated driving condition of BEB changing current. This is important to capture real use of electric buses in an effort to further model battery degradation and to predict the lifetime of the batteries if the bus is deployed on a particular route.

4.3 Recommendation For Future Work

The research and results described in this thesis open avenues to further investigations, experiments and research which are outlined in this section.

4.3.1 Improving the ECONS-M model

The ECONS-M has been developed as a research tool, but also to support the demonstration and integration of BEBs for three different Canadian jurisdictions during Phase I of the Pan-Canadian Electric Bus Demonstration & Integration Trial led by the Canadian Urban Transit Research and Innovation Consortium (CUTRIC).

Phase 1 of the project connects over 18 national and international consortium members, including Siemens and ABB on the charger side and Nova Bus and New Flyer on the BEB manufacturing side. 18 BEBs and 7 overhead chargers are in the process of being deployed over three different jurisdictions - Vancouver (TransLink), Brampton (Brampton Transit), and York (York Region Transit. The goal of phase I is to achieve standardized opportunity charging for on-route optimized charging, which is a world first. This project positions Canada as a global leader in low-carbon transit mobility [157, 158].

The second phase of the project aims to deploy 60 BEB across Canada and 10 additional standardized overhead charging systems, and standardized depot charging

systems. Another area of focus will be to integrate energy storage with the overhead chargers to buffer the load of the high-powered superfast chargers on the grid.

The ECONS-M was used during the planning of phase I and will be used for phase II as well. Each transit agency partner selects potential route candidate for electrification, then the model is run to estimate the charging requirements, costs and GHG savings for each route. These outcomes of the model have supported decision making for the members of the consortium and funding applications.

An interesting prospect of this project is that once the BEBs are deployed on the selected routes, a third party data logger will be installed on board to gather data to test the accuracy of the ECONS-M. These data will include the speed of the vehicle, GPS coordinates, SOC and overall energy consumption. Other sensors can be installed at the charger level to measure how much electricity is provided from the grid and actually delivered to the battery.

At this point of the research, the only available information that can validate the model is from the Altoona testing results. During the CUTRIC trial the model will be more rigorously tested, improved and validated.

Though the model can be constantly improved especially in terms of software development and user friendliness, one of the main recommendation for the next steps is to include varying auxiliary load according to the operating conditions. This is a key aspect according to the results found from the sensitivity analysis, section 3.1.2. In [151], He et al. developed a model that predicts the HVAC load of a BEB according to the number of passengers. The number of passengers influences the heat dissipated in the cabin temperature which can itself impact the energy consumption of the bus. Additionally, the air humidity could also impact the energy use of the bus, especially on the West Coast (according to conversations with BC Transit). Though the authors do not detail the value of the parameters used for their analysis

in this paper [151], they discuss how the AC thermal load was calculated using the summation of the convective heat flowing between the cabin and the bus surface, the solar radiation, the heat load of the passengers and additional loads due to auxiliaries. The next version of the model should implement a similar approach to model the energy consumption in the summer and winter time. That is, modeling both the AC and the electrical heating system will be important to model the energy consumption as close to reality as possible. Additionally, some manufacturers make the choice of having diesel heaters on board: this can also be modelled cost and emission wise, and compared to resistive heaters or full vapour-compressor AC-heat pump systems on board for purely electric function.

Additionally, the passenger count should be modelled more dynamically. As shown in the sensitivity analysis in section 3.1.2, the bus energy consumption varies greatly depending whether the bus is empty or full. Sensors such as the one developed by Clever Devices can perform passenger count that are 95% accurate. The sensors can either be overhead at the doors, that is counting "vertically" or dual beam sensors counting "horizontally". This kind of device can be used for accurate ridership information that can be fed to the ECONS-M to improve its accuracy.

Lastly, it would be of good use to develop a battery pack thermal modelling to assess the influence of battery temperature on the battery performance, especially in terms of efficiency. The impact of external temperature on the battery initial performance should also be modelled, to ensure that the bus can work given the harsh winter conditions in Canada.

4.3.2 Improving the Battery Degradation Model

The different limitations of the capacity fade and SPM model are described in section 2.2.6. These limitations can be addressed to improve the prediction of the lifetime of

batteries for heavy duty applications.

Specifically, it is important that a constant current - constant voltage (CC-CV) mode is implemented. Currently, the Matlab SPM model developed by Bizeray et al. [123] only supports constant current charging until a certrain time limit or a certain voltage is reached. Adding this constant voltage feature would require further software development and solving the SPM equations differently. During this thesis research, a more complex electrochemical model in Fortran developed by Doyle et al [84] in 1998 and available online was used before adopting the SPM model. Doyle's model took longer to run, and though the charge could be programmed to be constant voltage, it was not possible to specify a "cut-off" current. When the CC-CV is defined, the CC portion is performed until a certain cut-off voltage is reached, then the CV takes place until a very low current is reached. Therefore more work is required to allow this charging strategy to be modeled.

Another limitation is the fact that the model cannot be used for fast charging, i.e C-rates between 1 to 2C or more available for electric buses. To the knowledge of the author, the mathematical model of SEI formation has not been tested or validated at high charging rates. That would require ageing testing and further development of appropriate model equations. There is currently a lot of research and development in the area of fast DC chargers for battery electric bus. In Geneva in 2017, ABB was chosen to deploy 13 "flash stations" 600 kW each as part of the TOSA project, claiming that the BEBs deployed in the route can charge up at a stop in the amount of time it takes for passengers to get on and off [159]. Siemens also proposes off-board DC fast chargers ranging from 150kW-600kW. Fast chargers present many advantages, as the bus can have unlimited range as long as there are chargers allocated without needing to head back to depot in case the battery is depleted midday. This is a great motivator to study the impact of fast charging for battery degradation.

This limitation also comes from the fact that the SPM model assumption to neglect concentration gradient in the electrolyte is no longer true at higher C-rates. As such, it is crucial to use a more detailed mathematical model that describes the changes of concentration in the electrolyte such as the pseudo-2D model for C-rates higher than 1C.

The resistance increase during battery degradation was not considered in this research. To estimate the battery lifetime, the capacity fade is the only element required. However, resistance increase results in a decrease of the output power which is also crucial to quantify. In fact, a bus may not be able to perform the route it is initially scheduled for if the battery output power is insufficient. Future work needs to account for this change if one wants to obtain a fuller understanding of battery degradation.

Another important point to consider is the influence of temperature and calendar ageing on battery degradation. In this research the effect of temperature and storage ageing were neglected to simplify the development of the CFM. Future work should investigate the effect of these two parameters on battery power and capacity fade to improve the degradation model [83]. A good starting point to model the temperature fluctuations of the cell can be to replicate the methodology in [160], in which the authors coupled a thermal model with an enhanced SPM.

Finally, another important assumption that was made to scale the C-rate of the battery down to a cell level was that the battery and battery mangement system (BMS) were "ideal" which means that every cell behaved the same way. According to Baumhfer et al. in [161] every cell in a battery pack ages differently. This ageing difference is explained not only by the local operating conditions that vary from branches to branches, but also by the variances generated during the cell manufacturing process. In their research, the authors have tested 48 cells of the same type

from a mass production line and with the same charge and discharge protocol. Even when the cells are brand new, the measured capacity of the batteries vary +/- 1% from the mean. After ageing, an even greater variance in measured capacity is observed between -4.5% and 3.5% difference from the mean. The conclusion that can be drawn from these results is that mass production manufacturing processes lead to variations in the material properties and parameters, which in turn lead to different individual ageing of the cells. It was found that within these samples, in the worst case scenario one of the cell had a lifetime one quarter shorter than the lifetime of the best cell. Therefore, future research will have to investigate the scalability of the battery degradation process from the cell level to the battery pack level.

4.3.3 Potential Battery Ageing Experiments to be replicated on BEB cells

In section 3.2, the lack of available electrochemical data for LFP and NCM lithium-ion batteries was outlined, especially for high capacity cells such as the one used in BEBs. As stated in the introduction, deployment projects of BEBs are gaining momentum around the world, and are not viewed as pilot or test projects anymore because the technology has proven to be suitable for operations.

As such, there is an important research opportunity to carry out more testing on 40Ah lithium-ion cells with chemistries such as LFP, NMC or Lithium titanate. Battery ageing characterizations of these cell can especially advance the field to get a better understanding of the degradation.

Appendix C provides a literature review of the available testing methods to measure the degradation effects and mechanisms for electric vehicle batteries, especially the capacity and power fade and the increase in the system overall resistance. Such testing setup can be reproduced and/or improved on in future research to test electric

bus lithium-ion battery cells.

Bibliography

[1] C. G. Schneider and L. B. Hill, "Diesel and Health in America : The Lingering Threat," Tech. Rep. February, 2005. [Online]. Available: http://www.catf.us/resources/publications/files/Diesel_Health_in_America.pdf

[2] I. A. Reitolu, K. Altiniik, and A. Keskin, "The pollutant emissions from diesel-engine vehicles and exhaust aftertreatment systems," *Clean Technologies and Environmental Policy*, vol. 17, no. 1, pp. 15–27, 2014.

[3] "Table 6 2009 (preliminary) and 2008 (final) report," The Canadian Passenger Bus and Urban Transit Industries, Tech. Rep., 2009. [Online]. Available: http://www.statcan.gc.ca/pub/50-002-x/2011001/t007-eng.htm

[4] G. A. Ban-weiss and J. P. e. a. Mclaughlin, "Long-term changes in emissions of nitrogen oxides and particulate matter from on-road gasoline and diesel vehicles," *Atmospheric Environment*, vol. 42, pp. 220–232, 2008.

[5] "Adoption of the Paris Agreement. Proposal by the President." Tech. Rep. December, 2015. [Online]. Available: http://unfccc.int/resource/docs/2015/cop21/eng/l09r01.pdf

[6] R. Kühne, "Electric buses - An energy efficient urban transportation means," *Energy*, vol. 35, no. 12, pp. 4510–4513, 2010.

[7] T. Casey, "Electric Buses Could Beat CNG Buses By A Mile Or Nearly 6," 2015, [Accessed: 2017-06-29]. [Online]. Available: https://cleantechnica.com/2015/06/10/electric-buses-beat-cng-buses-mile-nearly-6/

[8] O. Delgado and R. Muncrief, "Assessment of Heavy-Duty Natural Gas Vehicle Emissions : Implications and Policy Recommendations," Tech. Rep., 2015. [Online]. Available: https://www.theicct.org/publications/assessment-heavy-duty-natural-gas-vehicle-emissions-implications-and-policy

[9] D. J. Rozell and S. J. Reaven, "Water Pollution Risk Associated with Natural Gas Extraction from the Marcellus Shale," *Risk Analysis*, vol. 32, no. 8, pp. 1382–1393, 2012.

[10] J. P. Stempien and S. H. Chan, "Comparative study of fuel cell, battery and hybrid buses for renewable energy constrained areas," *Journal of Power Sources*, vol. 340, pp. 347–355, 2017.

[11] F. Chen, T. R. Fernandes, M. Yetano Roche, and M. da Graça Carvalho, "Investigation of challenges to the utilization of fuel cell buses in the EU vs transition economies," *Renewable and Sustainable Energy Reviews*, vol. 11, no. 2, pp. 357–364, 2007.

[12] D. Simbeck, "Biggest Challenge for the Hydrogen Economy Hydrogen Production Infrastructure Costs," Tech. Rep., 2003. [Online]. Available: https://stephenschneider.stanford.edu/Publications/PDF_Papers/SimbeckAspenH2.pdf

[13] G. E. Gray, "Perceptions of public transportation," in *Public transportation*, 2nd ed., P. Hall, Ed., 1992, ch. 22.

[14] A. Innocenti, P. Lattarulo, and M. Grazia, "Car stickiness : Heuristics and biases in travel choice," *Transport Policy*, vol. 25, pp. 158–168, 2013.

[15] "Public Transportation: Benefits for the 21st Century," American Public Transportation Association, Tech. Rep., 2007. [Online]. Available: http://www.apta.com/resources/reportsandpublications/documents

[16] Apta.com, "Calculate Your Savings by Riding Public Transportation," [Accessed: 2017-06-29]. [Online]. Available: http://www.apta.com/resources/aboutpt/pages/transitcalculator.aspx

[17] B. Tuttle, "Driver Consensus: It's Silly to Upgrade Cars Every Couple of Years," 2012, [Accessed: 2017-06-29]. [Online]. Available: http://business.time.com/2012/07/27/driver-consensus-its-silly-to-upgrade-cars-every-couple-of-years/

[18] BYD.com, "K9 Electric Transit Bus Tech Specs," 2016, [Accessed:2017-05-09]. [Online]. Available: http://www.byd.com/usa/bus/k9-electric-transit-bus/

[19] Proterra.com, "The Proterra Catalyst 40-foot transit vehicle," [Accessed: 2017-05-09]. [Online]. Available: https://www.proterra.com/products/catalyst-40ft/

[20] Newflyer.com, "Xcelsior Electric Brochure," [Accessed: 2017-05-09]. [Online]. Available: https://www.newflyer.com/buses/zero-emissions/xcelsior-electric-bus

[21] Greenpowerbus.com, "Product line all electric transit and school buses," [Accessed:2017-05-09]. [Online]. Available: http://www.greenpowerbus.com/product-line/

[22] Proterra.com, "Proterra continues North American Market leadership with milestone deployment to San Joaquin RTD," 2017. [Online].

Available: https://www.proterra.com/press-release/proterra-continues-north-american-market-leadership-with-milestone-deployment-to-san-joaquin-rtd/

[23] B. Zhou, Y. Wu, B. Zhou, R. Wang, W. Ke, S. Zhang, and J. Hao, "Real-world performance of battery electric buses and their life-cycle benefits with respect to energy consumption and carbon dioxide emissions," *Energy*, vol. 96, pp. 603–613, 2016.

[24] M. Xylia, S. Leduc, P. Patrizio, F. Kraxner, and S. Silveira, "Locating charging infrastructure for electric buses in Stockholm," *Transportation Research Part C: Emerging Technologies*, vol. 78, pp. 183–200, 2017.

[25] A. Kontou and J. Miles, "Electric Buses: Lessons to be Learnt from the Milton Keynes Demonstration Project," *Procedia Engineering*, vol. 118, pp. 1137–1144, 2015.

[26] Autoblog.com, "Geneva's new 'flash-charge' electric buses refuel in 15 seconds," 2016, [Accessed: 2017-09-01]. [Online]. Available: http://www.autoblog.com/2016/07/18/genevas-new-flash-charge-electric-buses-refuel-in-15-seconds/

[27] "Electric bus feasibility study for the city of Edmonton," Edmonton, Tech. Rep. 9, 2016. [Online]. Available: https://www.edmonton.ca/documents/transit/ETS_Electric_Feasibility_Study.pdf

[28] Sanjoaquinrtd.com, "Clearly better zero-emission, all electric bus," 2012, [Accessed: 2017-05-09]. [Online]. Available: http://sanjoaquinrtd.com/electric-buses/

[29] tfl.gov.uk, "Mayor unveils first fully electric bus routes for central London," 2016, [Accessed: 2017-05-09]. [Online]. Avail-

able: https://tfl.gov.uk/info-for/media/press-releases/2016/september/mayor-unveils-first-fully-electric-bus-routes-for-central-lond

[30] J. Ayre, "China 100% Electric Bus Sales Grew To ˜115,700 In 2016," 2017, [Accessed:2017-05-09]. [Online]. Available: https://cleantechnica.com/2017/02/03/china-100-electric-bus-sales-grew-115700-2016/

[31] M. Mahmoud, R. Garnett, M. Ferguson, and P. Kanaroglou, "Electric buses : A review of alternative powertrains," vol. 62, pp. 673–684, 2016.

[32] M. Andersson, "Energy storage solutions for electric bus fast charging stations: Cost optimization of grid connection and grid reinforcements," Tech. Rep., 2017. [Online]. Available: http://uu.diva-portal.org/smash/record.jsfpid=diva2%3A1080948&dswid=1762

[33] P. Bansal, "Charging of Electric Vehicles : Technology and Policy Implications," *Journal of Science Policy & Governance*, vol. 6, no. 1, 2015.

[34] Z. Bi, L. Song, R. De Kleine, C. C. Mi, and G. A. Keoleian, "Plug-in vs. wireless charging: Life cycle energy and greenhouse gas emissions for an electric bus system," *Applied Energy*, vol. 146, no. 0, pp. 11–19, 2015.

[35] M. Yilmaz and P. T. Krein, "Review of charging power levels and infrastructure for plug-in electric and hybrid vehicles," *2012 IEEE International Electric Vehicle Conference, IEVC 2012*, vol. 28, no. 5, pp. 2151–2169, 2012.

[36] B.-R. Ke, C.-Y. Chung, and Y.-C. Chen, "Minimizing the costs of constructing an all plug-in electric bus transportation system: A case study in Penghu," *Applied Energy*, vol. 177, pp. 649–660, 2016.

[37] M. Rogge, S. Wollny, and D. Sauer, "Fast Charging Battery Buses for the Electrification of Urban Public TransportA Feasibility Study Focusing on Charging Infrastructure and Energy Storage Requirements," *Energies*, vol. 8, no. 5, pp. 4587–4606, 2015.

[38] F. Burmeister and L. Schnieder, "Simulation Based Studies on the Integration of Battery-Electric Vehicles in Regional Bus Services," *Intelligent Transportation Systems (ITSC), 2015 IEEE 18th International Conference*, pp. 1333–1338, 2015.

[39] P. Sinhuber, W. Rohlfs, and D. U. Sauer, "Study on Power and Energy Demand for Sizing the Energy Storage Systems for Electrified Local Public Transport Buses," *IEEE Vehicle Power and Propulsion Conference*, pp. 315–320, 2012.

[40] J. Miles and S. Potter, "Developing a viable electric bus service: The Milton Keynes demonstration project," *Research in Transportation Economics*, vol. 48, pp. 357–363, 2014.

[41] Z. Gao, Z. Lin, T. J. LaClair, C. Liu, J.-M. Li, A. K. Birky, and J. Ward, "Battery capacity and recharging needs for electric buses in city transit service," *Energy*, vol. 122, pp. 588–600, 2017.

[42] I. Karakitsios, E. Karfopoulos, and N. Hatziargyriou, "Impact of dynamic and static fast inductive charging of electric vehicles on the distribution network," *Electric Power Systems Research*, vol. 140, pp. 107–115, 2016.

[43] P. Bauer, Y. Zhou, J. Doppler, and N. Stembridge, "Charging of Electric Vehicles and Impact on the Grid," *Proceedings of the 13th International Symposium Mechatronika*, pp. 121–127, 2010.

[44] N. Leemput, F. Geth, J. Van Roy, P. Olivella-Rosell, J. Driesen, and A. Sumper, "MV and LV residential grid impact of combined slow and fast charging of electric vehicles," *Energies*, vol. 8, no. 3, pp. 1760–1783, 2015.

[45] G. Putrus, P. Suwanapingkarl, D. Johnston, E. Bentley, and M. Narayana, "Impact of electric vehicles on power distribution networks," *2009 IEEE Vehicle Power and Propulsion Conference*, pp. 827–831, 2009.

[46] Torontohydro.com, "Business electricity rates," [Accessed: 2017-07-18]. [Online]. Available: http://www.torontohydro.com/sites/electricsystem/business/rates/Pages/busrates.aspx

[47] Bramptonhydro.com, "Business electricity rates," [Accessed: 2017-07-18]. [Online]. Available: https://www.bramptonhydro.com/Business/BusinessRates/business_rates.html

[48] X. Luo, J. Wang, M. Dooner, and J. Clarke, "Overview of current development in electrical energy storage technologies and the application potential in power system operation," *Applied Energy*, vol. 137, pp. 511–536, 2015.

[49] H. Ding, Z. Hu, and Y. Song, "Value of the energy storage system in an electric bus fast charging station," *Applied Energy*, vol. 157, pp. 630–639, feb 2015.

[50] J. S. J. Song, A. Toliyat, D. Turtle, and A. Kwasinski, "A rapid charging station with an ultracapacitor energy storage system for plug-in electrical vehicles," *Electrical Machines and Systems (ICEMS), 2010 International Conference on*, 2010.

[51] Newflyer.com, "Brampton Transit To Participate in the CUTRIC Pan-Ontario Electric-Bus Demonstration and Integration Trial," 2016, [Accessed: 2017-07-04]. [Online]. Avail-

able: https://www.newflyer.com/rss/814-brampton-transit-to-participate-in-the-cutric-pan-ontario-electric-bus-demonstration-and-integration-trial

[52] G. De Filippo, V. Marano, and R. Sioshansi, "Simulation of an electric transportation system at The Ohio State University," *Applied Energy*, vol. 113, pp. 1686–1691, 2014.

[53] T. Kurzcvezil, L. Schnieder, and F. Burmeister, "Optimized Energy Management of Inductively Charged Electric Buses Reflecting Operational Constraints and Traffic Conditions," *Models and Technologies for Intelligent Transportation Systems (MT-ITS), 2015 International Conference*, no. June, pp. 273–279, 2015.

[54] L. Lindgren, "Full electrification of Lund city bus traffic: A simulation study," Industrial Electrical Engineering and Automation, Tech. Rep., 2015. [Online]. Available: http://www.iea.lth.se/publications/Reports/LTH-IEA-7255.pdf

[55] A. Lajunen, "Energy consumption and cost-benefit analysis of hybrid and electric city buses," *Transportation Research Part C: Emerging Technologies*, vol. 38, pp. 1–15, 2014.

[56] L. Johannesson, S. Pettersson, and B. Egardt, "Predictive energy management of a 4QT series-parallel hybrid electric bus," *Control Engineering Practice*, vol. 17, no. 12, pp. 1440–1453, 2009.

[57] E. Tazelaar, J. Bruinsma, B. Veenhuizen, and P. van den Bosch, "Driving cycle characterization and generation, for design and control of fuel cell buses," *World Electric Vehicle Journal*, vol. 3, no. 1, pp. 1–8, 2009.

[58] D. Krajzewicz, J. Erdmann, M. Behrisch, and L. Bieker, "Recent Development and Applications of {SUMO - Simulation of Urban MObility}," *International*

Journal On Advances in Systems and Measurements, vol. 5, no. 3, pp. 128–138, 2012.

[59] D. Pacella, T. Donateo, and D. Laforgia, "Simulation and Optimization of the Energy Management of ITAN500 in the SUMO Traffic Model Environment," in *EVER Ecologic vehicles renewable energies conference*, 2010.

[60] R. Maia, M. Silva, R. Araujo, and U. Nunes, "Electric vehicle simulator for energy consumption studies in electric mobility systems," *2011 IEEE Forum on Integrated and Sustainable Transportation Systems, FISTS 2011*, pp. 227–232, 2011.

[61] A. Pesaran, "Choices and Requirements of Batteries for EVs, HEVs, PHEVs (Presentation)," NREL, Tech. Rep., 2011. [Online]. Available: http://www.osti.gov/energycitations/servlets/purl/1018087-eXSTvN/%5Cnhttp://www.nrel.gov/docs/fy11osti/51474.pdf

[62] Epectec.com, "Battery cell comparison," [Accessed: 2017-07-18]. [Online]. Available: http://www.epectec.com/batteries/cell-comparison.html

[63] Targray.com, "Cathode Active Materials," [Accessed: 2017-09-06]. [Online]. Available: http://www.targray.com/li-ion-battery/cathode-materials/cathode-active-materials

[64] G. E. Blomgren, "The Development and Future of Lithium Ion Batteries," *Journal of The Electrochemical Society*, vol. 164, no. 1, pp. A5019–A5025, 2017.

[65] Batteryuniversity.com, "BU-205: Types of Lithium-ion," [Accessed:2017-09-06]. [Online]. Available: http://batteryuniversity.com/learn/article/types_of_lithium_ion

[66] E. S. Pampal, E. Stojanovska, B. Simon, and A. Kilic, "A review of nanofibrous structures in lithium ion batteries," *Journal of Power Sources*, vol. 300, pp. 199–215, 2015.

[67] J. Vetter, P. Novák, M. Wagner, C. Veit, K.-C. Möller, J. Besenhard, M. Winter, M. Wohlfahrt-Mehrens, C. Vogler, and A. Hammouche, "Ageing mechanisms in lithium-ion batteries," *Journal of Power Sources*, vol. 147, no. 1-2, pp. 269–281, 2005.

[68] N. Nitta, F. Wu, J. T. Lee, and G. Yushin, "Li-ion battery materials: Present and future," *Materials Today*, vol. 18, no. 5, pp. 252–264, 2015.

[69] X. Zhang, H. Xie, C. S. Kim, K. Zaghib, A. Mauger, and C. M. Julien, "Advances in lithiumsulfur batteries," *Materials Science and Engineering R: Reports*, vol. 121, pp. 1–29, 2017.

[70] N. Imanishi and O. Yamamoto, "Rechargeable lithium-air batteries: Characteristics and prospects," *Materials Today*, vol. 17, no. 1, pp. 24–30, 2014.

[71] Ahmad A. Pesaran, Gi-Heon Kim and M. Keyser, "Integration Issues of Cells into Battery Packs for Plug-in and Hybrid Electric Vehicles," *International Electrical Vehicle Symposium (EVS-24)*, no. May, p. 7, 2009.

[72] Nordkyndesign.com, "Lithium Battery Banks Fundamentals," [Accessed: 2017-06-30]. [Online]. Available: http://nordkyndesign.com/lithium-battery-banks-fundamentals/

[73] Auvac.org, "The Current Condition and Future Potential of Automotive Batteries," [Accessed: 2017-09-06]. [Online]. Available: http://auvac.org/newsitems/view/1082

[74] H. Berg, "The electrochemical cell," in *Batteries for electric vehicles: materials and electrochemistry*. Cambridge University Press, 2015, pp. 1–45.

[75] A. Barré, B. Deguilhem, S. Grolleau, M. Gérard, F. Suard, and D. Riu, "A review on lithium-ion battery ageing mechanisms and estimations for automotive applications," *Journal of Power Sources*, vol. 241, pp. 680–689, 2013.

[76] MIT.edu, "A Guide to Understanding Battery Specifications," MIT, Tech. Rep. December, 2008. [Online]. Available: http://web.mit.edu/evt/summary_battery_specifications.pdf

[77] V. Marano, S. Onori, Y. Guezennec, G. Rizzoni, and N. Madella, "Lithium-ion batteries life estimation for plug-in hybrid electric vehicles," *Vehicle Power and Propulsion Conference, 2009. VPPC '09. IEEE*, pp. 536–543, 2009.

[78] L. Gao and Shengyi Liu, "Dynamic lithium-ion battery model for system simulation," *IEEE Transactions on Components and Packaging Technologies*, vol. 25, no. 3, pp. 495–505, 2002.

[79] M. Einhorn, V. F. Conte, C. Kral, J. Fleig, and R. Permann, "Parameterization of an electrical battery model for dynamic system simulation in electric vehicles," *IEEE Vehicle Power and Propulsion Conference*, 2010.

[80] K. S. Ng, C.-S. Moo, Y.-P. Chen, and Y.-C. Hsieh, "Enhanced coulomb counting method for estimating state-of-charge and state-of-health of lithium-ion batteries," *Applied Energy*, vol. 86, no. 9, pp. 1506–1511, sep 2009.

[81] W. Gu, Z. Sun, X. Wei, and H. Dai, "A Capacity Fading Model of Lithium-Ion Battery Cycle Life Based on the Kinetics of Side Reactions for Electric Vehicle Applications," *Electrochimica Acta*, vol. 133, pp. 107–116, jul 2014.

[82] B. Saha, K. Goebel, S. Poll, and J. Christophersen, "An integrated approach to battery health monitoring using bayesian regression and state estimation," *Autotestcon, 2007 IEEE*, pp. 646–653, 2007.

[83] T. D. Finley, "Battery Degradation Modeling For Vehicle Applications," Ph.D. dissertation, University of Waterloo, 2014.

[84] M. Doyle, T. Fuller, and N. John, "Modeling of Galvanostatic Charge and Discharge of the Lithium/Polymer/Insertion Cell," *Journal of The Electrochemical Society*, vol. 140, no. 6, p. 1526, 1993.

[85] P. Ramadass, B. Haran, P. M. Gomadam, R. White, and B. N. Popov, "Development of First Principles Capacity Fade Model for Li-Ion Cells," *Journal of The Electrochemical Society*, vol. 151, no. 2, p. A196, 2004.

[86] M. B. Pinson and M. Z. Bazant, "Theory of SEI Formation in Rechargeable Batteries: Capacity Fade, Accelerated Aging and Lifetime Prediction," *Journal of the Electrochemical Society*, vol. 160, no. 2, pp. A243–A250, 2013.

[87] M. Safari, M. Morcrette, A. Teyssot, and C. Delacourt, "Multimodal Physics-Based Aging Model for Life Prediction of Li-Ion Batteries," *Journal of The Electrochemical Society*, vol. 156, no. 3, p. A145, 2009.

[88] M. T. Lawder, P. W. C. Northrop, and V. R. Subramanian, "Model-Based SEI Layer Growth and Capacity Fade Analysis for EV and PHEV Batteries and Drive Cycles," *Journal of The Electrochemical Society*, vol. 161, no. 14, pp. A2099–A2108, 2014.

[89] V. Ramadesigan, P. W. C. Northrop, S. De, S. Santhanagopalan, R. D. Braatz, and V. R. Subramanian, "Modeling and Simulation of Lithium-Ion Batteries

from a Systems Engineering Perspective," *Journal of the Electrochemical Society*, vol. 159, no. 3, pp. R31–R45, 2012.

[90] S. Santhanagopalan, Q. Guo, P. Ramadass, and R. E. White, "Review of models for predicting the cycling performance of lithium ion batteries," *Journal of Power Sources*, vol. 156, no. 2, pp. 620–628, 2006.

[91] D. Zhang, B. N. Popov, and R. E. White, "Modeling Lithium Intercalation of a Single Spinel Particle under Potentiodynamic Control," *Journal of The Electrochemical Society*, vol. 147, no. 3, p. 831, 2000.

[92] Q. Zhang and R. E. White, "Capacity fade analysis of a lithium ion cell," *Journal of Power Sources*, vol. 179, no. 2, pp. 793–798, 2008.

[93] M. Guo, G. Sikha, and R. E. White, "Single-Particle Model for a Lithium-Ion Cell: Thermal Behavior," *Journal of The Electrochemical Society*, vol. 158, no. 2, p. A122, 2011.

[94] M. Safari and C. Delacourt, "Modeling of a Commercial Graphite/LiFePO4 Cell," *Journal of The Electrochemical Society*, vol. 158, no. 5, pp. A562–A571, 2011.

[95] G. Ning, R. E. White, and B. N. Popov, "A generalized cycle life model of rechargeable Li-ion batteries," *Electrochimica Acta*, vol. 51, no. 10, pp. 2012–2022, 2006.

[96] X. Feng, M. Lewis, and C. Hearn, "Modeling and Validation for Zero Emission Buses," pp. 501–506, 2017.

[97] S. Pelletier, O. Jabali, G. Laporte, and M. Veneroni, "Battery degradation and behaviour for electric vehicles: Review and numerical analyses of several

models," *Transportation Research Part B: Methodological*, vol. 103, pp. 158–187, sep 2017.

[98] L. Burkitt, "The World's Largest Electric Vehicle Maker Hits a Speed Bump," 2017, [Accessed: 2017-10-09]. [Online]. Available: https://www.technologyreview.com/s/604335/the-worlds-largest-electric-vehicle-maker-hits-a-speed-bump/

[99] "Federal Transit Bus Test Performed, Manufacturer: BYD Motors," The Larson Institute, Altoona, Duncansville, Tech. Rep., 2015. [Online]. Available: http://altoonabustest.psu.edu/buses/441

[100] BYD, " A Thriving Alternative in Transit Bus Evolution BYD All-Electric Bus," Tech. Rep., 2013. [Online]. Available: https://www.stm.info/sites/default/files/affairespubliques/Communiques/Annexes/ap_fiche_

[101] A. Lajunen, "Powertrain design alternatives for electric city bus," *2012 IEEE Vehicle Power and Propulsion Conference, VPPC 2012*, pp. 1112–1117, 2012.

[102] I. Fernández, C. Calvillo, A. Sánchez-Miralles, and J. Boal, "Capacity fade and aging models for electric batteries and optimal charging strategy for electric vehicles," *Energy*, vol. 60, pp. 35–43, 2013.

[103] P. Arora, R. White, and M. Doyle, "Capacity Fade Mechanisms and Side Reactions in Lithium Ion Batteries," *Journal of The Electrochemical Society*, vol. 145, no. 10, pp. 3647–3667, 1998.

[104] D. Linden and T. B. Reddy, *Handbook of batteries*. McGraw-Hill, 2002.

[105] Z. Li, J. Huang, B. Yann Liaw, V. Metzler, and J. Zhang, "A review of lithium deposition in lithium-ion and lithium metal secondary batteries," *Journal of Power Sources*, vol. 254, pp. 168–182, 2014.

[106] M. Wohlfahrt-Mehrens, C. Vogler, and J. Garche, "Aging mechanisms of lithium cathode materials," *Journal of Power Sources*, vol. 127, no. 1-2, pp. 58–64, 2004.

[107] G. Sarre, P. Blanchard, and M. Broussely, "Aging of lithium-ion batteries," *Journal of Power Sources*, vol. 127, no. 1-2, pp. 65–71, mar 2004.

[108] B. Lunz, Z. Yan, J. Gerschler, and D. Sauer, "Influence of plug-in hybrid electric vehicle charging strategies on charging and battery degradation costs," *Energy Policy*, vol. 46, pp. 511–519, 2012.

[109] S. Drouilhet and B. L. Johnson, "A Battery Life Prediction Method for Hybrid Power Applications Preprint," *35th AIAAA Aerospace Science Meeting and Exhibit*, no. January, 1997.

[110] N. Omar, M. Monem, Y. Firouz, J. Salminen, J. Smekens, O. Hegazy, H. Gaulous, G. Mulder, P. Van den Bossche, T. Coosemans, and J. Van Mierlo, "Lithium iron phosphate based battery Assessment of the aging parameters and development of cycle life model," *Applied Energy*, vol. 113, pp. 1575–1585, 2014.

[111] G. Lacey and R. Kotter, "The Effect of Cycling on the State of Health of the Electric Vehicle Battery," in *Power Engineering Conference (UPEC)*, 2013, pp. 1–7.

[112] Comsol.com, "Background : Capacity vs Power Fade," 2015, [Accessed: 2017-01-01]. [Online]. Available: https://www.comsol.com/model/capacity-fade-of-a-lithium-ion-battery-12667

[113] T. R. Ferguson, "Lithium-Ion Battery Modeling Using Non-equilibrium Thermodynamics," Ph.D. dissertation, MIT, 2008. [Online]. Available: http://web.mit.edu/bazant/www/papers/pdf/Ferguson_Thesis.pdf

[114] J. Newman and W. Tiedemann, "Porous-electrode theory with battery applications," *AIChE Journal*, vol. 21, no. 1, pp. 25–41, jan 1975.

[115] L. L. Lam, "Determining optimal discharge strategy for rechargeable lithium- ion batteries using multiphysics simulation," Ph.D. dissertation, University of Washington, 2014. [Online]. Available: https://digital.lib.washington.edu/researchworks/handle/1773/26415

[116] W. Lai and F. Ciucci, "Mathematical modeling of porous battery electrodesRevisit of Newman's model," *Electrochimica Acta*, vol. 56, no. 11, pp. 4369–4377, apr 2011.

[117] T.-S. Dao, C. P. Vyasarayani, and J. McPhee, "Simplification and order reduction of lithium-ion battery model based on porous-electrode theory," *Journal of Power Sources*, vol. 198, pp. 329–337, 2012.

[118] R. Klein, N. A. Chaturvedi, J. Christensen, J. Ahmed, R. Findeisen, and A. Kojic, "Optimal charging strategies in lithium-ion battery," *American Control Conference*, pp. 382–387, 2011.

[119] P. Ramadass, B. Haran, R. White, and B. N. Popov, "Mathematical modeling of the capacity fade of Li-ion cells," *Journal of Power Sources*, vol. 123, no. 2, pp. 230–240, 2003.

[120] M. Farag, M. Fleckenstein, and S. Habibi, "Continuous piecewise-linear, reduced-order electrochemical model for lithium-ion batteries in real-time applications," *Journal of Power Sources*, vol. 342, pp. 351–362, 2017.

[121] A. M. Bizeray, S. Zhao, S. R. Duncan, and D. A. Howey, "Lithium-ion battery thermal-electrochemical model-based state estimation using orthogonal collo-

cation and a modified extended Kalman filter," *Journal of Power Sources*, vol. 296, pp. 400–412, 2015.

[122] N. A. Chaturvedi, R. Klein, J. Christensen, J. Ahmed, and A. Kojic, "Algorithms for advanced battery-management systems," *IEEE Control Systems Magazine*, vol. 30, no. 3, pp. 49–68, 2010.

[123] A. M. Bizeray, , J. Reniers, and D. A. Howey, "Spectral_lion_SPM: Initial release," [Accessed:2017-03-01]. [Online]. Available: https://doi.org/10.5281/zenodo.212178

[124] H. Binous, A. A. Shaikh, and A. Bellagi, "Chebyshev orthogonal collocation technique to solve transport phenomena problems with Matlab® and Mathematica," *Computer Applications in Engineering Education*, vol. 23, no. 3, pp. 422–431, 2015.

[125] A. Veneziani and U. Villa, "ALADINS: An ALgebraic splitting time ADaptive solver for the Incompressible Navier-Stokes equations," *Journal of Computational Physics*, vol. 238, pp. 359–375, 2013.

[126] MathWorks.com, "ode45," [Accessed:2018-01-23]. [Online]. Available: https://www.mathworks.com/help/matlab/ref/ode45.html

[127] M. B. Pinson and M. Z. Bazant, "Theory of SEI Formation in Rechargeable Batteries : Capacity Fade , Accelerated Aging and Lifetime Prediction," vol. 160, no. 2, 2013.

[128] J. Speirs, M. Contestabile, Y. Houari, and R. Gross, "The future of lithium availability for electric vehicle batteries," *Renewable and Sustainable Energy Reviews*, vol. 35, pp. 183–193, 2014.

[129] S. Saxena, C. Le, J. Macdonald, and S. Moura, "Quantifying EV battery end-of-life through analysis of travel needs with vehicle powertrain models," *Journal of Power Sources*, vol. 282, pp. 265–276, 2015.

[130] S. B. Walker, S. B. Young, and M. Fowler, "Repurposing Electric Vehicle Batteries for Energy Storage to Support the Smart Grid," *IEEE Canadian Review*, 2013.

[131] A. Franca, J. Fernandez, C. Crawford, and N. Djilali, "Assessing the impact of an electric bus duty cycle on the battery pack life span," in *2017 IEEE Transportation Electrification Conference and Expo (ITEC)*, 2017, pp. 679–683.

[132] P. Wesley and C. Northrop, "Multiscale Modeling , Reformulation , and Efficient Simulation of Lithium-Ion Batteries," Ph.D. dissertation, Washington University in St. Louis, 2014. [Online]. Available: https://openscholarship.wustl.edu/etd/1256/

[133] K. Kumaresan, G. Sikha, and R. E. White, "Thermal Model for a Li-Ion Cell," *Journal of The Electrochemical Society*, vol. 155, no. 2, p. A164, 2008.

[134] S. Basu, K. S. Hariharan, S. M. Kolake, T. Song, D. K. Sohn, and T. Yeo, "Coupled electrochemical thermal modelling of a novel Li-ion battery pack thermal management system," *Applied Energy*, vol. 181, pp. 1–13, 2016.

[135] O. Tremblay, L.-a. Dessaint, and A.-I. Dekkiche, "A Generic Battery Model for the Dynamic Simulation of Hybrid Electric Vehicles," *2007 IEEE Vehicle Power and Propulsion Conference*, no. V, pp. 284–289, 2007.

[136] all battery.com, "3.2V 40Ah LiFePO4 - Lithium Iron Phosphate (DGR)," [Accessed:2017-11-28]. [Online]. Available: http://www.all-battery.com/3.2V40AhLiFePO4LithiumIronPhosphate-30217.aspx

[137] O. Tremblay and L. A. Dessaint, "Experimental validation of a battery dynamic model for EV applications," *World Electric Vehicle Journal*, vol. 3, no. 1, pp. 289–298, 2009.

[138] BYD, "BYD EBUS 12 specifications," [Accessed: 2015-11-01]. [Online]. Available: http://www.bydeurope.com/vehicles/ebus/types/12.php

[139] Spytecinc.com, "Introduction - Tracking Key GPS Logger 2," [Accessed:2017-11-30]. [Online]. Available: http://www.spytecinc.com/tracking-key-gps-logger-2.html

[140] Nationalmap.gov, "3D Elevation Program (3DEP)," [Accessed:2018-02-01]. [Online]. Available: https://nationalmap.gov/3DEP/3dep_prodserv.html

[141] Y. Wang, Y. Zou, K. Henrickson, Y. Wang, J. Tang, and B.-J. Park, "Google earth elevation data extraction and accuracy assessment for transportation applications," *PLOS ONE*, vol. 12, no. 4, pp. 1–17, 04 2017.

[142] Landairsea.com, "Silver Cloud," [Accessed:2017-11-30]. [Online]. Available: https://www.landairsea.com/

[143] B. Zhou, Y. Wu, B. Zhou, R. Wang, W. Ke, S. Zhang, and J. Hao, "Real-world performance of battery electric buses and their life-cycle benefits with respect to energy consumption and carbon dioxide emissions," *Energy*, vol. 96, pp. 603–613, feb 2016.

[144] R. Frank, G. Castignani, R. Schmitz, and T. Engel, "A novel eco-driving application to reduce energy consumption of electric vehicles," *2013 International Conference on Connected Vehicles and Expo, ICCVE 2013 - Proceedings*, pp. 283–288, 2013.

[145] J. Asamer and A. Graser, "Sensitivity Analysis for Energy Demand Estimation of Electric Vehicles," *Transportation Research Part D Transport and Environment*, no. May, 2016.

[146] "Federal Transit Bus Test - New Flyer XE40," Larson Institute, Altoona, Tech. Rep., 2015. [Online]. Available: http://altoonabustest.psu.edu/buses/458

[147] "Federal Transit Bus Test - Proterra BE40," Larson Institute, Altoona, Tech. Rep. 814, 2015. [Online]. Available: http://altoonabustest.psu.edu/buses/454

[148] "Federal Transit Bus Test - Catalyst E2 Proterra," The Larson Institute, Altoona, Tech. Rep. 814, 2017. [Online]. Available: http://altoonabustest.psu.edu/buses/480

[149] X. Feng, M. Lewis, and C. Hearn, "Modeling and Validation for Zero Emission Buses," *Transportation Electrification Conference and Expo (ITEC), 2017 IEEE*, pp. 501–506, 2017.

[150] A. Lajunen, "Evaluation of battery requirements for hybrid and electric city buses," *World Electric Vehicle Journal*, vol. 5, no. 2, pp. 340–349, 2012.

[151] H. He, M. Yan, C. Sun, J. Peng, M. Li, and H. Jia, "Predictive air-conditioner control for electric buses with passenger amount variation forecast ," *Applied Energy*, no. January, pp. 0–1, 2017.

[152] Theicct.org, "BYD Electric Vehicles Presentation," [Accessed: 2017-10-05]. [Online]. Available: http://www.theicct.org/sites/default/files/BYD EV SEDEMA.pdf

[153] L. Eudy and M. Post, "BC Transit Fuel Cell Bus Project : Evaluation Results Report ," Tech. Rep. February, 2014. [Online]. Available: https://www.nrel.gov/docs/fy14osti/62317.pdf

[154] bchydro.com, "Generation type, rates & CO2 emissions," [Accessed:2017-12-11]. [Online]. Available: https://www.bchydro.com/accounts-billing/rates-energy-use/electricity-rates/residential-rates/generation-rates-co2-comparison.html

[155] M. Brander, "Greenhouse Gases , CO2 , CO2e , and Carbon : What Do All These Terms Mean?" *Ecometrica*, no. August, pp. 2–4, 2012.

[156] "Best practices methodology for quantifying grennhouse gas emissions," Ministry of Environment, Tech. Rep., 2016. [Online]. Available: https://www2.gov.bc.ca/assets/gov/environment/climate-change/cng/methodology/2016-17-pso-methodology.pdf

[157] Cutric-crituc.org, "Planning Session #1: Pan Canadian Electric Bus Demonstration and Integration Trial (Phase 2)," 2017, [Accessed:2017-12-20]. [Online]. Available: http://cutric-crituc.org/events/2017/11/17/planning-session-1-pan-canadian-electric-bus-demonstration-and-integration-trial-phase-2

[158] Globenewswire.com, "Dr. Josipa Petrunic honoured as one of Canada's 2018 Clean50 for demonstrated leadership in clean transportation partnerships," 2017, [Accessed: 2018-01-08]. [Online]. Available: https://globenewswire.com/news-release/2017/09/27/1133870/0/en/Dr-Josipa-Petrunic-honoured-as-one-of-Canada-s-2018-Clean50-for-demonstrated-leadership-in-clean-transportation-partnerships.html

[159] A. Kooser, "Battery-topped electric buses flash charge in 15 seconds," 2014, [Accessed:2018-01-25]. [Online]. Available: https://www.cnet.com/roadshow/news/battery-topped-electric-buses-flash-charge-in-15-seconds/

[160] N. Baba, H. Yoshida, M. Nagaoka, C. Okuda, and S. Kawauchi, "Numerical simulation of thermal behavior of lithium-ion secondary batteries using the enhanced single particle model," *Journal of Power Sources*, vol. 252, pp. 214–228, apr 2014.

[161] T. Baumhöfer, M. Brühl, S. Rothgang, and D. U. Sauer, "Production caused variation in capacity aging trend and correlation to initial cell performance," *Journal of Power Sources*, vol. 247, pp. 332–338, feb 2014.

[162] S. Naumann and H. Vogelpohl, "Cactus: Models and Methods for the Evaluation and the Optimal Application of Battery Charging and Switching Technologies for Electric Busses," IFAK, Tech. Rep., 2015.

[163] J. Sullivan, K. Fenton, F. El, G. Marquez, C. Harris, C. Carl, N. Hudak, K. Jungjohann, C. Kliewer, K. Mccarty, A. Mcdaniel, G. Nagasubramanian, D. Joshua, A. Talin, C. Tenney, and K. Zavadil, "The Science of Battery Degradation," no. January, 2015.

[164] X. Liu, J. Wang, S. Huang, and F. e. a. Fan, "In situ atomic-scale imaging of electrochemical lithiation in silicon," *Nature nanotechnology*, vol. 7, no. October, pp. 749–756, 2012.

[165] V. Stancovski and S. Badilescu, "In situ Raman spectroscopic-electrochemical studies of lithium-ion battery materials: A historical overview," *Journal of Applied Electrochemistry*, vol. 44, no. 1, pp. 23–43, 2014.

[166] L. O. Valoen and J. N. Reimers, "Transport Properties of LiPF6-Based Li-Ion Battery Electrolytes," *Journal of The Electrochemical Society*, vol. 152, no. 5, p. A882, 2005.

[167] M. S. Ding, K. Xu, S. S. Zhang, K. Amine, G. L. Henriksen, and T. R. Jow, "Change of Conductivity with Salt Content, Solvent Composition, and Temperature for Electrolytes of LiPF[sub 6] in Ethylene Carbonate-Ethyl Methyl Carbonate," *Journal of The Electrochemical Society*, vol. 148, no. 10, p. A1196, 2001.

[168] M. Broussely, S. Herreyre, P. Biensan, P. Kasztejna, K. Nechev, and R. J. Staniewicz, "Aging mechanism in Li ion cells and calendar life predictions," *Journal of Power Sources*, vol. 97-98, pp. 13–21, 2001.

[169] I. Bloom, B. Cole, J. Sohn, S. Jones, E. Polzin, V. Battaglia, G. Henriksen, C. Motloch, R. Richardson, T. Unkelhaeuser, D. Ingersoll, and H. Case, "An accelerated calendar and cycle life study of Li-ion cells," *Journal of Power Sources*, vol. 101, no. 2, pp. 238–247, 2001.

[170] A. Eddaheck, O. Briat, and J.-M. Vinassa, "Performance comparison of four lithiumeion battery technologies under calendar aging," *Energy*, vol. 84, pp. 542–550, 2015.

[171] T. Waldmann, M. Wilka, M. Kasper, M. Fleischhammer, and M. Wohlfahrt-Mehrens, "Temperature dependent ageing mechanisms in Lithium-ion batteries A Post-Mortem study," *Journal of Power Sources*, vol. 262, pp. 129–135, 2014.

[172] J. Groot, M. Swierczynski, A. I. Stan, and S. K. Kær, "On the complex ageing characteristics of high-power LiFePO4/graphite battery cells cycled with high charge and discharge currents," *Journal of Power Sources*, vol. 286, pp. 475–487, 2015.

[173] W. Gu, Z. Sun, X. Wei, and H. Dai, "A new method of accelerated life testing based on the Grey System Theory for a model-based lithium-ion battery life evaluation system," *Journal of Power Sources*, vol. 267, pp. 366–379, 2014.

[174] T. Guan, P. Zuo, S. Sun, C. Du, L. Zhang, Y. Cui, L. Yang, Y. Gao, G. Yin, and F. Wang, "Degradation mechanism of LiCoO2/mesocarbon microbeads battery based on accelerated aging tests," *Journal of Power Sources*, vol. 268, pp. 816–823, 2014.

Appendix A

ECONS Model Validation Inputs

Parameter	**Value**	**Unit**	**Source**
Bus physical characteristics			
Weight	16,914	kg	[99]
Frontal area	8.66	m^2	$width \times height$
Seated passengers	37	-	[99]
Tire radius	0.50	m	[99]
Motor performances			
Maximum motor torque	700	Nm	[100]
Maximum motor power	180	kW	[100]
Motor maximum revolutions per minute	7500	RPM	[100]
Powertrain and battery performances			
Gear ratio	15	-	Assumed
Transmission (wheel to motor) efficiency	95%	-	[162]
Converter efficiency	97%	-	Assumed

Regenerative braking power split	40%	-	From conversations with BEB manufacturers
Charger power	80	kW	[100]
Battery capacity	324	kWh	[99]
Environmental characteristics			
Air density	1.225	kg/m^3	Assumed
Drag coefficient	0.6	-	Assumed
Rolling resistance coefficient	0.01	-	[101]

Table A.1: ECON-M input to simulate Altoona's results for a 2013 BYD K9

Appendix B

Capacity model code developed in Python

```
"""
@author: anaissia
"""

#import the required modules

import matlab.engine
import numpy as np
import scipy.integrate
import matplotlib.pyplot as plt
import math

eng = matlab.engine.start_matlab()
```

```
def degradation():
#list of input
    Rf=8.7*10**-3
    Cnom=1.67
    Tref = 25 + 273.15
    Rc = 20.0*10**-4
    thick1 = 75.0*10**-6
    thick2 = 25.0*10**-6
    thick3 = 74.0*10**-6
    As = 0.087
    Rs1 = 2.0*10**-6
    Rs3= 2.0*10**-6
    eps1s = 0.51
    eps3s = 0.48
    cs1max = 30550.0
    cs3max = 51555.0
    x1soc0 = 0.009
    x1soc1 = 0.62
    y3soc0 = 0.94
    y3soc1 = 0.50
    Ds1ref = 3.8*10**-14
    Ds3ref = 1.0*10**-13
    EaDs1 = 35.0*10**3
    EaDs3 = 29.0*10**3
    k1ref = 1.0*10**-6
    k3ref = 10.*10**-6
```

```
    Eak1=20.0e3
    Eak3=58.0e3
    ceavg = 1.0*10**3
    Cs_N= 25342    #x1soc0*cs1max
    Cs_N_disc= x1soc1*cs1max
    cycle=2
    N=[1,2]
    c=0



#run Matlab model
    result=eng.SPM(Cnom,\
    Tref,\
    Rc,\
    thick1,\
    thick2,\
    thick3,\
    As ,\
    Rs1,\
    Rs3,\
    eps1s,\
    eps3s,\
    cs1max,\
    cs3max,\
    x1soc0 ,\
```

```
        x1soc1,\
        y3soc0  ,\
        y3soc1  ,\
        Ds1ref,\
        Ds3ref  ,\
        EaDs1,\
        EaDs3  ,\
        k1ref,\
        k3ref,\
        Eak1,\
        Eak3,\
        ceavg,\
            c)
#Run degradation
        j_p=result['j1']._data.tolist()
        phase_diff_p=result['phase_diff']._data.tolist()
        t_p=result['time']._data.tolist()
        temp_p=result['temperature']._data.tolist()
        j_para=calc_j_side(phase_diff_p,j_p,Rf,temp_p)
        Rf,diff_R=increase_resistance(Rf,j_para,t_p)
        Rc=Rc+diff_R
        Cs_N,diff_C=decrease_concentration(Cs_N,j_para,t_p)
        print(diff_C,"degradation C",diff_R, "resistance deg")
        print('Cs_N', Cs_N, 'R_n', Rf)
        Cs_N=float(Cs_N)
        Rf=float(Rf)
```

```
Rc=float(Rc)
x1soc0=float(Cs_N/cs1max)
x1soc1=float((Cs_N_disc-diff_C)/cs1max)
for c in range(1, cycle):
    print('Model running for cycle:',c,'/n')
    Cs_N,diff_C=decrease_concentration(Cs_N,j_para,t_p)
    if c in N:
        print(diff_C,"degradation C",diff_R, "resistance deg")
        print('Cs_N', Cs_N, 'R_n', Rf)


    Cs_N=float(Cs_N)
    x1soc0=float(Cs_N/cs1max)
    x1soc1=float((Cs_N_disc-diff_C)/cs1max)
    if c==cycle:
        result=eng.SPM(Cnom,\
        Tref,\
        Rc,\
        thick1,\
        thick2,\
        thick3,\
        As ,\
        Rs1,\
        Rs3,\
        eps1s,\
        eps3s,\
```

```
                cs1max,\
                cs3max,\
                x1soc0  ,\
                x1soc1,\
                y3soc0  ,\
                y3soc1  ,\
                Ds1ref,\
                Ds3ref  ,\
                EaDs1,\
                EaDs3  ,\
                k1ref,\
                k3ref,\
                Eak1,\
                Eak3,\
                ceavg,\
                    c)
def calc_j_side(phase,j_p,Rf,temp):
    # calculated the local current of the side reaction

    Upara=0.38 # side reaction voltage (V)
    j0=0.8*10**-7
    F=96485.3329 #faraday's constant
    R=8.3144598 # J/mol k
    alpha_c=0.5
    overpotential=[]
    jpara=[]
```

```
    for i in range(0,len(phase)):
        overpotential.append(abs(phase[i])-Upara-Rf*(abs(j_p[i])))
        jpara.append(-j0*math.exp ..
        (alpha_c*F*abs(overpotential[i])/(R*temp[i])))

    return jpara

def decrease_concentration(Cs_N,j_para,time):

    #calculates the decrease in concentration

        eps_e=0.440 #electrolyte volume frac
        eps_fl=0.07 #conductive filler volume frac
        rs=2*10**-6 #radius particule m
        eps_s=(1-eps_e-eps_fl)
        a_neg=3*eps_s/rs
        F=96485 #C/mol (C=A.s) Faraday
        Q=[]


        Q_tot=abs(scipy.integrate.trapz ..
        (j_para[1:len(time)],time[1:len(time)])*a_neg)

        Cs_N1=Cs_N-(Q_tot)/(eps_s*F)
        diff_C=  (Q_tot)/(eps_s*F)
```

```
        return Cs_N1, diff_C

degradation()
```

Appendix C

Review on Battery Ageing Experiments

Various methods are used to observe the battery ageing level on electrodes and electrolytes experimentally, especially using spectroscopy and electrochemical techniques. Transmission electron microscopy (TEM) especially in-situ or "on-site" TEM are efficient techniques to observe and analyze nanoscale mechanisms associated with electrode lithiation, delithiation, cycling, mechanical fatigue and failure [163]. In [164], Liu et al. have shown that real-time lithiation of lithium-ion battery anodes can be observed using TEM. TEM provides extremely high spatial resolution for thin active electrode particles but when observing thicker particle the results are negatively impacted due to a limited chemical sensitivity. The scanning transmission x-ray microscopy (STXM) addresses this issue. STMX creates an x-ray absorption map with a 20 nm spatial resolution of a sample by using highly collimated x-ray beam [163]. Recent advances in the development of in-situ Raman spectroscopy, especially the integration of Raman spectrometers into non-optical microscopes such as atomic force microscope (AFM) or scanning electron microscope (SEM) have shown great

prospects for studying the electrochemical degradation in lithium ion battery [165]. These techniques allow a deeper insight into the degradation phenomenon in batteries and into the creation and dynamic change of the SEI.

Ex-situ or "off-site" testing can be performed to measure the characteristics of an electrolyte [166]. The conductivity, density and viscosity of the electrolyte can be measured through experiments such as the ones described in [167]. Electrolytes typically used in LPF batteries are prepared by mixing EC and EMC solvents and LPF salts in a dry glove box filled with argon. The temperature is controlled in an environmental chamber. To determine the conductivity, the electrolyte impedance is scanned from 1MHz to 20Hz at various temperatures. This method is called impedance spectroscopy. A Nyquist plot is then obtained and the conductivity is obtained at the intersection of the impedance curve with the real "X" axis.

In section 2.2.1, several factors influencing the battery lifetime were identified that were not taken into account in this research. High temperature was shown to have a significant impact on increasing calendar and cycling ageing. In [168], Broussely et al. investigate the effect of temperature on calendar ageing by using $LiCoO_2$ or $LiNiO_2$ electrode material cells and by storing them at various temperatures (14 ^{o}C, 30^{o}C, 40^{o}C, 60^{o}C) at a constant voltage. The cell capacities are diagnosed by either discharging or charging the cells at different ambient temperatures.

In [169] and in [170], the authors also investigated the effect of temperature on calendar ageing and accounted for the SOC level (60% and 80% and 30%, 65% and 100% respectively). The fully charged cells are first discharged at a constant C-rate until the desired SOC is reached. The cells are then heated to the desired temperature and their voltage is recorded for a period of four weeks. A second experiment was conducted to study cycling ageing using an "accelerated cycle life" testing procedure. The goal of this procedure is to shorten the experiment time to not have to wait for

the "natural" EOL to occur. The cells are exposed to various temperatures, SOC and ΔSOC, defined as the amount of nominal capacity discharged during a current pulse. The various ΔSOC represent different driving conditions, such as a few seconds of regenerative breaking or "charge pulse" and some constant discharge and charge events.

Wadmann et al. in [171] tested lithium-ion cells cycled with a constant 1C charge and discharge at constant temperatures between -20^{0}C and 70^{0}C, which represents the expected temperature range of an electric vehicle. Several research efforts have been carried to identify the impact of various charging rates on batteries but there is a gap in the literature to experimentally study how fast charging conditions would impact battery life.

In [172], the capacity and power degradation in $LiFePO_4$ are quantified for different current rates, temperatures and SOC ranges. Current rates of 1 and 2C are chosen to be within the operating condition range for electric vehicles. The influence of current rate and asymmetric cycles on cell degradation for various ΔSOC is investigated in this research. For the testing four main pieces of equipments were used:

- a cell tester - Maccor Series 4000: this is a fully automated test system with high level accuracy and time resolution to calibrate the capacity of the cells. The main parameters that can be controlled are the current and the voltage, it can contain between 1 to 192 individual test channels

- an environmental chamber to keep the temperature constant

- a potentiostat/galvanostat - Gamry Reference 3000: used to perform electrochemical impedance spectroscopy up to 1 MHz at a constant current or voltage

- a computer equipped with a post-processing analysis tool - TrueData-EIS: an impedance analyzer to measure the electrochemical impedance spectrum of com-

ponents during operation under different loads

There are several kinds of brands with different characteristics for each of these testing apparatus. Depending whether the experiment is to be performed on a pack or a single cell, the equipment should be different. The same testing apparatus can be used to test for calendar and accelerated cycling ageing. Similar testing procedure are used in [173] and in [174].

The figure below shows how the apparatus setup are linked together. Note that the potentiostat/galvanostat is optional if a constant current/constant voltage testing is not required. These equipments are required to setup ageing experiments on high capacity lithium-ion cells.